PV Lifetime Energy Yield

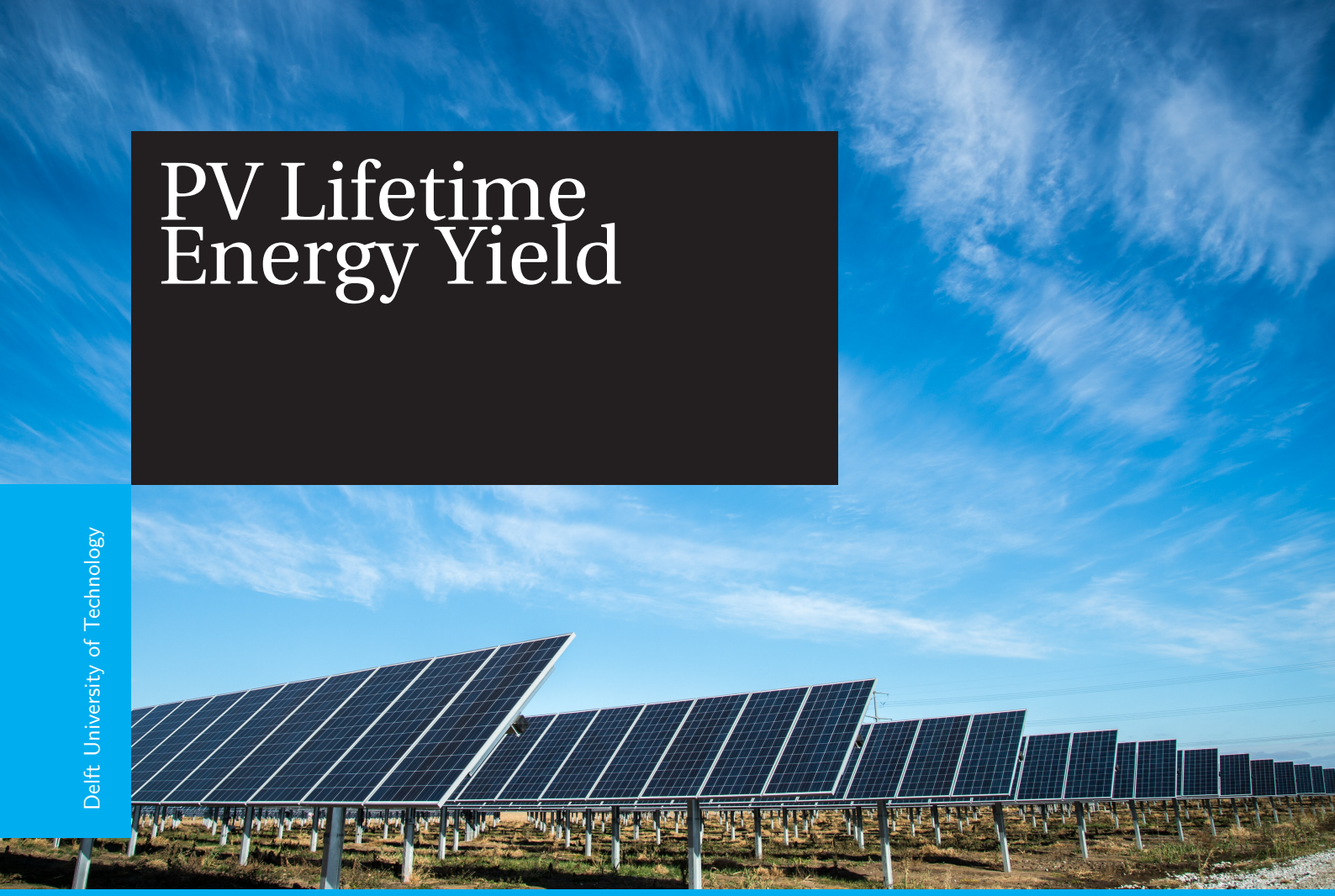

Delft University of Technology

TU Delft Delft University of Technology

Challenge the future

PV lifetime energy yield modelling and implementation in PVMD toolbox

by

Abhishek Velpuru

to obtain the degree of Master of Science in

Sustainable Energy Technology

at the Delft University of Technology,

to be defended publicly on Friday August 6, 2021 at 14:30

Student number: 5050316

Project duration: 16 November 2020 - 6 August 2021

Thesis Committee:

Dr. Rudi Santbergen	Assistant Professor - PVMD	Supervisor
Dr. Ivan Gordon	Professor - PVMD	
Dr. Babak Gholizad	Assistant Professor	External committee member
Dr. Malte Ruben Vogt	Postdoc-PVMD	Daily supervisor

TU Delft

PVMD Delft University of Technology

PREFACE

I've always been fascinated by the world of engineering and technology, particularly when it comes to the huge impact they've have on the evolution of civilization, and one such technology that amazed me was sustainable technology. My master's degree in sustainable energy technology at Delft University of Technology has been an enthralling voyage through diverse people and cultures over the last two years. I had time to enrich my knowledge and passion for photovoltaic technology, which resulted in the creation of this project.

I would like to thank and show my gratitude to *Dr. Rudi santbergen* for his support, knowledge, and experience, which made this project achievable. I'd like to express my gratitude to *Dr. Malte Ruben Vogt*, who has consistently motivated me and pushed me to exceed my limitations; he has been more than a mentor and supervisor during these difficult pandemic times. I'm blessed to have my friends Amith, Rohit, and Sushanth who are always there for me; this journey would not have been the same without them. Finally, but certainly not least, my housemates Jack and Ivan have provided me with an environment to work and have fun.

I would want to appreciate *Dr. Ismail Kaaya,* who works at the ISE Fraunhofer solar energy institute. Who has been gracious enough to spend time discussing various aspects of the project. It has been an honor to collaborate with him and his studies. I appreciate your willingness to share your knowledge and skills.

Finally, I'd like to convey my gratefulness for this journey to my parents and fate for providing me with this opportunity to expand my wings. Many thanks to the people and experiences that provided me with lifelong memories.

Delft, July 26^{th} 2021
Abhishek Velpuru

ABSTRACT

The global share of photovoltaic electricity has been expanding at a breakneck pace with CAGR of 27% over the last decade. This resulted in remarkable advancements in photovoltaic technology and design. The performance of the majority of PV modules is determined in laboratories under controlled conditions. Perhaps the climatic conditions on-site are not always stable when the PV module is installed. As a result, modules are subjected to changing environmental stressors such as temperature, relative humidity, UV radiation, and cyclic temperatures. Each of these environmental factors results in a distinct mode and mechanism of degradation, resulting in a loss of performance over time. As a result, determining the rate of degradation of a photovoltaic module is crucial for performance prediction and financial analysis.

Primarily, this research identifies a degradation model that is adaptable to various of photovoltaic technologies and designs while maintaining long-term accuracy such model is implemented into PVMD toolbox. We use this model to explore the degradation of photovoltaic modules in a variety of locations around the world, as each site has its own distinct environment. We explore a few well-known climates, namely tropical, steppe, temperate, desert, and cold. According to the study's findings, the lifetime of $Cold > Steppe > Desert > Temperate > Tropical$ and inverse for degradation rates.

Financial analysis is critical for determining the value and social impact of a project. Thus, the levelized cost of electricity metric is utilized to determine the economic value of photovoltaic modules under the various climatic conditions indicated previously. To perform this study an LCOE model is incorporated in PVMD toolbox consisting of economic and system variables along with growth rate per year parameter to determine future costs of PV modules. Tropical, steppe, and cold regions are evaluated financially using a variety of economic scenarios and discount rates in order to compare the effect of degradation on LCOE. Tropical zones have the highest LCOE values and the greatest influence on LCOE when the scenario is changed. Cold zones exhibit the greatest range of LCOE values in sensitivity analysis.

Finally, as crystalline silicon modules approach their theoretical limit, we discovered the tandem module in quest of more efficient technologies. Due to its broad compatibility with silicon modules, this study focuses on perovskite/silicon tandem modules. Despite this, new research indicates that perovskite/silicon tandem modules are susceptible to degradation. As a result, a model is designed with the objective of assessing the total degradation of tandem modules. We focused on the ability of the perovskite layer degradation to affect the overall degradation of the tandem module by employing normalized power in tandem degradation research. To investigate correlations, the energy production loss owing to degradation in tandem modules is compared to that of an independent crystalline silicon module. Following that, the LCOE of tandem modules is assessed and compared to that of crystalline silicon modules in order to determine the economic impact. According to the study, the perovskite layer in 4T tandem modules degrades at a greater rate than the perovskite layer in 2T tandem modules in order to maintain the same lifetime as independent crystalline silicon modules at the location. When perovskite layers in 2T and 4T degrade at optimal rate, they reach economic equilibrium at 5% and 10% additional module cost over crystalline silicon module.

ABBREVIATIONS AND SYMBOLS

STC:	Standard Test Conditions
IEC:	International electrotechnical commission
a-Si:	Amorphous silicon
CdTe:	Cadmium telluride
KGPV :	Köppe Geiger Photovoltaic
PET:	Polyethylene Terephthalate
PID :	Potential induced degradation
IC:	Inter-connection circuit
PLR:	Performance loss rates
PM:	Performance metrics
CSD:	Classical seasonal decomposition
STL:	Seasonal trend decomposition using loess
TMY:	Typical mean year
NPV:	Net present value
W_{peak}:	Rated MPP power
V_{oc} :	Open circuit voltage
R_{sh} :	Shunt resistance
FF:	Fill Factor
AC:	Alternating current
Y_f:	Final yield
a:	Slope
c:	Frequency factor
E_a:	Activation energy
K_p:	Photo-degradation rate
μ:	Shape factor
UV:	Ultra Violet radiation
k_i:	Total or per mechanism degradation rate
n:	Relative humidity impact factor
θ:	Temperature impact factor
T_{max}:	Module maximum temperature
C_N:	Cyclic rate
P(t):	Power at time t after degradation
R_d:	Degradation rate
I:	Irradiation zones
BK:	Desert very high radiation
DH:	Temperate high radiation
r:	Discount rate
d_t:	Power loss in year t
I_t:	Annual Investment
T:	Estimated operational duration
P_{STC}:	Power at STC conditions
Si:	Silicon layer
2T:	Two terminal tandem module
I_1:	Top layer short circuit current
I_2:	Bottom layer short circuit current
NP:	Normalized power
PTC:	PVUSA Test Conditions
LCOE:	Levelized cost of electricity
CIGS:	Copper indium gallium selenide solar
c-Si;	Crystalline silicon
PV:	Photovoltaic
EVA :	Ethyl vinyl acetate
IV:	Current - Voltage
TCO:	Transparent conductive oxide
CSI:	Clear sky index
LR:	Linear regression
HW:	Holt winter
GUI:	Graphical user interface
GHG:	Green house gases
I_{sc}:	Short circuit current
P_{max} :	Maximum power
R_s :	Series resistance
γ:	Temperature cefficient
DC:	Direct current
Y_{ref}:	Reference yield
b:	Y-intercept
RMSR:	Root mean squared error
k_h:	Hydrolysis degradation rate
k_{Tm}:	Thermo-mechanical degradation rate
τ:	Power susceptibility
RH:	Relative humidity
A:	Arrhenius constant
X:	UV impact factor
T_m:	Module mean temperature
T_{min}:	Module minimum temperature
A_N:	Normalized constant
P_0:	Ideal power without degradation
TP:	Temperature-precipitation zones
AH:	Tropical high radiation
CH:	Steppe high radiation
EM:	Cold medium radiation
E_t:	Energy generated at year t
I_0:	Initial investment
M_t:	Maintenance cost
BOS :	Balance of system
pvk:	Perovskite layer
pvk/si:	Perovskite silicon tandem module
4T:	Four terminal tandem module
V_1:	Top layer open circuit voltage
V_2:	Bottom layer open circuit voltage
x:	Additional manufacturing cost percentage

CONTENTS

List of Figures

List of Tables

1

INTRODUCTION

The status of renewable energy sources is given to pollution free energy resources such as the solar, wind, tidal and biomass used for electrical generation. Renewable energy sources have exploded in popularity in recent years, owing to the depletion of conventional fossil fuels and pollution. This advancement was made possible by the evolution of technology and the decisions made by policymakers [7]. Renewable energies have the primary advantage of abundant supply, sustainability, and zero emissions. Solar energy, which is converted to electricity using photovoltaic modules, is one of the most abundant renewable energy sources. Annual installation volume of photovoltaic technology has surpassed 100 GW [8]. Crystalline silicon is now the dominant technology in the PV market. Technical specifications defining these modules' operational features are validated in laboratories under STC circumstances. When these modules are put on-site, they are exposed to harsh and uncontrollable environmental conditions, which adversely affect the module's functionality. Thus, makers of photovoltaic modules claim a general lifetime of 25 years and a degradation rate of 0.8% per year when assessed under controlled settings. Due to the fact that environmental conditions differ globally, there is a need for a consistent process for determining the degradation and lifetime of modules based on their location.

Continuous cycles of environmental elements like as humidity, UV radiation, temperature, and soiling can have an influence on the module in both reversible and irreversible forms. Humidity, ultraviolet radiation, temperature, and cyclic temperatures are all considered irreversible degradation factors, but soiling is considered a reversible degradation factor. Irreversible degradation factors result in degradation modes such as delamination, corrosion, hot spots, and cell cracks, which significantly impair the modules' performance [9]. As a result, accurate performance forecasting with degradation is critical for both the manufacturer and the investor. At the moment, there are two approaches to resolving this issue: (1) simulating outdoor conditions in acceleration testing facilities in accordance with International electrotechnical commission (IEC) standards, and (2) using mathematical models to estimate module degradation rates [10]. Due to the inability of testing facilities to adequately simulate outdoor conditions, mathematical models are necessary. Mathematical models are developed in one of two ways: physically or data-driven. The physical method is represented by the degradation mechanisms involved, while the data-driven approach is represented by the long-term monitoring of performance data from the location. Data-driven models are site-specific and incorporate operational data, making them precise. A key difficulty is the lack of long-term performance data for all technologies in all the locations. A physics-based model is built for indoor acceleration test facilities, making them adaptable with any type of photovoltaic technology and different stress factors, with the problem being the model's accuracy due to the controlled environment of acceleration tests [11]. As a result, a hybrid model is required that incorporates both data-driven precision and physics-based compatibility. Recent research on hybrid models has resulted in the presentation of few models by Bala Subramaniyan [12] and Ismail Kaaya [5]. In this thesis, we integrate Ismail Kaaya's hybrid model into the PVMD toolbox and assess degradation under a variety of environmental conditions around the world.

The system's energy output decreases over time as degradation caused by various mechanism giving rise to different modes have an effect on the module's performance. Economic estimations made previous to installation would become unstable as a result of this occurrence. Therefore it is vital for the investor to incorporate degradation into the economic assessment. There are several economic measures that can be used for financial assessment, but the most commonly used statistic for comparing the costs and performance of renewable energy sources is the levelized cost of electricity (LCOE). It is computed by using the investment cost of the complete system and the amount of energy generated by the system over its lifetime [13]. The reliability of PV modules owing to degradation is a significant component in determining the levelized cost

of energy (LCOE) based on the energy production parameter. Climates such as hot and humid in tropical locations have demonstrated significant degradation, with PV products having a limited lifetime and not living up to the manufacturer's warranty. Investigating LCOE values and variation in such location can be pivotal. Because degraded modules must be replaced at the end of their useful life, applying a replacement factor can precisely compute the LCOE of the plant in the site. As a result, in our thesis, we incorporate financial analysis of LCOE into the PVMD toolbox, along with a degradation factor and a replacement parameter used to forecast the future cost of PV module that are to replace degraded modules.

In 2015, at the COP21 climate change summit in Paris, InstitutPhotovoltaqued'Ile-de-France (IPVF) set the 30/30/30 target of producing photovoltaic modules with energy conversion efficiencies greater than 30% for 0.30$ per W_{peak} by 2030 [14]. Crystalline silicon technology has achieved its zenith, achieving their theoretical maximum of 29%, necessitating the development of new technologies to push beyond these boundaries. Tandem modules are one such technology, in which different cells are placed one on top of the other to reach high efficiency that beyond the theoretical limits of crystallin silicon cells. Perovskite cells have the generic structure ABX3, with A representing an inorganic cation (often lead), B representing an organic cation (methylammonium), and X representing a halogen anion (halogen group elements). Due to their ability to react to a broad spectrum of wavelengths, flexibility, tunable bandgaps, and transparency, perovskite cells in combination with silicon cells have been a game-changing tandem structure [15]. Perhaps even perovskite suffers from the drawback of degrading in the presence of environmental stressors such as moisture. As a result, we develop a mathematical model to evaluate the degradation of perovskite silicon tandem modules into the PVMD toolbox in this work. Further explore the overall variation in performance of the power and energy generation in tandem module due to the different degradation rates of perovskite layer. To assess the costs and benefits of tandem modules, these predicted performance characteristics are compared to those of crystalline silicon modules.

1.1. THESIS OBJECTIVES:

The primary objective of this thesis is to analyze the yield of photovoltaic modules made of crystalline silicon and perovskite/silicon tandem modules subjected to degradation and to conduct financial analysis under a variety of climatic circumstances. As a result, the primary objective of the research is:

"Evaluate lifetime yield of crystalline silicon and perovskite/silicon tandem module along with financial analysis and implementation in PVMD Toolbox"

The following subgoals were established to aid in the achievement of the project's primary objective:

Objective 1: Implementation of degradation model for crystalline silicon modules and evaluation at various climatic conditions

Identification and incorporation of an appropriate degradation model for crystalline silicon modules into the PVMD toolbox as a new section named "DEGRADATION." The report's literature review section explains why the Kaaya hybrid model was chosen. For accuracy and precision, the model was evaluated using data from the reference article and from independent sources. Various locations throughout the world are used to imitate different climatic zones according to the KGPV classification. These locations are computed in order to investigate degradation and lifetime.

Objective 2: financial assessment modelling of LCOE included with degradation and replacement parameter

As a financial metric, the levelized cost of electricity (LCOE) is utilized. In the Toolbox, a section titled "LCOE" is established where the LCOE mathematical model is used in conjunction with the degradation parameter to calculate energy produced as a function of time and the replacement parameter is designed as a mathematical function to calculate the future cost of a PV module to replace degraded modules. Sensitivity analysis is carried out by altering the discount rate variable.

Objective 3: Application of degradation for perovskite/Si tandem module

This section discusses tandem perovskite/silicon cells. The pre-existing "ELECTRICAL" section of the PVMD toolbox has been upgraded to incorporate degradation into IV parameters in order to examine tandem module performance over time. The linear degradation of the perovskite layer is projected to occur in conjunction with the non-linear power loss of the silicon bottom cell as calculated using the Kaaya model. The results include an investigation of the normalized power, energy produced per year, total energy produced over a lifetime, and levelized cost of electricity (LCOE) as function of degradation rates of perovskite top layer for a perovskite/silicon tandem module.

1.2. OUTLINE OF THE PROJECT:

This report contains five chapters, as detailed below:

Each chapter is provided with respective introduction and conclusion

Chapter 2 provides details on various degradation model available, including physical and data-driven models, and their associated drawbacks. The final sub-section details the knowledge gaps and their solutions.

Chapter 3 explains the degradation model that was selected to address the knowledge gaps revealed in the previous chapter. It describes the model's implementation in the PVMD toolbox and the analysis of degradation in various climatic zones, thereby achieving the first objective.

Chapter 4 discusses the second objective in detail, specifically the significance of the LCOE. Application of the LCOE model to the PVMD toolbox with degradation and replacement parameters included.

Chapter 5 discusses the application of degradation into IV parameters to study the performance and behavior of perovskite/silicon tandem modules in response to changes in the degradation rate of the perovskite layer, as well as the LCOE calculation for tandem modules.

2

LITERATURE REVIEW

This chapter gives an overview of various core concepts related to the current topic along with available literature data. The section 2.1 discusses various degradation modes in photovoltaic modules, the section 2.2 discusses the stressors causing degradation, the section 2.3 discusses power degradation due to various degradation mechanisms and climates, the section 2.4 discusses the degradation rates of IV parameters specific to technology and climate, and the section 2.5 discusses methods for calculating degradation rates.

2.1. DEGRADATION MODES IN PV MODULES

The sections that follow provide an overview of various irreversible degradation modes.

2.1.1. DELAMINATION

When the adhesion between the various layers of the photovoltaic module, such as the glass, the encapsulant, the photovoltaic cell, and the back layer, is weakened, delamination of the layers occurs. Additionally, delamination results in the collection of contaminants, such as moisture, which causes corrosion[16].

2.1.2. BACK-SHEET ADHESION LOSS

It is similar to delamination; typically, the phrase 'delamination' refers to front side adhesion loss, whereas 'back-sheet adhesion loss' refers to rear side adhesion loss. The rear sheet shields electrical components from environmental damage. Generally, the back sheet is made of Polyethylene Terephthalate (PET) material, which is susceptible to delamination when exposed to UV light. There have been proposals to make the rear sheet of glass, but this may fail owing to breakage. This breakage is result of poor mounting, hail, wind-driven, or mechanical stressors. Cracks in the glass may allow current to pass through, resulting in an electric arc. If the delamination occurs in close proximity to the junction box, it could be dangerous. Because of moisture accumulation in these areas, eventually creating a straight channel to the ground[17].

2.1.3. EVA DISCOLORATION

Between the glass and the photovoltaic cells, an Ethyl Vinyl Acetate (EVA) layer is employed to protect the photovoltaic module from environmental degradation. When EVA is exposed to heat and UV radiation over an extended period of time, acetic acids can develop, resulting in discolouration. This degradation is responsible for the loss of short circuit current[18].

2.1.4. CELL CRACKS

PV cells are extremely fragile, which makes them susceptible to cell breaks. Numerous manufacturing procedures can result in cell cracks that are invisible to the naked eye. Minor cell cracks that are not visible to the human eye have a significant probability of developing into longer and broader cracks later causing large power loss[19].

2.1.5. SNAIL TRACKS

This mode of failure is characterized by the discoloration of silver paste on the front metal connectors of pho-

tovoltaic cells. Snail trails vary in intensity and speed according to environmental variables. They generally develop more rapidly in warmer settings. This failure is mainly dependent on EVA and back-sheet materials rather than the type of silver used[20].

2.1.6. POTENTIAL INDUCED DEGRADATION

Potential induced degradation (PID) occurs as a result of the potential difference between the module's cell and frame. PID degradation occurs in two distinct forms: (1) PID-p and (2) PID-s. PID-p degrades the passivation layer in a reversible manner. PID-s, on the other hand, is an irreversible degradation process triggered by sodium ion diffusion into the silicon lattice, creating a shunt channel. It is discovered that PID has a declining effect on fill factor, open circuit voltage, and short circuit current.[21].

2.1.7. DISCONNECTED CELL AND STRING INTERCONNECTION

Each cell in the photovoltaic module is connected to the next cell in a pattern from front to back. Frequently, these cell-to-cell connections have a weak point as a result of insufficient soldering during the production stage. These weak points are prone to fatigue failure as a result of temperature cycling or as a result of a hot spot created by partial shade, which causes mechanically weak kinks to break[22].

2.2. PHOTOVOLTAIC DEGRADATION BY STRESSORS

The major stressors that contribute to the degradation of photovoltaic modules include temperature, humidity, temperature cycling, dust, snow, and solar irradiation. Among these climatic challenges, we are particularly interested in mechanisms of irreversible degradation that result in permanent losses in the photovoltaic system. In this case, we include temperature, temperature cycling, humidity, and UV impacts as elements that contribute to permanent degradation. The other stressors, such as dust and snow, are excluded since their impacts can be minimized by scheduling periodic maintenance on the site. With time, the intensity of these climatic stresses on photovoltaic modules increases, resulting in a decrease in their performance. Accurate forecasting of PV module yield is critical for distribution and financial planning. As a result, modeling of these degradation rates becomes critical.

Degradation can occur at any level of the photovoltaic system, including the cell, module, array, and system. The following are some of the degradation modes that result in irreversible degradation: corrosion, fractured cells, and light-induced degradation at cell level; and delamination, connector breakage, glass breakage, discolouration, diode failures, moisture ingress, and hot-spots at the module level[23]. The figure 2.1 illustrates several climatic stresses that contribute to each degradation mechanism.

Degradation mechanism, corresponding stress factors and accelerated aging tests.

Degradation mechanism	Stress factor					Accelerated stress test
	High temperature	Moisture	Thermal cycling	UV	High voltage	
Broken interconnect	✓	✓			✓	Thermal cycle
Broken cell	✓				✓	
Solder bond failures	✓	✓	✓		✓	
Junction box failure	✓	✓				
Open circuits leading to Arcing	✓				✓	
Corrosion	✓	✓			✓	Damp heat exposure
Delamination of encapsulant	✓	✓	✓	✓	✓	
Encapsulant loss of adhesion and elasticity	✓	✓	✓		✓	Humidity freeze
Encapsulant discoloration	✓			✓		UV test
Hot spots	✓					Hot spot test
Shunts at the scribe lines	✓	✓				
Electrochemical corrosion of TCO	✓	✓			✓	Dry and wet insulation resistance
Ground fault		✓			✓	
Bypass diode failures	✓		✓			bypass diode thermal test

Figure 2.1: Degradation mechanisms with respect to stress factors.

2.2.1. EFFECT OF DEGRADATION MODES ON IV PARAMETERS

The I-V characteristic analysis has always been regarded as the most effective method for determining the influence of each type of degradation on the module's power output. The I-V parameters are as follows:

short circuit current, open-circuit voltage, fill factor, and maximum power point as shown in figure 2.2a. By defining the slope at each intercept, we can gain additional insight into the degradation process. The slope at the horizontal intercept(i.e. open circuit voltage) determines the circuit's series resistance, whereas the slope at the vertical intersection (i.e. short circuit current) defines the circuit's shunt resistance 2.2b. As series resistance increases as a result of corrosion and connect failures, the slope at the horizontal point increases (red curve in figure 2.2b), resulting in a decrease in fill factor. With more shunt routes available for current to bypass the active circuit, the shunt resistance decreases. As shunt resistance reduces, current leakage increases, as illustrated by the blue curve in the figure 2.2b [17].

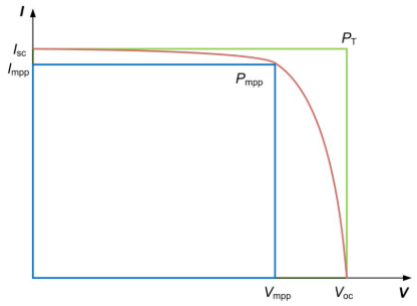

(a) IV parameters.

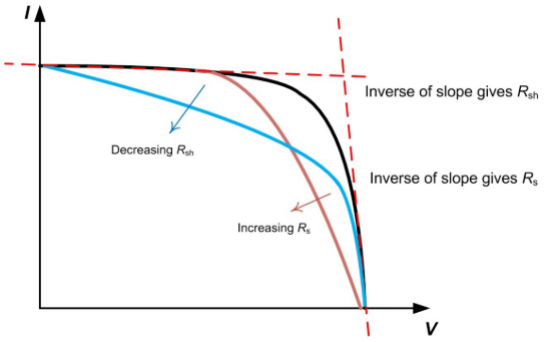

(b) Series and shunt resistance of IV parameters.

Figure 2.2: IV parameters and behaviours.

The modes of degradation for each IV parameter are listed below [17].

- Short- circuit current I_{sc} deviation is illustrated in case S1 in table 2.3. This is frequently due to a decrease in transparency induced by browning and delamination. These factors have an effect on the module's optical characteristics.
- Open circuit voltage V_{oc} deviation is illustrated in case S2 in the table 2.3. V_{oc} decreases as a result of bypass diode failure, short circuits, and cell connections failures. Additionally, it is influenced by potential induced degradation (PID) and light-induced degradation (LID)
- Series resistance R_s deviation is illustrated in case S3 in the table 2.3. The rise in series resistance can be attributed to an increase in interconnection resistance, loose joints, or corrosion.
- Shunt resistance R_{sh} deviation is illustrated in case S4 in table 2.3. Shunt resistance increases as the number of shunt channels in the photovoltaic cell grows. Cell mismatch or non-uniform yellowing may play a slight role in affecting the shunt resistance.

Failure	Safety	Power	P_{max}	S1: I_{sc}	S2: V_{oc}	S3: R_{oc}	S4: R_{sc}
							
Disconnected bypass diode	B	A					
Short-circuit bypass diode	B	E	x		x		
Inverted bypass diode	B	E	x		x		
Homogeneous loss of transparency	A	C	x	x			
Heterogeneous loss of transparency	A	E	x	x			x
Homogeneous glass corrosion	A	D	x	x			
Heterogeneous glass corrosion	A	D	x	x			x
Homogeneous delamination	B	D	x	x			
Heterogeneous delamination	B	D	x	x			x

(a)

Homogeneous corrosion AR coating of the cells	B	C	x	x			
Heterogeneous corrosion AR coating of the cells	B	C	x	x			
Passivation degradation	A	D	x		x		
PID polarization induced degradation	A	C	x		x		
LID light-induced degradation for crystalline solar cells	A	D	x	(X)	x		
Short-circuited cells, e.g. by cell interconnection ribbon	A	E	x		x		
Solder corrosion	A	C	x			x	
Homogeneous soldering disconnections	B	E	x			x	
Broken cell interconnect ribbons	B	E	x			x	
Cracked cells	A	E	x	x			

(b)

Figure 2.3: IV parameters effected due to various degradation processes.

2.3. PV DEGRADATION IMPACT ON POWER LOSS

This section describes the severity of each degradation's impact on power loss. The severity of power is determined by kuitche et al., as illustrated in figure 2.4a. The ranking is from 1 to 10, with 1 denoting the least impact on power and 10 denoting the most impact on power. The impact of degradation modes on power loss is depicted in figure 2.4b. The term 'Back sheet insulation compromise' refers to adhesion loss, cracking, peeling, and flaking, as well as weaker solder bonding caused by discolouration and thermal cycling. Additionally, hotspots and PID are thought to be significant drivers in power losses [24].

Severity	Rating
Major effect on power and safety	10
Major effect on power	8
Moderate effect on power	5
Slight deterioration of performance	3
No effect on performance	1

(a) Severity rank relative to power loss.

Mode	Severity
Encapsulant discoloration	3
Major delamination	5
Minor delamination	1
Backsheet insulation compromise	10
Backsheet other	1
Internal circuitry discoloration, series resistance increase	5
Internal circuitry failure, solder bond failure	8
Hot spots	10
Fractured cells	5
Diode/J-box problem	5
Glass breakage	5
Permanent soiling	2
Potential induced degradation	8
Frame deformation	3

(b) Degradation relative to severity ranking.

Figure 2.4: Degradation as function power loss ranking.

2.3.1. DEGRADATION MODES

Degradation modes can occur at various stages during the PV module's lifetime, as illustrated in figure 2.5. The degradation process that occurs over the lifespan of a photovoltaic module is classified into three stages: (1) Infant-failure (2) Failure in midlife; and (3) Wear-out failure. It is critical to note that we use the term failure rather than degradation, as DeGraff defined failure as the stage at which rated power falls to 80% of its initial value (which is degradation of 20%). Infant failures occur at the beginning of the photovoltaic mod-

ule's lifetime and are typically caused by manufacturing or transportation problems. It is mostly comprised of glass breakage, connector failure, loose frame failure, and delamination. The next stage is midlife failure, which occurs between 11 and 20 years into the module's working life. This stage of degradation is characterized by PID, diode failure, and cell interconnection breakage. The final stage is wear-out failure, which is characterized by cell cracks, delamination, and discolouration of the EVA [25].

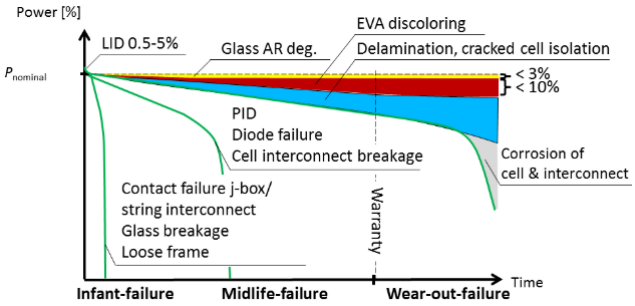

Figure 2.5: Degradation mechanisms with respect to time.

2.3.2. DEGRADATION MODES ON THE EXPOSURE TIME AND CLIMATE

The figure 2.6a illustrates the number of modules affected as a function of exposure time. It is divided into three categories: fewer than ten years, ten to twenty years, and more than twenty years. Color-coded degradation processes are established, and degradations with identical mechanisms are assigned the same color. Challenges such as delamination and backsheet insulation are highlighted in red. Green indicates hotspots and potential degradation. The number of impacted modules, weighted according to the severity rating stated above, is shown in figure 2.6b The fraction of modules weighted by severity and the total number of affected modules given by figure 2.6a and presented in figure 2.6c. In a moderate climate, the majority of modules exhibit encapsulant discolouration and delamination during the 11–20 year exposure period. Perhaps, when weighted against its severity, the intensity of encapsulant discoloration reduced relative to delamination and internal circuitry discoloration. When considering newer installations, they are significantly impacted by hotspots and PID degradations once severity is taken into account, as illustrated in figure 2.6b. Encapsulant discolouration, along with delamination, is the most typical mode of failure in hot and humid climates and older installations. Hotspot,internal circuitry discoloration and J-box degradation are more severe in newer systems. The majority of medium-aged installations are impacted by major delamination. In a desert climate, older installations exhibit discoloration of the encapsulant [24].

Using all available data, a Pareto chart (figure 2.7b) is created with two sections: (1) the last decade of data and (2) the remaining data. It is the sum of the number of modules affected by a degradation weighted by the severity of the degradation. As illustrated in figure 2.7a, We notice strong dominance of hot-spots, interconnection circuit (IC) discolouration, and PID throughout the last decade of data. We see domination by major delamination and hot-spots in the remaining data, despite the fact that encapsulant discolouration is more frequent but less extreme. In the thin-film module, considerable glass breakage, TCO discoloration, and hotspot formation are detected[24].

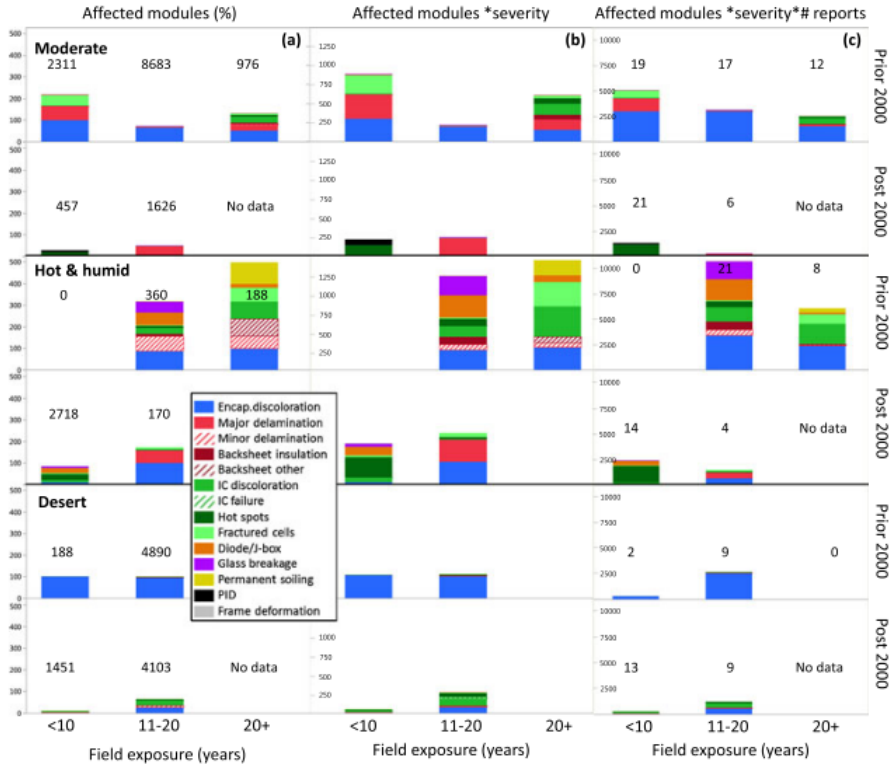

Figure 2.6: Degradation intensity as function of field exposure and climate.

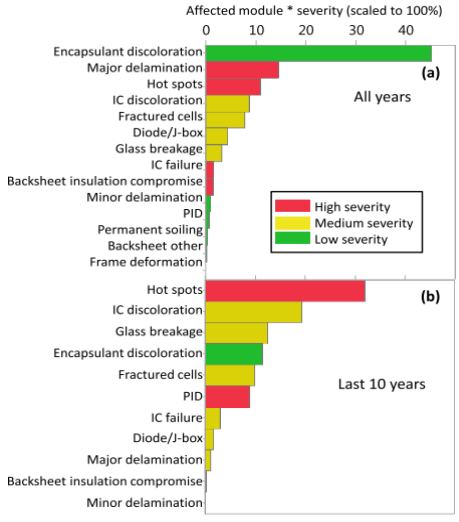

(a) Pareto chart of the most significant degradation modes for all years for crystalline silicon.

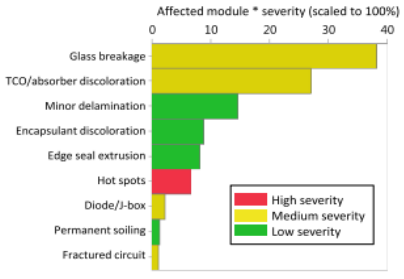

(b) Pareto chart of the most significant degradation modes for all years for Thin film modules.

Figure 2.7: Pareto chart for degradation modes

2.4. DEGRADATION RATES OF IV PARAMETERS

Depending on the climate, all of the aforementioned degradation mechanisms result in a reduction in power, short circuit current, and open circuit voltage. This section reviews the available literature on the effect of climate and technology on IV parameter loss.

2.4.1. IV PARAMETER DEGRADATION RATES IN GENERAL

D.C Jordan et al. have conducted an extensive amount of research on the topic at hand. The consistent pattern seen in mono and multicrystalline silicon is that the largest degradation occurred in Pmax and is approximately identical to the value of I_{sc}, followed by FF and finally V_{oc}. The majority of degradation occurred in I_{sc} as a result of EVA discolouration, broken cells, and delamination. The least degradation occurred in FF as a result of corrosion and solder fracture, which resulted in an increase in series resistance[24].
The most frequently observed degradation in all thin film technologies (a-Si, CIGS, and CdTe) is that FF degradations are greater than power degradation, which might be due to light-induced degradation in a-Si and series resistance increase in CIGS.

2.4.2. DEGRADATION RATES OF IV PARAMETERS WITH RESPECT TO CLIMATE

In many climatic zones, I_{sc} degradation is the most major influencing factor in power degradation for mono and multi silicon technologies. According to current research, the I_{sc} degradation rate is greater than the power degradation rate in the desert climate, as illustrated in figure 2.8a. Additionally, it is noted that the FF varies the most in polar climes compared to other climates. Probably as a result of snow accumulation damaging the front glass/cells or as a result of connector fracture at lower temperatures caused by EVA's brittleness.
For thin-film technologies, it is observed that FF has a greater variation and influence on power degradation in maritime and hot-humid zones than other factors, as illustrated in figure 2.8b.

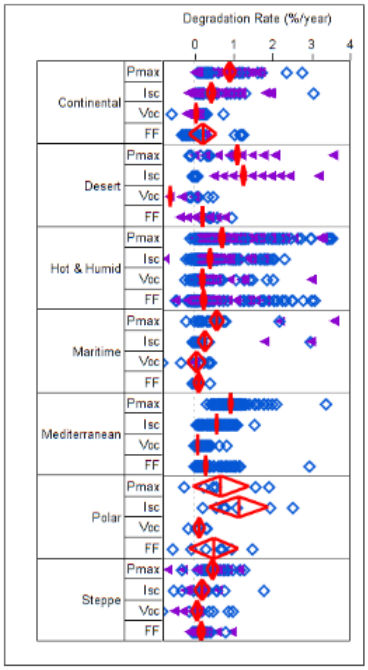

(a) Mono and multi silicon modules degradation rates with respect to climate.

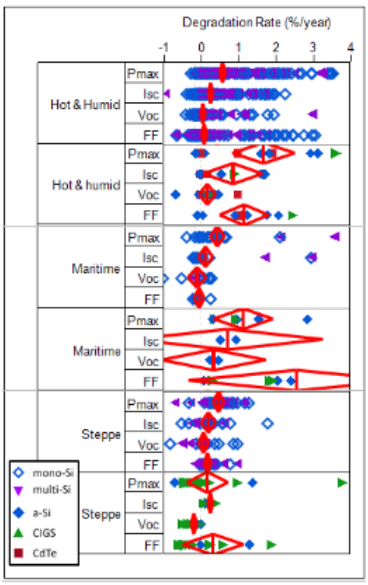

(b) Thin film modules degradation rates with respect to climate.

Figure 2.8: Degradation rates with respect to climate.

A correlation is drawn between the rate of power degradation and various IV parameters for mono and multi silicon technologies, as shown in figure 2.9. It is divided into two zones: one that was hot and humid and an-

other that is not. Perfect Correlation is depicted by a solid red line in the correlation graph since correlation is a linear property, whereas no correlation is represented by dashed lines. The figure 2.9a demonstrates that the majority of degradation data in hot-humid environments fall between the correlation and non-correlation lines. It usually often follows correlation lines in another climate. Referring to Figure 2.9b, a considerable fall in Voc is observed in a few cases in the hot-humid zone, most likely due to sub-string failure and the figure 2.9c reveals that FF degrades significantly in a hot-humid climate, most likely as a result of a rise in series resistance[26][27].

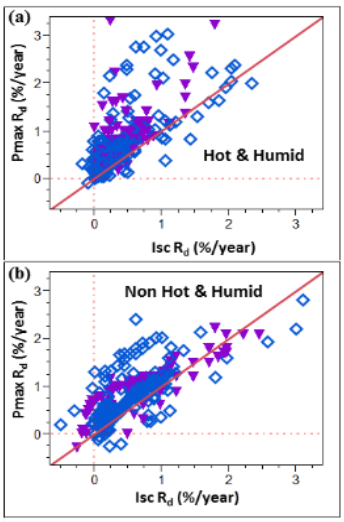

(a) Correlation between power and Isc degradation rates.

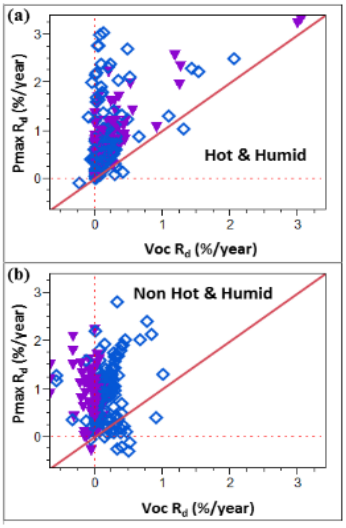

(b) Correlation between power and Voc degradation rates.

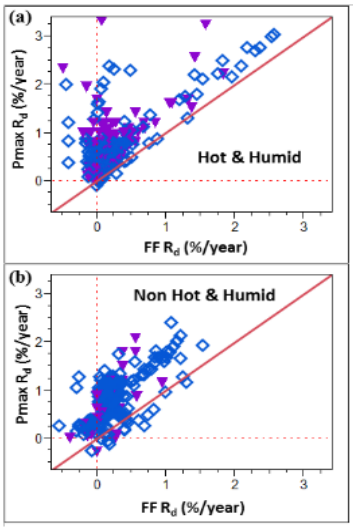

(c) Correlation between power and FF degradation rates.

Figure 2.9: Correlation between power and IV parameters.

2.4.3. OBSERVED DEGRADATION RATE'S

Many mono-silicon technologies degrade at less than 1% per year, while thin-film technologies degrade at more than 1% each year. In terms of performance, amorphous silicon technologies have the highest scattering. Multi-silicon technologies have consistently demonstrated lower degradation rates than mono-silicon technologies. After three years, CIGS technologies demonstrated a little improvement due to light soaking [28].

Mono Crystalline silicon Reis et al [29] discovered a degradation rate of 0.4% per year during their exami-

nation of a mono-silicon setup in Arcata, California, USA. According to Sakamoto and Oshiro, the average degradation rate for mono-silicon technologies is less than 0.5% per year, with high losses in FF and I_{sc} [30]. King et al [31] discovered a median degradation rate of 0.5% per year in mono technologies due to deterioration of solder connections. The majority of research indicates that modules in open circuit situations and with silicon encapsulant (as opposed to general EVA encapsulant) exhibit less degradation than modules linked to an inverter. Realini et al, observed a small degradation rate of 0.2% per year in southern Switzerland [32]. Saleh et al[33] reported that degradation in Libya's arid climates was roughly 1% each year.

Amorphous silicon Dhere et al [34] reported a degradation rate of 0.5% per year in the hot-humid climate of Florida, USA. Adelstein and Sekulic observed a 1% degradation per year in a triple junction roof configuration [35]. McNutt et al. observed a degradation rate of greater than 1% per year for twin junction configurations [36]. Apicella et al. reported a degradation rate of roughly 1% per year for single-junction configurations in Italy[37]. We observe that rates in amorphous silicon vary widely, from less than 1% to greater than 1%. Even though amorphous technologies degrade at a faster degradation than monocrystalline technology, they compensate by being less expensive than monocrystalline modules.

CIGS and CdTe Musikowski [38] states that there were no significant degradation rates in the CIGS module despite temperature and irradiation variations. Jordan et al. conducted a few observations in Colorado, USA [28] the observations revealed no substantial change after five years of life. Foster et al. measured a degradation rate of between 0% and 1% per year for the deployed system in Mexico's hot-humid climate [39].

2.5. DEGRADATION CALCULATIONS METHODOLOGIES

In general, two approaches are used to calculate the degradation rate of photovoltaic modules: a statistical method [driven by performance data] and an analytical method [driven by physics].

2.5.1. STATISTICAL METHOD

These are empirical models that are applied on the PV system's output data in order to calculate degradation rates. The primary objective is to analyse the data and then distinguish the trend from seasonal variations and noise. The slope of the trend is utilized to determine the performance loss rate(PLR). These models analyze performance loss rather than module degradation, as performance data includes impacts such as shade, soiling, module mismatch, and snow. Data is filtered and performance metrics are calculated prior to using statistical models. Filtering techniques are applied in accordance with the irradiance or standard deviation ranges. This is done to decrease sensor-generated outliers, noise, and other inhomogeneous data. After data filtering, performance metrics are applied to the filtered data, and then trend and PLR are determined [1].

2.5.2. DATA FILTERING

PV time series are filtered to remove the influence of outliers and other external variables. Different irradiance layoffs are used to reduce outliers. The first filter is 0 $W/m^2$to eliminate data with little or no light discrepancies. Following that, filters for low and high irradiance are applied. Finally, the data is subjected to clear sky filters such as the clear sky index (CSI) and the Reno 5C of the PV lib. The CSI approach is based on the ratio of measured irradiance to anticipated clear sky irradiance by weather models[40]. The 5C model employs a moving average of magnitude and stability across the sensor's lifetime and modeled irradiance data [41]. The following figure illustrates all of the filters that have been applied.

Filter	Power Threshold	Irradiance Threshold	Clear sky filter
0	$> 1\%$ Max P_{MP}	$G > 0W/m^2$	None
1	$> 1\%$ Max P_{MP}	$G > 200W/m^2$	None
2	$> 1\%$ Max P_{MP}	$G > 800W/m^2$	None
3	$> 1\%$ Max P_{MP}	$G > 200W/m^2$	RdTools CSI
4	$> 1\%$ Max P_{MP}	$G > 200W/m^2$	Reno 5C (PVlib)

Figure 2.10: Various filters applied to measured output data.

2.5.3. PV PERFORMANCE METRICS

Certain performance parameters are subjected to statistical modeling. Due to the overwhelming amount of output data, incorporating performance metrics(PM) simplifies the process. PM are applied on data over a certain time span. For instance, data from each day of a month is averaged to provide a single number for the month. There are three types of performance metrics: (1) evaluation of IV parameters; (2) empirical parameters such as PVUSA, the 6 K model, and Sandia models; and (3) normalized parameters such as the performance ratio[2].

IV PARAMETERS EVALUATION

All IV parameters are continuously recorded and performance degradation is reported. If there is a degradation in performance, the modules are evaluated in indoor testing facilities. Nonetheless, transporting PV modules from the field to the testing facility and back can be time consuming and may cause damage to the modules during transportation[2].

EMPIRICAL PARAMETERS

The objective is to use empirical coefficients and weather data to compute performance characteristics such as efficiency or maximum power. **6K model** calculates performance as a function of irradiance and module temperature using a relative efficiency metric associated to STC[42].

$$\eta(G,T) = 1 + k_1 * \ln(G) + k_2 * (\ln(G)^2) + k_3 * T + k_4 * T * \ln(G) + k_5 * T * (\ln(G)^2) + k_6 * (T^2) \tag{2.5.1}$$

equation 2.5.1 is fitted to the output data in order to derive the empirical coefficients k1–k6. Normalizing the irradiance and temperature by $G = G_{AOI}/G_{STC}$ and $T = T_{mod} - T_{stc}$. **PVUSA**, The power output is a function of the current and voltage. Current is believed to be a function of irradiance in PVUSA, but voltage is assumed to be a function of module temperature, which is a function of irradiance, wind speed, and ambient temperature[43][44].

$$P_{MPP} = G_{POA}[A + B(G_{POA}) + C(T_{am}) + D(U_w)] \tag{2.5.2}$$

The above equation is fitted to measured data in order to yield the coefficients A,B,C, and D. Following that, these coefficients are utilized to determine monthly ratings at PTC (Gptc = 1000 W/m^2, Tptc = 20°C, Uw= 1 m/s). It should be emphasized that this approach has been refined specifically for crystalline silicon. An extra coefficient E is utilized for thin films.

NORMALIZED METRICS

Due to the fact that this performance metric is a normalized value, it is extremely useful for comparing different photovoltaic technologies and climates. It is a no-unit metric that has been modified for outdoor conditions. The performance ratio (PR) is the most often used normalized performance metric. PR is calculated as the ratio of final yield (Y_f) and reference yield (Y_{ref}) as seen in equation 2.5.3. Depending on the application, either measured AC power or DC power output can be used [2]. Belluardoet al. offered a corrected formula. It is power corrected for irradiance and temperature at STC conditions, as shown in equation 2.5.4. γ is the temperature coefficient of the photovoltaic module [45].

$$PR = \frac{Y_f}{Y_{ref}} = \frac{P_{AC}/P_{STC}}{G_{POA}/G_{STC}} \tag{2.5.3}$$

$$PR_{T,G_{corr}} = P_{max}\frac{G_{STC}}{G}\frac{1}{1+\gamma(T_{mod} - T_{STC}} \tag{2.5.4}$$

COMPARISON BETWEEN PERFORMANCE METRICS

The 6k model has more seasonal variations, with winter being noisier than summer. The performance ratio model, called the XBX model, has a high degree of seasonality and possibly minimal noise. Even seasonality can be suppressed when high irradiance filters are employed, however utilizing high filters may diminish extrapolation data. The XBX and 6K models exhibit a nearly identical trend, with the XBX model exhibiting fewer outliers. The figure 2.11 illustrates the comparison of several models as a function of the applied filter and time [1].

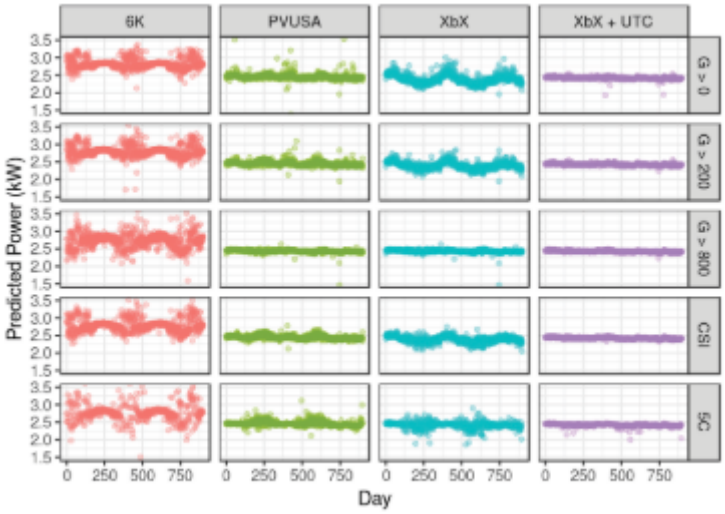

Figure 2.11: Various Performance metrics comparison[1].

2.5.4. STATISTICAL METHODS

The statistical approaches used to calculate performance loss have a significant effect. The purpose of statistical models is to analyze the slope of the trend curve (% per year) using a separate trend from the performance metric produced in the preceding section. Several statistical models include linear regression, traditional seasonal decomposition, holt-winter exponential smoothing, seasonal trend decomposition utilizing loess (STL), and auto-regressive integrated moving average (ARIMA).

LINEAR REGRESSION MODEL

Linear regression (LR) is a first-degree polynomial model in which the polynomial is fitted to the PR data after it has been filtered. In this equation, $\hat{y}$ is the fitted value, a is the slope of the trend, and b is the line's y-intercept. LR fits the data using ordinary least squares, which minimizes the sum of squared residuals. It is susceptible to outliers and seasonal volatility, and hence carries a high degree of uncertainty [46].

$$\hat{y} = at + b \tag{2.5.5}$$

CLASSICAL SEASONAL DECOMPOSITION

The classical seasonal decomposition (CSD) technique is distinguished by the fact that it employs a constant seasonal variation to mitigate the seasonality effect on fitting data. It derives the trend component and seasonal index of data using a centered moving average. CSD is applied using the equation 2.5.6, where $\hat{y}$ represents the fitted value, T_t represents the trend, S_t represents the seasonality, and e_t represents the residual components. It employs either an additive or multiplicative equation, depending on the seasonal component's stability [47].

$$\begin{aligned} \hat{y} &= T_t + S_t + e_t \\ \hat{y} &= T_t * S_t * e_t \end{aligned} \tag{2.5.6}$$

HOLT WINTER MODEL

The Holt Winter model (HW) is a triple exponential model that is used to smooth seasonal variance. It accounts for seasonal variance, as opposed to CSD, which is seasonal constant. The HW model employs the equation 2.5.7, where l_t denotes level, b_t denotes slope, and s_t denotes seasonal components [48].

$$\begin{aligned} \hat{y} &= l_t + b_t + s_t \\ l_t &= \alpha(y_t - s_t - m) + (1-\alpha)(l_{t-1} + b_{t-1}) \\ b_t &= \beta(l_t - l_{t-1}) + (1-\beta)b_{t-1} \\ s_t &= \gamma(y_t - l_{t-1} - b_{t-1}) + (1-\gamma)s_{t-m} \end{aligned} \tag{2.5.7}$$

SEASONAL TREND DECOMPOSITION USING LOESS

Seasonal trend decomposition with Loess (STL) is a robust approach that is used to decompose time series in a variety of ways. It smooths the data using locally weighted linear regression. A approximation of the smoothed data is made using neighboring points within the range. STL employs the equation 2.5.8 , here T_t is trend component, S_t is seasonal and R_t is residual components of time series[49].

$$\hat{y} = T_t + S_t + R_t \tag{2.5.8}$$

ARIMA

ARIMA is the most precise model of the ones discussed thus far. It takes into account outliers, seasonal volatility, level shifts, and errors, and so lacks any form of auto-correction. ARIMA employs the equation 2.5.9, here p,d,q denote the order, difference, and moving average of the autoregression, respectively. ARIMA defines P, D, and Q as seasonal auto regressive order, seasonal differencing order, and seasonal moving average, respectively [50].

$$\Phi(T)\phi_s(T^s)\nabla^d\nabla_S^D y_t = \theta(T)\theta_S(T^S)e_T \tag{2.5.9}$$

PERFORMANCE LOSS CALCULATION

Using the statistical model stated above, PR data is classified as trend, seasonality, and noise. PLR is calculated using the equation 2.5.10, here b denotes the y-intercept, a denotes the slope, and c is the frequency factor (if the data is in intervals of months over an year - it is 12).

$$PLR = c * \frac{a}{b} * 100\% \tag{2.5.10}$$

The root mean squared error is used to quantify the disparity between fitted and measured data.

$$RMSE = \sqrt{\frac{1}{N}\sum_{1}^{N}(x - \hat{x})^2} \tag{2.5.11}$$

COMPARISON AND FLOW CHART OF STATISTICAL MODEL

The comparison of all statistical models is shown in the figure 2.12. It should be remembered that SLR cannot provide precise measurements. CSD is calculated using a moving average that excludes the earliest and last few months of data. While STL and ARIMA produce the greatest results, one must keep in mind that ARIMA is a computationally costly model[2].
The flow chart figure 2.13 depicts the complete process of statistical method development, from data collection to filtering, performance indicator development, and statistical model development [3].

Characteristic	SLR	CSD	HW	ARIMA	STL
Different technologies	PLR with highest uncertainty	Not well suited	Not that well suited	PLR with high accuracy	PLR with high accuracy
Filtering, outlier handling	Crucial, outlier have big impact	Crucial, outlier have big impact	Robust through weighted average	Robust through models flexibility	Robust through locally weighted regression
Time period	Longer time-series better suited	Removing of first & last observations	Shorter time series can be evaluated	Shorter time series can be evaluated	shorter time series can be evaluated
Seasonality	Sensitive to seasonality	Sensitive to seasonality	Insensitive to seasonality	Insensitive to seasonality	Insensitive to seasonality
Stationarity of time-series	Not necessary	Not necessary	Not necessary	Stationarity necessary	Not necessary

Figure 2.12: Summary of different statistical models [2].

2.5.5. OVERVIEW OF STATISTICAL MODELS

For the long term, statistical models can accurately estimate performance losses (which encompass losses in the entire system, such as inverter failures, shadowing, and mismatches). These models filter daily data

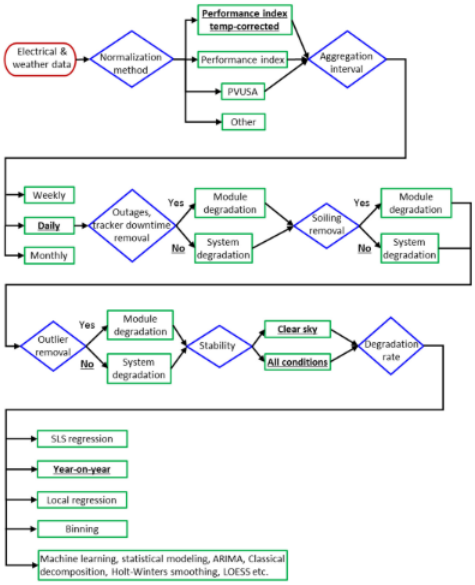

Figure 2.13: Overview of Statistical data driven method [3].

and then interpolate monthly values using performance measures. In PM measurements, the trend is distinguished from seasonality and noise; the slope of the trend curve represents the degradation rate. Perhaps statistical models demand a minimum of 3-4 years of measured data for each technology, and the results should be site-specific.

2.5.6. ANALYTICAL MODELS

These models are generated through an understanding of the physical and chemical degradation processes. Developed primarily to aid in the comprehension of experimental data pertaining to various degradation processes. Fitting the model to the experimental observation yields the unknown parameters. Following the derivation of unknown parameters, the model is applied to the appropriate weather conditions in order to forecast degradation. These models can be used to forecast IV parameters such as P_{max}, I_{sc}, R_{sh} and R_s. There are two types of analytical models: (1) degradation indicator models and (2) degradation rate models. Models of degradation indicator discuss the degree of degradation in an indication such as power and current etc. Models of degradation rate examine the rate of degradation of a specific indication [51].

CORROSION DEGRADATION MODELS

Corrosion weakens the metallic connections between the cells, resulting in a decrease in the adhesive strength between the cell and the frame. This impact raises the module's series resistance and results in leakage current. Corrosion occurs in climates with high temperatures and humidity. High temperatures cause the backsheet or EVA to delaminate, allowing moisture to enter the module. This moisture combines with EVA to generate acetic acid, which causes corrosion [52][53]. Power and resistance are used as degradation indicators, and the following models are presented to fit the observed degradation pattern.

(1) Pan Model [54]:

$$\frac{P_{max}}{P_0} = e^{-R_D t^{\beta}} \tag{2.5.12}$$

(2)Braisaz Model [55]:

$$P_{max} = \frac{1 + e^{-B}}{1 + e^{R_D t - B}} \tag{2.5.13}$$

$$R_s = R_0 + e^{R_D t - B} \tag{2.5.14}$$

P_{max} represents the output power at the highest power point, Rs represents the series resistance at time t, P_0 represents the initial power output at time zero, and R_0 represents the initial series resistance at time zero. β denotes the experimental parameter, B is the coefficient to be defined, and R_D denotes the degradation rate in percent per hour.
It is noted that the precision of fitting is dependent on the degradation pattern. Few degradation patterns fit well described by the pan model 2.5.12, while others by the Braisaz model 2.5.13. It is critical to remember that a flawlessly fitting model for historical data does not imply faultless forecasting, and these models are ineffective for calculating long-term degradation.

The degradation rates utilized in the aforementioned models (equation 2.5.13 and 2.5.12) can be computed using 3 degradation rate models which are a function of temperature and relative humidity. (1) the Pecks model; (2) the Eyring model; and (3) the Exponential model [56] [57]. These are predicated on the premise that the degradation rate is proportional to the module's water content and that the rate constant has an Arrhenius temperature dependence.

(1) Pecks model

$$R_{D.Peck} = Ae^{\frac{-E_a}{K_\beta T}} RH^n \tag{2.5.15}$$

(2) Eyring Model

$$R_{D.Eyring} = Ae^{\frac{-E_a}{K_\beta T} - \frac{b}{RH}} \tag{2.5.16}$$

(3) Exponential Model

$$R_{D.Exp} = Ae^{\frac{-E_a}{K_\beta T}} e^{m*RH} \tag{2.5.17}$$

As the exponential model expresses relative humidity in exponential terms, it is found to be more sensitive to relative humidity than other models. This sensitivity to relative humidity in addition to temperature may result in inaccurate estimates. Pecks model exhibits consistent sensitivity to both temperature and relative humidity.
A,n,b, and m are referred to as model parameters in each of the preceding models. The model parameters (A,n,b,m) and activation energy (Ea), are determined by fitting the equations 2.5.15, 2.5.16 and 2.5.17 to observable experimental data. These can also be given on a logarithmic scale as the following equation to aid with fitting comprehension. The data is plotted as $\ln R_D$ versus $1/T$, with the slope equal to E_a/K_β and intercept is $\ln A$

$$\ln R_{D.Peck} = \ln A - \ln \frac{-E_a}{K_\beta T} + n \ln RH \tag{2.5.18}$$

$$\ln R_{D.Eyring} = \ln A + (\frac{-E_a}{K_\beta T} - \frac{b}{RH}) \tag{2.5.19}$$

$$\ln R_{D.Exp} = \ln A - \ln (\frac{-E_a}{K_\beta T}) + (m * RH) \tag{2.5.20}$$

POTENTIAL INDUCED DEGRADATION MODELS

PID is formed as a result of a potential difference between structure of the module and cell. As previously stated, there are two types of PID degradation: PID-P and PID-S. PID-p is a temporary and reversible degradation, whereas PID-s is a permanent degradation [58]. PID-s occurs as a result of sodium ion diffusion into the silicon lattice, resulting in current leakage due to shunting. Sodium ion diffusion has the greatest effect on the cell's fill factor, followed by open circuit voltage and finally short circuit current. PID can be triggered by elevated temperatures, relative humidity, system voltage, or injected carriers [59]. The following are several models for predicting PID degradation.

(1) PID-HACKE model [60]

$$\frac{P_{max}}{P_0} = 1 - Ae^{\frac{-E_a}{K_\beta T}} RH^n t^2 \tag{2.5.21}$$

This model is frequently used to describe the initial phase of degradation dominated by PID-s because it fits the initial phase of the PID sigmoid better than the stabilization phase. It is a parabolic model that fits the

power degradation of c-si modules, as documented in report [60]. By fitting the equation to experimental data, the A and n model parameters are determined. Parameters must be customized for each module technology.

(2) PID - Annigoni model [61] :

$$\frac{P_{max}}{P_0} = 1 - Ae^{\frac{-E_a}{K_\beta T}} RH^n t^2 U \tag{2.5.22}$$

It is a modified version of the PIDHACKE model (equation 2.5.21) that includes voltage (U). As with the prior model, parameters are established through fitting to experimental data and then used to predict degradation for needed climatic stress values.

(3) PID-Hattendorf model [62]:

$$\begin{aligned} P_{max}(U,T,RH,t) &= P_0(1-P(t)) \\ P(t) &= P_\infty \frac{1-e^{\frac{t}{\tau_1}}}{1-e^{\frac{t-t_0}{\tau_2}}} \end{aligned} \tag{2.5.23}$$

It is based on experimental data gathered by varying the humidity, voltage, and temperature and then deriving a matrix from them. The model parameters are determined by fitting the power degradation model to experimental data using a variable voltage U and a constant RH-T.

(4) PID-Taubitz model [63] :
Shunting phase

$$R_{sh}(t) = a_S e^{\frac{-t}{b_S(t)}} \tag{2.5.24}$$

Regeneration phase

$$R_{sh}(t) = C_R + a_R e^{\frac{t}{b_R(t)}} \tag{2.5.25}$$

Transition phase

$$R_{sh}(t) = a_T(T)(t + b_T(T))^2 + C_T \tag{2.5.26}$$

Taubitz model is primarily concerned with calculating the shunt resistance created in the module as a result of PID. As illustrated above, shunt resistance is divided into three phases. Fitting for each module type determines $a_S, b_S, C_T, b_T, a_T(T), b_S(T), b_T(T), C_R$ and a_R.

(5) PID-Braisaz model [55]:

$$R_{sh}(t) = \frac{R_s h(0)}{1 + aR_D t} \tag{2.5.27}$$

$$R_D = AU \frac{B}{1 + e^{-C(RH)+D}} e^{\frac{-E_a}{K_\beta T}} \tag{2.5.28}$$

Shunt resistance is described in this model as a function of voltage, relative humidity, and temperature. A,B,C, and D are model parameters, U is the applied voltage, and R_D is the degradation rate as a function of RH,T, and U.

UV DEGRADATION

Continuous UV irradiation results in discolouration and delamination of the encapsulant [64][65]. These kinds of degradation result in a decrease in short circuit current. UV degradation is shown to follow an exponential rather than a linear trend.

(1) UV - Braisaz model [55]:

$$I_{sc}(t) = I_{sc(o)} - aD_{UV}(t) - b(1 - e^{-CD_{UV}(t)}) \tag{2.5.29}$$

$$D_{UV}(t) = \int_0^t E(u) \times 5.5\% du \tag{2.5.30}$$

D_{UV} is UV dose measured in MJ/m^2 or kWh/m^2.The model parameters are a,b, and C. 5.5% is the proportion of the ultraviolet spectrum (280nm - 400nm) in the entire light spectrum E(u), according to article [66].

DELAMINATION, SOLDER FAILURE AND CELL CRACKS DEGRADATION

(1) Coffin-masons equation [56]:

$$N = \frac{\sigma}{(\delta T)_1^{\beta}} \tag{2.5.31}$$

Delamination, solder failure, and cell cracking are all caused by temperature cycling. This model quantifies the number of cycles required to reach failure. δT denotes the temperature range, whereas σ and β denote the material and test setup parameters. This model is adjusted to add cycling rate, which is defined in the following equation. where freq denotes the frequency of cycling and E_a denotes the activation energy.

$$N = \frac{\sigma}{(\delta T)_1^{\beta}} \frac{1}{freq_2^{\beta}} e^{\frac{E_a * 11605}{T_{max}(K)}} \tag{2.5.32}$$

(2) Crack propagation model [55]

$$C_a(t) = C_a(t-1) + \frac{1}{x(\frac{125}{T_a})^m} \tag{2.5.33}$$

This model determines the activation of cracks at time (t) and is used to simulate the degradation of short circuit current caused by cell crack expansion. m is the model parameter, while x denotes the number of heat cycles.

(3) Damage accumulation model [67]

$$D = C(\delta T)^n (r(T))^m e^{\frac{-Q}{K_\beta T_{max}}} \tag{2.5.34}$$

This model is used to determine the extent of solder fatigue. C is the scaling constant, Q is the activation energy, r(T) is the number of times that temperature increases or decreases across the reversal temperature, T is the period of year, and n and m are the model parameters identical to those in the coffin-mason equation.
(4) Backsheet degradation model

$$R_D = I^X (b + mTOW)(T_f)^{\frac{T-T_0}{10}} \tag{2.5.35}$$

It is used to calculate the degradation of backsheets. I denotes the intensity of light, X, b, and m denote model parameters, TOW denotes time of wetness, and T_f denotes a multiplier for the increase in degradation with each 10°increase in temperature [68].

COMBINED DEGRADATION MODEL

Some authors have proposed models that take all climatic stresses into account when determining the degradation rate.

(1) Gaines model

$$\frac{P_{max}}{P_{max(0)}} = [1 - R_D t]^{\frac{1}{\beta}} R_D = A f_T f_R H f_M f_G f \tag{2.5.36}$$

Gaines suggested this model for estimating power degradation while accounting for all climatic conditions. where $f_t, f_{RH}, f_M f_G f$ are temperature, relative humidity, mechanical stress, gaseous concentration, and excursion frequency influences. The article discusses the mathematical formulas for each stress element [69].

(2) Subramaniyan model [70]

$$Rate(T, \delta T, UV, RH) = \beta_0 e^{\frac{-\beta_1}{k_\beta T_{max}}} (\delta T_{daily})^{\beta_2} (UV_{daily})^{\beta_3} (RH_{daily})^{\beta_4} \tag{2.5.37}$$

Bala Subramaniyan suggested another model for estimating degradation rates that takes into account all environmental stresses. where T_{max} denotes the daily maximum module temperature, δT denotes the daily module temperature range, UV_{daily} denotes the daily average irradiance, and RH_{daily} denotes the daily average relative humidity. All β factors are estimated using fitted data.

OVERVIEW OF ANALYTICAL MODELS

Along with IV parameters, an analytical model can be employed to determine degradation owing to a certain degradation mechanism. Indoor experimental data are utilized to determine module characteristics, which are then used to determine degradation under specified climatic conditions. Nonetheless, analytical models are accurate for short-term forecasting(1-1.5 year), and the majority of models developed for crystalline technology are accurate. As a result, we require a model that can be used for long-term prediction while also being compatible with a variety of technologies.

2.5.7. FUTURE GOALS(KNOWLEDGE GAPS)

Following an extensive examination of the literature, the following knowledge gaps are identified:

- While statistical models are accurate for long-term forecasting, they provide information on performance losses (such as shading, module mismatch, and so on) rather than degradation owing to environmental stress factors. Nevertheless, we are focused on models that describe degradation rate under any environmental condition than in models that represent performance loss at a specific site.
- For investigation of specific module degradation, statistical models require at least 3-4 years of collected data. This is not flexible enough for investigation because they require performance data for each site to be evaluated. We are particularly interested in models that require little or no data.
- Analytical models are accurate for short-term forecasting of degradation caused by climatic stress factors but are insufficient for long-term forecasting. We require physical models capable of accurate long-term forecasting.
- Analytical models are fitted models that are dependent on the degradation pattern. These models can be modified to adapt to different technologies and degradation modes. As a result, we are interested in models that are flexible to a variety of technologies and degradation modes.
- **Hybrid models** combining analytical and statistical models are investigated. These hybrid models have the potential to increase accuracy for long-term forecasting and are compatible with a number of technologies. They accommodate for non-linear evaluation of power loss due to the variety of degradation mechanisms produced by environmental conditions based on the technology and design.

3

DEGRADATION MODEL

The purpose of this work is to identify the computational approach for estimating photovoltaic module degradation under a variety of environmental circumstances and to incorporate it into the PVMD toolbox. We selected to address the gaps in knowledge identified throughout the literature research by implementing Ismail Kaaya's hybrid outdoor degradation model (referred to as Kaaya model). This model considers the nonlinear behavior of technology or design, the material evolution of solar modules, the accuracy of long-term forecasting, and the possibility of location-independent evaluation. Additionally, we investigate the effect of various environmental conditions on crystalline silicon module degradation.

3.1. METHODOLOGY

In this chapter, we will examine the properties of the Kaaya model. In Section 3.1.1, we provide the environmental parameters that were taken into account when creating the model. In Section 3.1.2, we explain the model's features.

3.1.1. ENVIRONMENTAL FACTORS

Numerous environmental factors have an effect on the performance of a photovoltaic module in outdoor operation. Several environmental stressors are identified as crucial for the primary degradation modes defined in the preceding chapter 2.2. Temperature, relative humidity, UV radiation, and cyclic temperature all contribute to the irreversible degradation of photovoltaic modules. It is crucial to keep in mind that reversible degradation mechanisms caused by stress factors such as dust or snow are not included. As dust or snow degradation can be avoided through routine module operational maintenance.

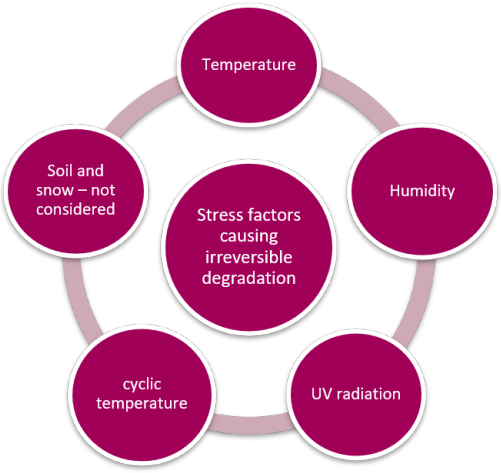

Figure 3.1: Environmental stress factors.

3.1.2. MODEL ASPECTS AND ASSUMPTIONS

To account for all potential factors, a lengthy and complex simulation may be required. As a result, a few simplifying assumptions are made [4].

- The degradation model for each process is considered to be an Arrhenius dependent equation. The activation energy (E_a) contained in the Arrhenius equations can be used to characterize the material dependence.
- Three degradation mechanisms are regarded to be the most prevalent: hydrolysis, photodegradation, and thermomechanical degradation.
- All model constants are regarded to be same regardless of their location. These constants remain same unless the module's technology or design changes.

As stated below, certain aspects are taken into account. [4].

- Material impact: Due to the frequent updates to the materials used in photovoltaic modules, the material impact parameter is considered while calculating degradation and measuring power loss via activation energy (E_a) and power susceptibility.
- Location conditions: Because photovoltaic modules are used in a wide variety of environmental conditions found throughout the world. The settings are intended to take location-specific stressors into account.
- PV technologies: Due to the fact that photovoltaic modules are classified according to their design (glass-glass or glass-back sheet) and technology (crystalline silicon or thin-film etc). Shape factor (μ) is used to account for these characteristics.

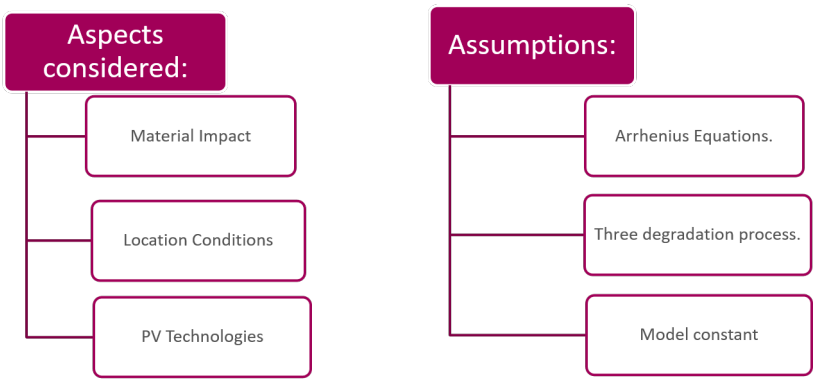

Figure 3.2: Aspects and Assumption of Kaaya model.

3.2. MATHEMATICAL MODELS

The mathematical model for each mechanism is determined by the combination of climatic stress elements. These combinations were chosen because they correspond to separate modes, as demonstrated in figure 3.3, and because controlled testing facilities are easily available in acceleration test laboratories. To begin, we use indoor testing facilities to determine the impact constants (X,n, and $theta$) in rate equations. The model is then calibrated and applied to outdoor conditions to generate the outdoor parameters (τ and μ).

3.2.1. DEGRADATION MECHANISM MODEL:

The following equations are used to determine the degradation for three major mechanisms: hydrolysis, photo-degradation, and thermo-mechanical degradation [4].

$$k_h = A_h * Rh_{eff}^n * exp(\frac{-E_{ah}}{k_B * T_m}) \tag{3.2.1}$$

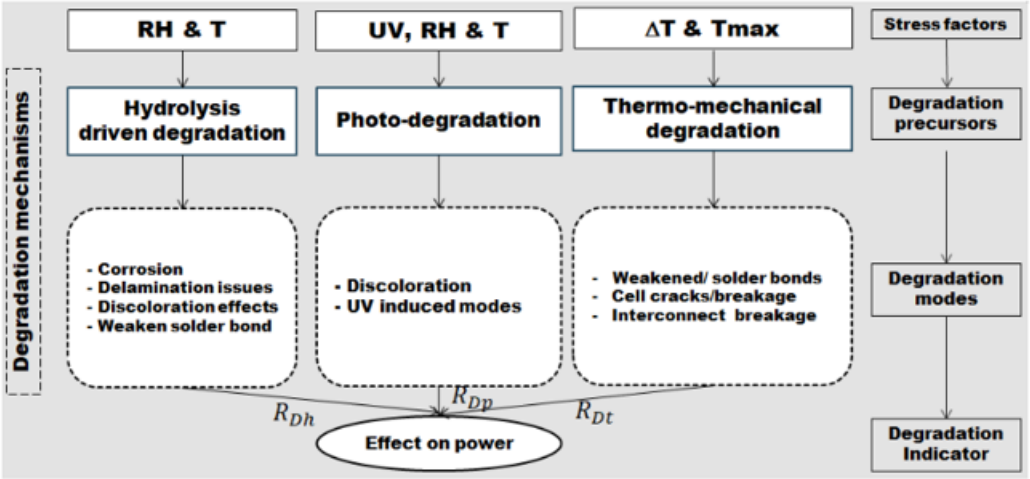

Figure 3.3: Characteristics of Mathematical model [4].

$$Rh_{eff}(\%) = \frac{100}{1+98*exp(-9.4*\frac{RH}{100})} \tag{3.2.2}$$

$$k_p = A_p * UV^X * (1+(Rh_{eff}^n)) * exp(\frac{-E_{ap}}{k_B * T_m}) \tag{3.2.3}$$

$$k_{Tm} = A_t * C_N * (273+\Delta T)^\theta * exp(\frac{-E_{at}}{k_B * T_{max}}) \tag{3.2.4}$$

Stress parameters such as module mean temperature and relative humidity (RH) are taken into account in the hydrolysis model expressed by the equation 3.2.1. UV and relative humidity are taken into account in the photodegradation process (RH is included again since its interaction with UV results in degradation that is not accounted for in the hydrolysis mechanism), as defined in equation 3.2.3. The thermomechanical degradation mechanism given by the equation 3.2.4 takes cyclic temperatures into consideration.

Here, k_h denotes the annual rate of hydrolysis degradation, k_p denotes the annual rate of photo degradation, and k_{Tm} denotes the annual rate of thermomechanical degradation. Arrhenius constants are defined as A_h $[year^{-1}]$, A_p $[m^2/kWh]$ and A_t $[°C^{-1}/cycle]$ constants. E_{ah},E_{ap} and E_{at} denote the activation energies of the corresponding mechanisms. The Boltzmann constant is denoted by k_B. n,X, and θ are impact factors that reflect the influence of effective relative humidity [%], UV dosage $[kWh/m^2 - year]$, and module temperature ((T_m)[K]) on the module(these impact parameters are determined by indoor experimental data). $\Delta T = T_{max} - T_{min}$[K] is the difference in temperature between the location's maximum and minimum temperatures, C_N[cycles/year] is the cycling rate, T_{max} is the module's greatest temperature in [K], and T_{min} is the module's lowest temperature in [K]. The table 3.1 holds the impact and module parameters' values.

Table 3.1: Impact and model parameter values

Parameters	A_h	A_p	A_t	E_{ah}	E_{ap}	E_{at}	n	X	θ	C_N	A_N
Values	4.91e7	71.8	2.04	0.74	0.45	0.43	1.9	0.63	2.24	1	1

The total degradation rate for a module is calculated using following equation 3.2.5

$$k_T = A_N * \prod_{i=1}^{n} (1 + k_i) - 1 \tag{3.2.5}$$

where k_T is total degradation, A_N is normalization constant , n is number of degradation processes(3 processes) and k_i is the degradation rate per mechanism.

3.2.2. STRESS FACTOR MODELING

The stressors indicated in the equations 3.2.1, 3.2.3 and 3.2.4 are modeled using site-specific meteorological data.

Module temperature: The temperature of the module is determined using a fluid dynamic model that incorporates conduction heat transfer to the environment, convection heat transfer due to ambient temperature, radiation heat transfer from the module's back, and front, as specified in equation 3.2.6 [71].

$$mc\frac{dT_M}{dT} = \alpha G_M - h_c(T_M - t_a) - \epsilon_{back}\sigma(T_M^4 - T_{gr}^4) - \epsilon_{top}\sigma(T_M^4 - T_{sky}^4) \tag{3.2.6}$$

We shall investigate the steady state condition of the fluid dynamic model in this thesis project. As a result, using steady state assumptions, equation 3.2.6 can be rearranged as equation 3.2.8. α represents the module's absorptivity, T_a represents ambient temperature, T_{gr} represents ground temperature, T_{sky} represents sky temperature, h_c represents convection thermal coefficient, and $h_{r,gr}$ and $h_{r,sky}$ represent radiative rearranged terms for sky and ground. G_M denotes the irradiation plane of the array, which is determined using the sky map, sensitivity map, and solid angle indicated in the equation 3.2.7 [72].

$$G_M = \int_{sky} (skymap)(sensitivitymap)d\Omega \tag{3.2.7}$$

$$T_M = \frac{\alpha G_M + h_c T_a + h_{r,gr} T_{gr} + h_{r,sky} T_{sky}}{h_c + h_{r,gr} T_{gr} + h_{r,sky}} \tag{3.2.8}$$

Ultraviolet irradiation UV irradiation acquired through measurement generally encompasses UV radiation between 280nm and 420nm. However, the stated model accounts for UV light between the wavelengths of 280nm and 400nm; thus, the mathematical model is employed to describe UV irradiation. The wald model is used to simulate ultraviolet radiation as shown in equation 3.2.9 [73].

$$\begin{aligned} c_{teff} &= max(0.1, min(c_t, 0.7)) \\ UV_A &= (7.210 - 2.365 * c_{teff}) * 0.001 * E_{POA} \\ UV_B &= (1.897 - 0.860 * c_{teff} * 0.01 * E_{POA} \\ UV_{total} &= UV_A + UV_B \end{aligned} \tag{3.2.9}$$

Relative humidity As shown in equation 3.2.10, relative humidity is computed using ambient temperature and dew point temperature via water vapour pressure. Buck model is used to estimate the WVP [74] as presented in equation 3.2.11.

$$RH[\%] = \frac{WVP(T_{dew})}{WVP(T_{amb})}.100 \tag{3.2.10}$$

$$\begin{aligned} WVP(T < 0) &= 0.61115.exp((23.036 - (T)/333.70).((T)/(279.82 + (T))) \\ WVP(T >= 0) &= 0.61121.exp((18.678 - (T)/234.84).((T)/(257.14 + (T))) \end{aligned} \tag{3.2.11}$$

3.2.3. NON-LINEAR NORMALIZED POWER

Manufacturers of photovoltaic modules use power as a generic criterion to establish a guarantee. The power loss curve might be linear, exponential, or step in shape. As a result, dealing with non-linearity is critical for calculating power loss. To calculate power loss, a simple non-linear model is presented in the form of equation 3.2.12. P(t) signifies the output of the module at time t, including degradation, and P_0 denotes the ideal module's output. k_i signifies either the total degradation rate or the degradation rate by mechanism.

τ denotes power susceptibility, which is considered a material property. It is used to describe a performance enhancement caused by material changes to a solar module. τ streamlines the process of computing module parameters for each module using new material. μ is a form factor that takes nonlinearity into consideration; it is a factor that is design and technology dependent. Module design, such as glass-glass constructions, results in fewer moisture routes, which results in increased degradation throughout the product's later stages of life. As a result of this, μ can be utilized to optimize the patterns of the degradation's as shown in figure 3.4.

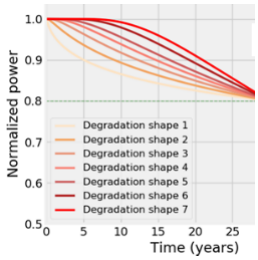

Figure 3.4: Shape factor μ variations [5].

The methodology is illustrated in figure 3.5, from the first data collection to the final computation of power loss. The process is divided into five parts, as illustrated on the left of the flowchart: data processing, input processing, degradation rate per mechanism processing, overall degradation rate processing, and power loss and levelized cost of electricity (LCOE) processing. The data processing step takes meteorological data and initializes all essential parameters using meteonorm software. The input processing step generates all of the variables necessary for degradation analysis, including irradiation, relative humidity, UV radiation, module temperature, and impact constants. The degradation rate per mechanism approach gives degradation rates for hydrolysis, photo, and thermomechanical degradation depending on the prior process's data. The total degradation rate procedure adds the degradation rates of each mechanism together to get a single overall degradation rate. Annual normalized power estimates are generated by the power degradation process utilizing the overall degradation rate, shape factor, and power susceptibility factor; these data can then be used to calculate the LCOE and failure lifetime.

$$\frac{P(t)}{P_0} = 1 - exp(-(\frac{\tau}{k_i * t})^{\mu}) \tag{3.2.12}$$

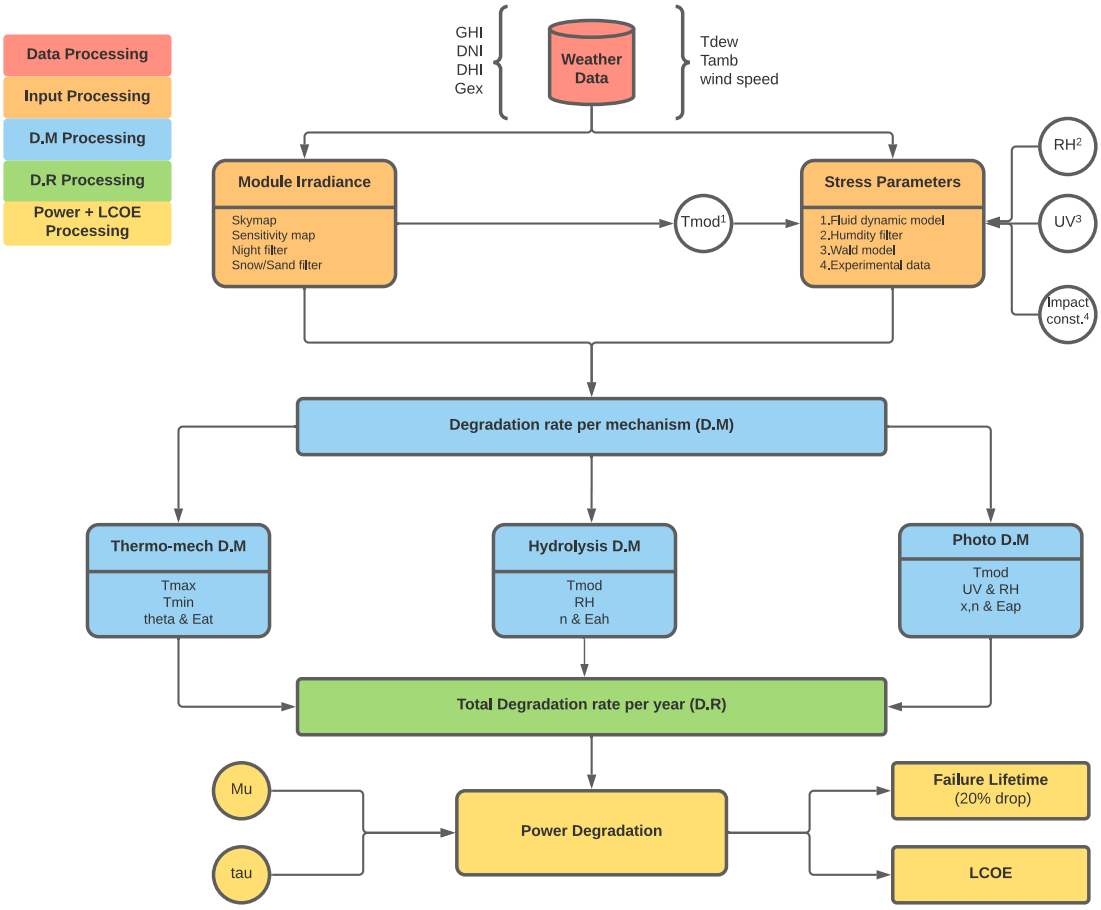

Figure 3.5: Methodology flowchart.

3.3. IMPLEMENTATION IN PVMD TOOLBOX

The model outlined is implemented in the PVMD toolbox via the methodology flowchart in figure 3.5. The process flow is illustrated in figure 3.6; the initial graphical user interface (GUI) prompts the user to activate the degradation model. The second graphical user interface requests information about the place and the time period for which normalized power should be calculated. Following the model's computation in the outputs, we have two graphical representations and two MATLAB structural variables labeled DEGRADATION_OUTPUT and NORMALIZEDPOWER_OUTPUT in the MATLAB workspace. The first graphical output depicts the normalized power consumed by each mechanism over the module's lifetime. The second graphical output depicts the module's normalized power consumption as a result of overall degradation and the module's lifetime for a 20% performance degradation. The proportion of degradation rate induced by each mechanism and the total degradation are stored in the DEGRADATION_OUTPUT variable. NORMALIZEDPOWER_OUTPUT consists of normalized power for each year due to each degradation mechanism and combined along with lifetime of the system till 20% drop in performance. Additionally, NORMALIZEDPOWER OUTPUT contains normalized power up to the set time period in the second GUI (which is then used in the LCOE calculation scenario (1) in section 4.2.2).

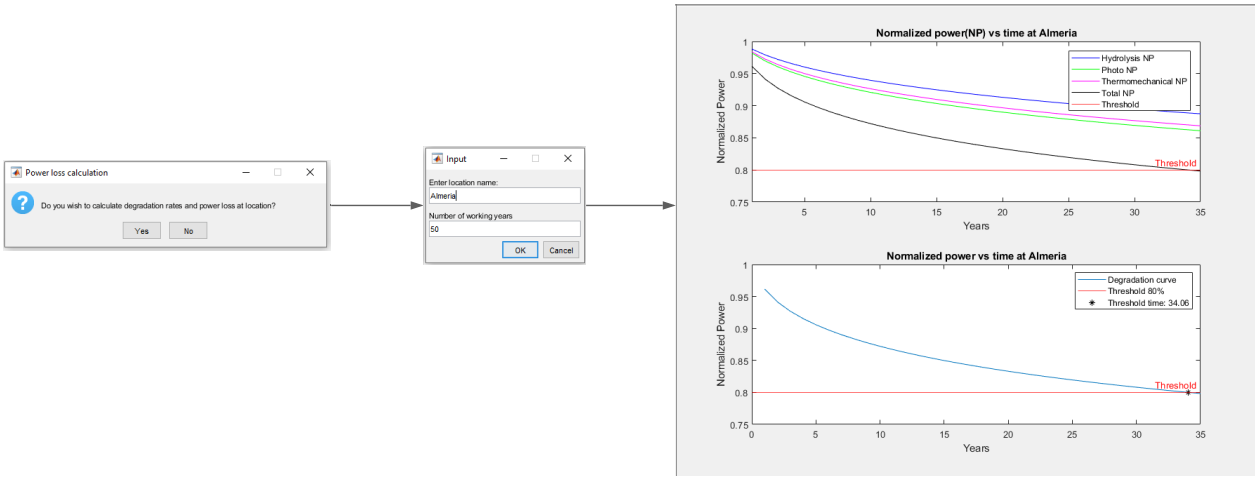

Figure 3.6: PVMD Toolbox implementation.

3.4. VALIDATION OF MODEL

The degradation rates for each mechanism are calculated using the equations 3.2.1, 3.2.3 and 3.2.4. Which will be used to calculate the total degradation rate using the equation 3.2.5. The equation 3.2.12 is used to compute the normalized power after degradation at a certain location. The equations 3.2.6, 3.2.10 and 3.2.9 are used to calculate stress factors such as relative humidity, ultraviolet light, and temperature. Additionally, stress factors are filtered to guarantee that they are examined efficiently. Irradiation filters for two conditions: (1) high irradiation for snow or sand regions to eliminate soiling losses; and (2) low irradiation for nighttime parameter elimination (radiations happening below the frequent radiation range between 50-200W/m^2).

Table 3.2: Input data of stress variables at the locations.

location	RH[%]	UV[kWh/m^2]	Tm[°C]	T_{max} [°C]	T_{min} [°C]
Canaria	65	128.4	30.77	43.95	19.12
Zugspitze	66.6	100.5	23.70	42.12	8.7

By comparing the model to two locations indicated in the paper [4] the model is validated. The validation locations are Canaria (Maritime) and Zugspitze (Snow Mountains), while Negev is utilized to represent individual outputs. The table 3.2 contains the modelled stress variables for each site. The stress factors variables are generated using typical meteorological year (TMY) data from meteonorm software's.

The calculated degradation rate for the selected locations and reference degradation rate are shown in table 3.3 (the calculations were done using the stress parameters from the table 3.2) along with lifetime of the modules to reach 80% performance. The deviation is observed between evaluated and reference degradation rate due to the usage of different climatic data - TMY data in our case. The deviation is between 4.1 to 32.3% of the prescribed uncertainty [75]. When output variables are correlated among themselves and other locations, there was no correlation found. Output variables were purely location depend. Locations with high average module temperature are more sensitive for a unit change in input parameters. Locations with low average module temperature are less sensitive to a unit change in input parameters.

Table 3.3: Calculated and reference degradation rate.

location	Estimated Rd[%/$year$]	Reference Rd[%/$year$]	Deviation[%]	Lifetime [years]
Canaria	0.506	0.50	-	34.7
Zugspitze	0.33	0.30	10	53.16

Power loss is computed for each location using the equation 3.2.12 and the degradation rate from the table

3.3. τ is assumed to be 190 and μ is assumed to be 0.19, as specified in the report [76] for crystalline silicon modules. The figure 3.7 illustrates the power loss graphically. Where the blue curve denotes power loss owing to the simulated degradation rate, the red line denotes an 80% power limit, and the dotted curve denotes power loss due to reference degradation rates.

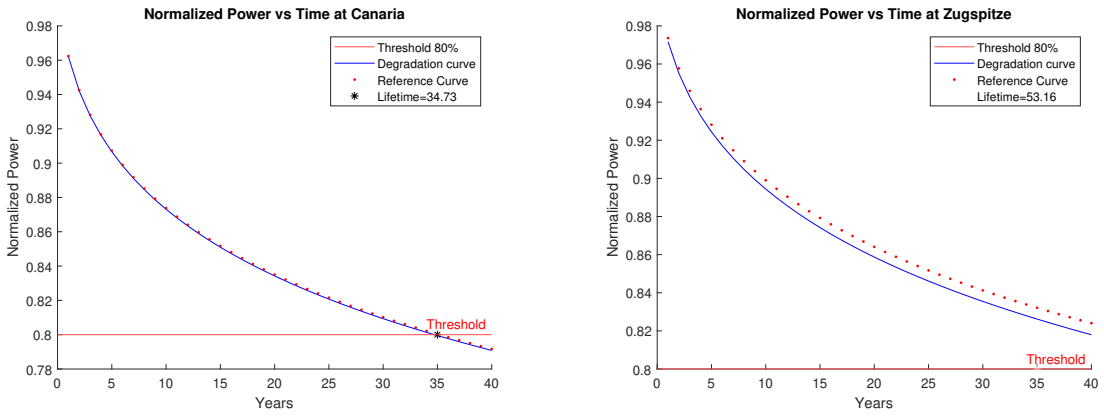

(a) Canaria degradation rate.

(b) Zugspitze degradation rate.

Figure 3.7: Degradation rates validation at two locations.

The degradation and estimation of power loss are repeated for a different site - Negev (desert) to evaluate individual degradation rates and normalized powers. The Negev's stress factors are listed in table 3.4. The total degradation rate in this region is projected to be 0.74% per year, with a life expectancy of 24 years. The figure 3.8 illustrates the individual normalized power after degradation caused by each process. The blue curve represents normalized power due to hydrolysis degradation at a rate of 0.14% per year, the green curve represents normalized power due to photo degradation at a rate of 0.21 % per year, the violet line represents normalized power due to thermomechanical degradation at a rate of 0.26% per year, and the black curve represents normalized power due to total degradation at a rate of 0.74 % per year in the Negev. Due to the lack of humidity in the desert, hydrolysis degradation has the least effect.The major process begins thermomechanical degradation, due to the desert's extreme temperature cycling. Degradation condition in deserts could be further improved in future with development of materials that are resistant to UV rays.

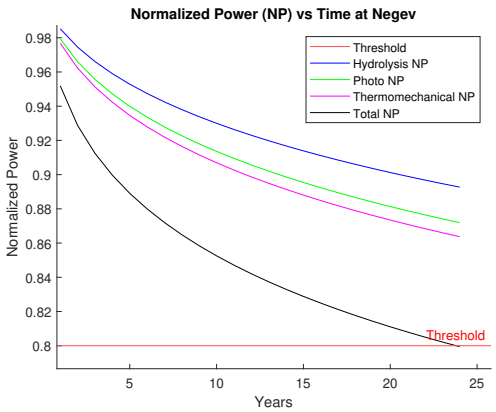

Figure 3.8: Power loss due to various degradation mechanism at Negev.

Table 3.4: Input data for Negev

location	RH[%]	UV[kWh/m^2]	Tm[°C]	T_{max}	T_{min}
Negev	60	125.7	38.45	58.94	13.5

3.5. VALIDATION WITH INDEPENDENT DATA

In this section, we compare the degradation model to measured degradation data available from independent sources to confirm the irradiation and temperature models. Bouaichi [77] provided a brief overview of degradation rates at various locations. Based on the discussion, three sites that are relevant to our model are chosen for validation with independent data : Mesa (USA), Perth (Australia), and Hamamatsu (Japan) (Japan). The criteria as seen in table 3.5 contribute to the site selection process are crystalline modules at the site meet the model requirement, outdoor exposure to dissimilar years ensures the model's temporal dependence, and visual inspection protects the modules from soiling and cell cracking, which also meets the model requirement.

Table 3.5: Criteria for selection of site.

Criteria	Mesa,USA	Perth,AUS	Hamamatsu,Japan
crystalline silicon modules	x	x	x
long-term outdoor exposure (2-10 years)	x	x	x
visual inspected	x		x

Table 3.6: Degradation rates with independent data.

Location	Measured degradation rate [%]	Modelled degradation rate [%]	Deviation[%]
Mesa,USA	0.4	0.34	15
Perth,AUS	0.5-2.7	0.67	-
Hamamatsu,Japan	0.62	0.488	21.2

We inspect data for the specified locations in Table 3.6. The measured degradation rate column refers to degradation rates measured at a specific site [77], while the modelled degradation rate column refers to degradation rates determined by our model. The deviation column indicates the deviation between the modelled and measured rates. As seen, the variation of the modelled degradation rate between the three locations is between 15% and 21%. This discrepancy is expected due to assumption used in the model for simplification along with usage of typical mean year (TMY) data from the Meteonorm database to determine degradation. Nonetheless, the observed deviation range is within the uncertainty range specified in the model [75].

3.6. RESULTS AND DISCUSSION

This section discusses the project's findings. Here, we select a few suitable locations for PV modules and use the Kaaya model to simulate their performance at those places.

3.6.1. DEGRADATION IN VARIOUS CLIMATIC ZONES

We examine the degradation across many climate around the globe. To eliminate researcher confusion on climate classification, Köppen-Geiger-Photovoltaic climate classification system (KGPV) standardizes the working climate for photovoltaic modules based on temperature, precipitation, and irradiance. The KGPV climates are classified into two categories: Temperature-precipitation (TP) zones and Irradiation (I) zones. Temperature-precipitation zones are classified as A-tropical, B-desert, C-steppe, D-Temperate, E-cold, and F-polar, whereas irradiation zones are classified as L-low, M-medium, H-high, and K-very high. Permutations of TP zones and I zones (a total of 24 combinations) account for nearly all of the solar photovoltaic working conditions.

For our study, Five climatic zones are evaluated in relation to the KGPV climates from these combinations of TP and I. The places were chosen using a specific parameter called the "surface-population density indicator." This indicator combines the population density with the land surface density per climatic zone facilitating PV plant installation criteria. The chosen five locations are represented with the highest surface population density indicator. The table presented in figure 3.9 represents surface population indicator values for the Köppen-Geiger-Photovoltaic climate classification system. AH, BK, CH, DH, and EM are the five zones with

the highest surface population density indication. According to author Vásquez, the key geographical locations reflecting these distinct zones are AH-Bangkok (Thailand), BK-Atacama (Chile), CH-Almeria (Spain), DH-Atlanta (USA), and EM-Minneapolis (USA) [6]. It is assumed that the TMY weather data acquired using meteonorm software from 2000 to 2009 will remain constant for further investigation. The environmental stressors that are utilized to determine the degradation rate of each mechanism at selected sites are listed in table 3.7. The first value reflects the module's maximum temperature, followed by the module's average temperature and finally the module's minimum temperature. The 3^{rd} column contains relative humidity data with irradiation filter , followed by UV radiation values.
These values are substituted into the equations 3.2.1, 3.2.3, 3.2.4 and 3.2.5 to determine the hydrolysis, photo, thermomechanical, and total degradation rates for each climatic zone. Then, using the obtained degradation rates for each mechanism, equation 3.2.12 is utilized to determine the nonlinear normalized power after degradation.

Surface-Population Density indicator		*I*-zones			
		L	*M*	*H*	*K*
TP-zones	*A* – Tropical	0.59	0.66	8.95	1.20
	B – Desert	0.00	0.01	1.04	1.68
	C – Steppe	0.00	0.13	4.26	1.14
	D – Temperate	1.14	6.53	9.79	0.62
	E – Cold	0.95	2.96	0.87	0.02
	F – Polar	0.00	0.00	0.05	0.01

Figure 3.9: Surface-population density indicator per climate zone for Köppen-Geiger-Photovoltaic climate classification[6].

Table 3.7: Stress factors for degradation mechanism at 5 KGPV locations.

location	Climatic zones	T_{max} [K]	T_{mean} [K]	$T_{min}[K]$	RH [%]	UV $[kWh/m^2 - year]$
Bangkok, Thailand	Tropical (AH)	332.08	319.16	306.60	58.16	111.83
Atacama, Chile	Desert (BK)	319.04	299.723	283.843	54.2	334.28
Almeria, Spain	Steppe (CH)	323.45	305.44	288.63	50.4	104.25
Atlanta, USA	Temperate (DH)	326.94	308.72	286.9	55.2	106.94
Minneapolis, USA	Cold (EM)	328.57	312.21	281.87	39.7	87.71

The degradation rates and lifetime required for the modules to reach 80% of their initial power were calculated for the specified location. The table 3.8 contains information about the degradation rate and lifetime for each of the 5 locations. We observe that tropical-high irradiation zones and cold-medium irradiation zones have the highest and lowest degradation values. The maximum degradation rate seen was 1.31 % over a lifetime of 13.36 years, while the minimum degradation rate observed was 0.33 % over a lifetime of 55.9 years. The declining trend in module lifespan is as follows: $Cold > Steppe > Desert > Temperate > Tropical$, and the inverse pattern in degradation rates is as follows.

The figure 3.10 illustrates the non-linear normalized power as function of time for each degradation process (hydrolysis, photodegradation, and thermomechanical degradation) up to their lifetime in each zone. In the same figure, 80% of the original power threshold is represented by a red horizontal line, while blue indicates a temperate environment, magenta curve indicating tropical climate, yellow indicates a desert climate, black indicates a steppe climate, and green indicates a cold climate..

Table 3.8: Degradation rates with KGPV climate zones.

location	Climatic zones	Modelled degradation rate [%]	Lifetime [80% of initial power]
Bangkok, Thailand	Tropical (AH)	1.31	13.36
Atacama, Chile	Desert (BK)	0.53	33.41
Almeria, Spain	Steppe (CH)	0.52	34
Atlanta, USA	Temperate (DH)	0.67	26.24
Minneapolis, USA	Cold (Em)	0.33	55.9

Hydrolysis degradation: The graphs in figure 3.10a depict the normalized power associated with hydrolysis degradation. As indicated in the illustration, the tropical zone, denoted by the magenta curve, suffers the most loss of power, whereas the cold zones suffer the least. Tropical locations are especially vulnerable due to the climate's high amounts of precipitation and Temperature. Tropical climates, as indicated in the table 3.7, have a maximum temperature of 332.08 K and a relative humidity of 58.16%. It is crucial to note that Atacama, due to its proximity to the coast, has a higher relative humidity than other desert locations. Due to the fact that the relative humidity in Atacama and Atlanta is similar, locations with a high mean module temperature degrade more rapidly.

Photo degradation: The graphs in figure 3.10b indicate the normalized power due to module photodegradation. The tropical zone experiences the most loss in power, while the cold zone experiences the least. It's odd to see that tropical areas lose more energy than deserts. As tropical zones with a high concentration of stress factors (module mean temperature, humidity, and UV radiation) outweigh desert zones with a high concentration of UV radiation but a low humidity and temperatures as seen in table 3.7. Due to the high concentration of ultra-violet irradiation in desert regions, photo degradation data indicate that PV modules perform worse than those in temperate and steppe climates.

Thermo-mechanical degradation: The graphs in figure 3.10c indicate the normalized power caused by module thermo-mechanical degradation. This degradation is more evident in areas where temperatures fluctuate significantly. The largest power loss occurs in cold zones and the least in desert zones. Desert regions outperform temperate and steppe regions in thermomechanical degradation studies. Nonetheless, it was surprising to discover that the photovoltaic module performs poorer in cold climates than in other regions in temperature cycling effect due to high difference in temperature between the maximum and minimum temperatures as indicated in table 3.7.

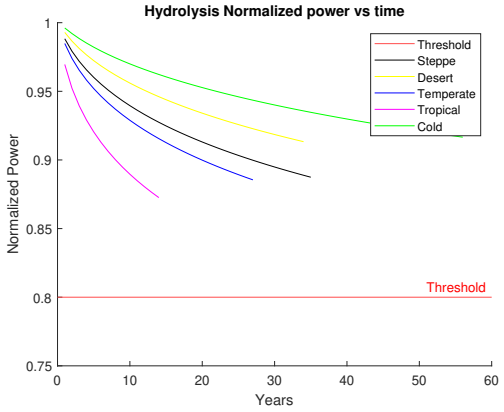

(a) Normalized power due to Hydrolysis degradation mechanism.

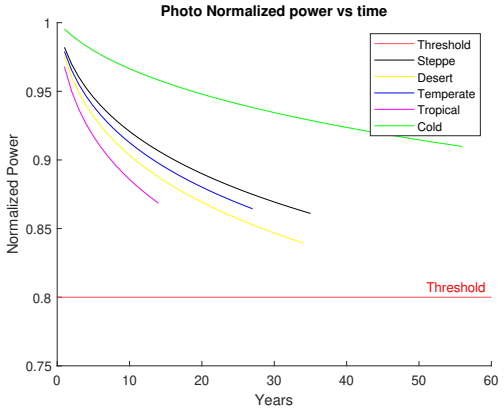

(b) Normalized power due to Photo(UV) degradation mechanism.

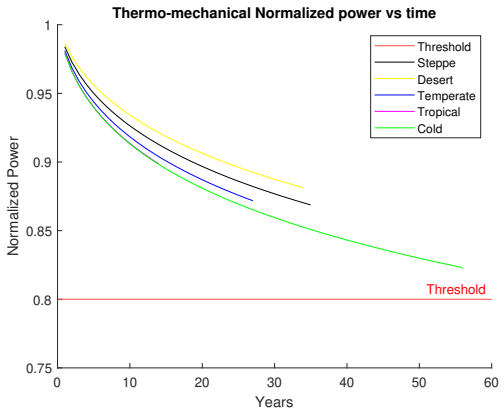

(c) Normalized power due to Thermo-mechanical degradation mechanism.

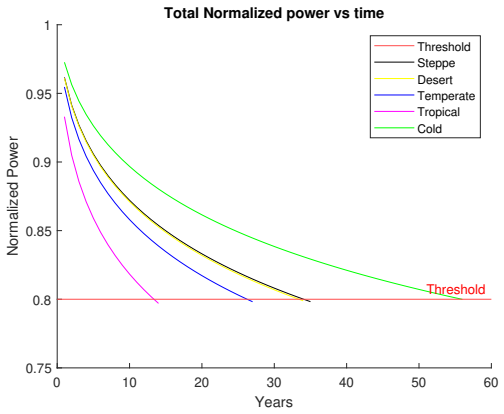

(d) Total Normalized power vs time.

Figure 3.10: Normalized power vs time for all the climatic zones.

The non-linear normalized power generated by the cumulative influence of all processes until the lifetime time is reached is depicted in figure 3.10d. A horizontal red line indicates that 80% of the initial power threshold has been reached, while a magenta curve indicates a tropical climate, blue indicates a temperate environment, yellow indicates a desert climate, black indicates a steppe climate, and green indicates a cold climate (same notation as before). All of the normalized power numbers in the figure are accounted to the crystalline silicon module's lifetime under the specified climatic conditions. Tropical climates have the highest power loss ratios($= 1 - NP$), followed by temperate climates, steppe and desert climates, and finally cold climates. It was interesting to observe that deserts, due to their low thermomechanical stress and low hydrolysis, as well as their high photodegradation, had an average climate stress similar to that of the steppe climate. This was possibly due to Atacama being near to ocean having almost similar RH as Atlanta.

3.7. CONCLUSION:

In this study, we identify a degradation model that is meteorological-specific. We account for stress variables that result in irreversible degradation of photovoltaic modules, such as module temperature, relative humidity, UV radiation, and cyclic temperatures. Soiling and snowing stress elements are excluded because their effects are reversible with proper module maintenance. A few assumptions were made to streamline the computation: the model's material and structure dependencies are accounted for by the activation energy (E_a) and power susceptibility constant, three degradation mechanisms (hydrolysis, photo, and themomechanical degradation) play a significant role in determining module degradation, and module parameters such as impact constants, shape factor and power susceptibility are independent of the location. We determine the stress factor combinations that are considered in each mechanism: hydrolysis degradation accounts for the module's temperature and humidity, photo degradation accounts for UV and other effects triggered by the combination of UV and RH, and thermomechanical degradation accounts for the location's cycling temperatures. All three degradation modes are mathematically combined to provide a single overall degradation factor that is used to calculate the normalized power of the photovoltaic module at the site. The degradation model implemented in the PVMD toolbox was further validated with the results presented in report [4] for precision. The model was later validate with independent data from various regions that are represented in the article [77] due to usage of mathematical models such as sky-maps, sensitivity maps for irradiation calculation and fluid dynamic model for temperature calculations that are different from the models used in the reference article [4] for accuracy. The deviation between predicted and reference values in validation of model and independent data are within the model's uncertainty bounds.

Further, the degradation model was used to assess degradation under diverse climatic conditions. Five major climate zones were chosen for the study from the 24 combinations in the "Koppen Geiger photovolatic climate classification" based on the surface-population density indicator. These five areas consisted of a mix of temperature-precipitation and irradiation zones. Tropical with high irradiation (AH), Desert with extremely high high irradiation (BK), steppe with high irradiation (CH), temperate with high irradiation (DH), and cold with medium irradiation(EM) were chosen five combinations. These locations denote the availability of radiation, population, and available surface area for a photovoltaic plant. According to the study, the tropical zones have highest degradation of 1.31% and lifetime of 13.36 years for 20% drop in performance, while cold zones have least degradation of 0.33% and lifetime of 55.9 years. After simulating the normalized power for each mechanism at each location, it is discovered that hydrolysis degradation is greatest in tropical regions due to the presence of high humidity, followed by temperate zones; photo degradation is greatest in tropical regions, contrary to popular belief to be desert, due to the combined effect of UV and relative humidity; and thermomechanical degradation is most in cold climates due to huge temperature variations and least in desert. The combined degradation data indicate that tropical regions see the greatest loss of power, followed by temperate zones. It is peculiar that steppes and deserts have the almost similar power loss since averaged stressors in the steppe balance out the single major stressor in the desert, with cold regions being the least affected. It is critical to notice that Atacama, a desert zone located close to the ocean, experienced a higher relative humidity than expected.

4

FINANCIAL ANALYSIS

Lately, there has been intense focus on renewable energy technologies, particularly solar PV technology, to replace fossil fuels as a result of the impending energy crisis, the rising cost, the decreasing availability, as well as extensive emissions of greenhouse gases (GHG) [78]. Despite this, the application of renewable energy technology has not yet reached its full potential, primarily as a result of intermittent energy generation and economic constraints. Solar photo-voltaic (PV) technology is currently considered to be the fastest expanding industry for affordable renewable energy. Since 2000, solar photo-voltaic (PV) technology has grown at an annual average rate of 42%, resulting in a total capacity of 512 gigawatts (GW) [79]. Solar PV has the lowest marginal cost when viewed economically, as there are no fuel expenditures and only operational costs. As a result, solar energy's production costs are lower than those of coal and natural gas, implying that natural gas and coal energy will be phased out of the electricity market [80].

Despite ongoing demand growth and subsidies for renewable energy, solar PV has not yet become a significant source of electricity [81]. When the market attains "Grid parity," photovoltaic technology will triumph. Grid parity is reached when the cost of power generated by a photo-voltaic module is less than or equal to the market price (generally set by conventional plants). At the moment, it is only possible in a limited number of circumstances, dependent on the source's availability, the plant's capacity, the modules' degradation, their efficiency, and their cost [82]. Many different economic measures can be used to calculate the price of power that is supplied. Among the different economic indicators, the levelized cost of electricity (LCOE) is a popular one. The LCOE is used to determine the lowest price at which energy produced by a certain energy source should be sold in order to recover the investment expenses (fuel price, operation and maintenance costs, and fixed costs) over the course of the source's lifetime [83]. The LCOE is computed as a function of the amount of energy produced by the plant over its lifetime and the cost of the generation plant; as a result, it is expressed in Euros per kilowatt-hour (€ per kWh). But because LCOE is a volatile measuring unit, even a little change in the input variables or assumptions might cause it to alter significantly. Investment cost, system lifetime, degradation in the system, discount rate, and incentives are the most essential input and volatile variables in the computation of the LCOE. Fixed costs, operation and maintenance costs, and fuel costs are all included in the investment costs of available renewable energy sources such as solar PV. However, there is no fuel cost associated with solar PV. As a result, accurate forecast and evaluation of energy produced over the module's lifespan as well as the module's lifetime play a significant part in determining the LCOE of PV modules.

The goal of this study is to determine the LCOE values for various climatic conditions around the world with differing rates of degradation and conditions required for grid parity along with investment return. Three economic scenarios are considered when determining the LCOE: (1) the same modules are used throughout the planned operating period of the PV plant, (2) degraded modules are replaced with new modules at same price until the planned operating period of the PV plant is completed, and (3) degraded modules are replaced with new modules at newer lower prices until the planned operating period of the PV plant is completed. The estimated LCOE is subjected to sensitivity analysis utilizing the discount rate variable for scenario (3). Finally, the financial model is included into the PVMD toolbox together with economic scenarios.

4.1. LCOE METHODOLOGY

As previously stated, LCOE is defined as the economic evaluation of a generation system as a function of the energy generated by the system during its lifetime and the cost of establishing the system. This statistic can be used to compare economic and technical performance of various technologies. The LCOE calculation takes into consideration the system's cost, operation and maintenance costs, and fuel costs, as well as the energy

produced, and converts them to a single measuring unit defined in Euro(€) per kWh [83]. The following equation 4.1.1 can be used to calculate the LCOE.

$$LCOE = \frac{\textit{Total cost till the lifetime(Euro)}}{\textit{Total energy produced in lifetime (kWh)}} \tag{4.1.1}$$

Total cost and total energy produced over the course of a lifetime are computed using the "discount cash flow" approach. The term "discount cash flow" refers to the worth of a commodity adjusted for the time value of money. After calculating the needed parameters using the discount cash flow approach, the 'Net present value'(NPV) are calculated and NPV ratio are utilized to determine the LCOE. The net present values of each commodity are represented in Equations 4.1.2 and 4.1.3 [84]. In equation 4.1.2, we note that the initial condition $t = 0$ is used to account for the initial investment cost before the plant begins producing. Finally, LCOE is determined as a ratio of net present values, which is ratio of the sum of discounted present values for investment costs and discounted present values for energy, as specified in equation 4.1.4 [85].

$$\textit{Net present value of investment} = \sum_{t=0}^{T} \frac{C_t}{(1+r)^t} \tag{4.1.2}$$

$$\textit{Net present value of production} = \sum_{t=1}^{T} \frac{E_t}{(1+r)^t} \tag{4.1.3}$$

$$LCOE = \frac{\sum_{t=0}^{T} \frac{C_t}{(1+r)^t}}{\sum_{t=1}^{T} \frac{E_t}{(1+r)^t}} \tag{4.1.4}$$

PV module energy production decreases with time, as previously discussed in the chapter 2. This also indicates the need for a degradation term in LCOE calculations. The degradation of the photovoltaic module is factored into the LCOE by multiplying E_t, the system's rated energy, by $(1-(dt))$, where d_t is a nonlinear power loss variable ($= 1 - \textit{Normalized power ratio}$) computed in the preceding chapter 3.2.3. As a result, equation 4.1.4 can be restructured as 4.1.5. I_0 denotes the initial investment, which comprises module and inverter expenses, as well as structural and electrical BOS costs. I_t annual investment, which may include inverter or battery replacement costs. M_t is the system's maintenance cost, E_t is the system's rated energy yield, d_t is the system's nonlinear power loss, r is the discount rate, and T is the system's estimated operating duration.

$$LCOE = \frac{I_0 + \sum_{t=1}^{T} \frac{I_t + M_t}{(1+r)^t}}{\sum_{t=1}^{T} \frac{E_t(1-d_t)}{(1+r)^t}} \tag{4.1.5}$$

4.2. IMPLEMENTATION IN PVMD TOOLBOX

This section will explain the introduction of LCOE calculations into the PVMD toolbox and the toolbox's nomenclature.

4.2.1. USER INPUT

The graphical user interface (GUI) is used to retrieve input variables from the user, and the flowchart figure 4.1 describes the GUI sequence step by step. The first graphical user interface dialog box is used to specify the system's design. It contains the following information: the number of modules, the discount rate, the module cost, the inverter cost, the structural BOS cost, the electrical BOS cost, the OM cost, the estimated length of operation, the inverter lifetime, and the installation year.
The following table details the function and definition of each variable in the graphical user interface dialog boxes.

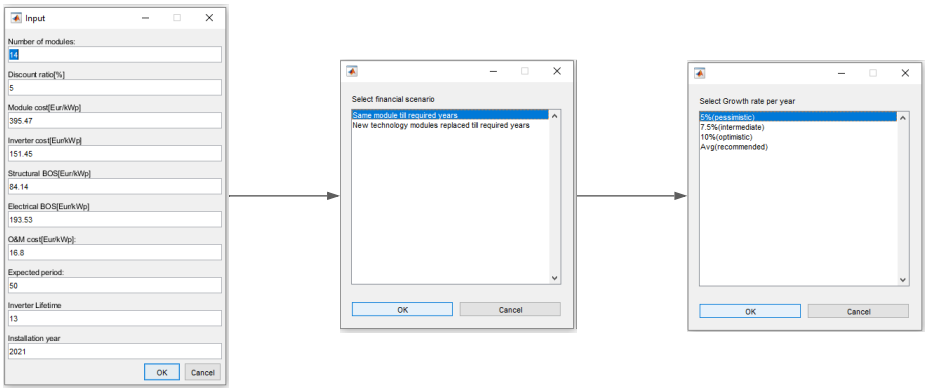

Figure 4.1: GUI dialog box flowchart.

Table 4.1: Input GUI

Variable	Purpose and definition
Number of modules	The total number of photovoltaic modules in the system. This variable is used to determine the system's total rated power. *Default value-14.*
Discount rate [%]	It is used to add the attribute of value of time to money, the value of which is determined by a variety of circumstances. High discount rates are employed to maximize short-term earnings and low discount rates to optimize long-term benefits [86]. *Default value- 5%*
Module cost [€/kW_p]	It is a cost assessment of each module's manufacturing and is given in euros per kWp (rated power). *Default value- 395.47 €/kW_p*
Inverter cost [€/kW_p]	It is a cost estimate for the entire system's inverter, expressed in euros per kWp (rated power). *Default value-151.45 €/kW_p*
Structural BOS cost [€/kW_p]	It is an estimate of the cost of mounting, installation, and infrastructure for the entire system, expressed in euros per kWp (rated power). *Default value- 84.14 €/kW_p*
Electrical BOS cost [€/kW_p]	It is used to describe the cost of DC cabling and grid connection for the entire system and is expressed in euros per kWp (rated power). *Default value- 193.53 €/kW_p*
Operation and maintenance cost [€/kW_p]	It is used to determine the operating and maintenance costs of the entire system and is expressed in euros per kWp (rated power). *Default value- 16.8 €/kW_p*
Expected period [$years$]	This variable is used to specify how long the system should remain functional at the site regardless of the module's lifetime. *Default value- 50 years*
Inverter lifetime [$years$]	It is used to interpret the replacement cycle of the inverter till projected expected period. *Default value- 13 years*
Installation year [$year$]	The future cost of new technology is calculated using this variable as a reference point. *Default value- 2021*

4.2.2. OUTPUT

Following the processing of financial section in the toolbox. The output includes a single graphical output and the creation of an LCOE variable in the MATLAB workspace. Each scenario is inscribed with four variables in "LCOE" structure variable presented in MATLAB workspace. They are the levelized cost of electricity at which the energy should be sold as a function of the time in years, the energy produced by the system

Table 4.2: Financial scenario

Scenario	Purpose and definition
Same module till required years	Scenario 1: PV module are not replaced after their 20% drop in performance. They are continued till the expected operation period is completed.
New modules replaced till required years	This economic scenario occurs when modules are replaced after a 20% degradation. This scenario is subdivided into two parts. • Scenario 2: PV modules that have degenerated by 20% are replaced with new modules at the same price as the first installation. • Scenario 3: PV modules that have degraded by 20% are replaced with new module available at cheaper price in the market during that time-frame. The cost of new module's in this scenario are calculated using a mathematical model constructed from the report's data [87] *It is critical to emphasize that all scenarios involve just price increases, not improvement in the efficiency of new modules.*

Table 4.3: Growth rate per year for second financial scenario from table 4.2

Growth rate	Purpose and definition
5%	This option is chosen if the market for photovoltaic technology is predicted to expand at a rate of 5% per year. Perhaps this is a pessimistic market framework [87].
7.5%	This option is chosen if the market for photovoltaic technology is predicted to increase at a rate of 7.5% per year. This option is viewed as a middle ground between pessimistic and optimistic market frameworks [87].
10%	This option is taken if the market for photovoltaic technology is predicted to develop at a 10% annual rate. This is seen as an optimistic market framework [87].
Avg	This option is selected if the market for photovoltaic technology is predicted to increase at an annual rate equal to the average of pessimistic, intermediate, and optimistic courses of action. This option is regarded to be recommended in light of the present market environment [87].

until the expected period, Discounted energy produced (used for LCOE) and total investment cost including replacement module cost, inverter cost and operation & maintenance cost of the system.

In the graphical output, the LCOE is plotted as a function of the number of operational years using data from the reference table 4.1 and a scenario selected from the reference table 4.2 along with growth rates from table 4.3. The X axis depicts the operating period of the photovoltaic system, while the Y axis depicts the LCOE necessary to recover the investment cost measured for the X value set in the graphical interface. On a graphical interface, a pointer can be used to pick the required X (years) or Y (LCOE). The figure 4.2 illustrates an example of scenario 1 situation, where Y equals 0.044 when $X = 27$. This means that for a solar photovoltaic system erected at this location to recovery its investment cots within 27 years, the levelized cost of electricity should be 4.4 cents per kWh for the first 27 years. We find that the value of Y is 0.039 in other selected period of $X = 39$. This means that until 39 years after installation, the levelized cost of electricity for a photovoltaic system at the installed location should be 3.9 cents per kWh to recover investment costs in 39 years.

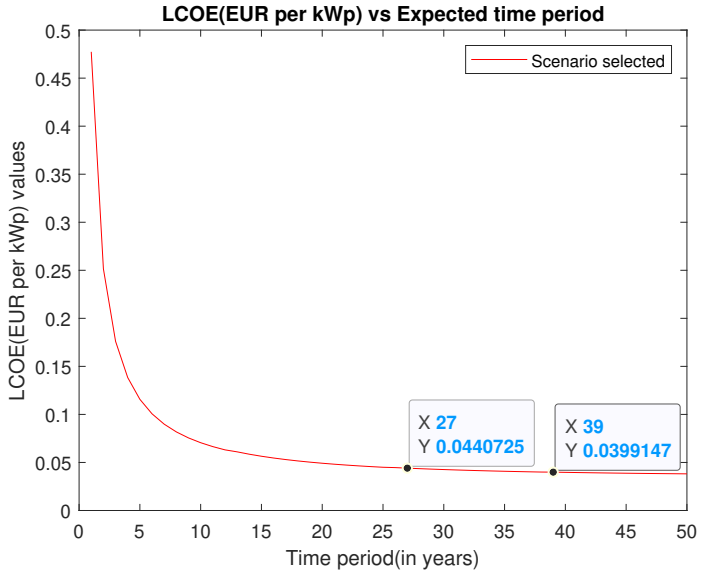

Figure 4.2: Graphical output.

4.3. VALIDATION OF THE MODEL

The PVMD toolbox model is validated using the exercise described in the cited presentation [88]. We have a 5 kW_p system with an energy yield of 950 kWh/kW_p, system cost of 1300€ per kW_p, an operation and maintenance cost of 20 € per kW_p, and a 5% discount rate. The degradation rate is estimated to be 0.36% per year, and the module's life expectancy at this location is 25 years. In comparison to the aforementioned numbers, the LCOE is computed to be 0.12€ per kW_p . A similar model is created with the PVMD toolbox; ten modules with a rated power of 500 Watts are used in the LCOE input GUI table 4.1 to establish a 5kW system, while the remaining inputs are adjusted to correspond to the required reference system. As shown in the figure 4.3, the LCOE values at 25 years is 0.12€ per kW_p using the LCOE model included in the PVMD toolbox, which is comparable to the number in the cited presentation[88].

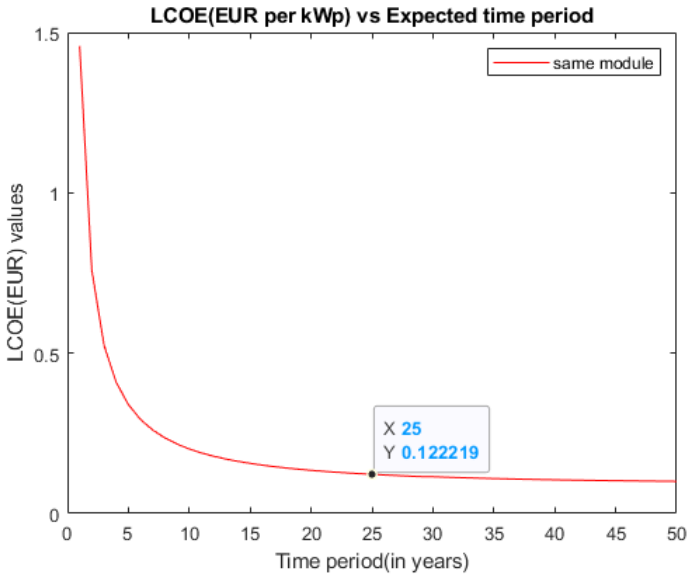

Figure 4.3: Validation of LCOE model.

4.4. RESULTS AND DISCUSSION

As we are interested in the effect of climate on the performance of photovoltaic modules in various places. We chose three locations to investigate the effect of climate on LCOE computation. Tropical (severe degradation), steppe (medium degradation), and cold (least degradation) climates are selected and available in the locations specified in the section 3.6.1 , namely Bangkok, Almeria, and Minneapolis. A hypothetical average residential system of 6.5 kW with fixed-tilt PV modules and grid connection is used to evaluate LCOE. PV technology characteristic used for this purpose are 14 mono-crystalline PV modules with a rated power of P_{STC} = 458 watts and an efficiency of 24.3% are used.

The financial input data for the system are as follows: module costs per watt, inverter costs per watt, structural BOS cost per watt, and electrical BOS cost per watt and are obtained from the given report [89]. To ensure economic viability, prices are converted from USD to EURO at a rate of 1 USD = 0.84 EUR. The investment costs after converting each category from USD per Watt to EURO per kilo-Watt are 395.47 €/kW for modules, 151.45 €/kW for DC power optimizer string inverters, 84.14 €/kW for structural BOS, and 193.53 €/kW for electrical BOS. Operating and maintenance costs are maintained at 16.8 €/kW. For analysis purposes, a discount rate of 5% is utilized. The system's expected term is set to 50 years, computing the facility LCOE for each year up to 50 years. PV modules are replaced on a periodic basis if their output power decreases by 20% or more over a 50-year period, and the costs of new PV modules in future required for the calculation of investment costs to replace degraded modules are retrieved using a mathematical function developed in the PVMD toolbox from data in the cited report[87]. Inverters are changed on a periodic basis of 13 years up to a 50-year expected term, with the price remaining constant throughout the duration. All configuration parameters are listed in table 4.4.

Table 4.4: System inputs

Variable	Value
Number of modules	14 (each module with rated power P_{STC} = 458 watts)
Discount rate[%]	5%
Module cost [€/kW_p]	395.47
Inverter cost [€/kW_p]	151.45 (DC power optimizer string inverter)
Structural BOS cost [€/kW_p]	84.14
Electrical BOS cost [€/kW_p]	193.53
Operation and maintenance cost [€/kW_p]	16.8
Expected working period [years]	50
Inverter lifetime [years]	13
Installation year	2021
Growth rate per year	recommended

4.4.1. FINANCIAL ANALYSIS AT STEPPE CLIMATE - ALMERIA

The LCOE values for Almeria, Spain, are presented in the figure 4.4a for three scenarios: (1) same module for 50 years, (2) after the module's lifetime is reached, it is replaced with a new module at a same cost to ensure the system's functionality till 50 years, and (3) new modules at an average growth rate having lower cost are used to replace the degraded module after it reaches its lifetime to maintain system functionality for 50 years. The LCOE calculation for the hypothetical system at the site is subjected to a sensitivity analysis with discount rates ranging as 3%,5%,7% and 10% that are commonly used[90]. The analysis's findings are depicted in figure 4.4c.

As reviewed in section 3.6.1, it is estimated that Almeria has a lifetime of 34 years in a steppe climate. The

graphic representation is shown in 4.4b , along with an increase in LCOE at the 35^{th} year owing to module replacement. Thus, to maintain the system's functionality for 50 years, the photovoltaic module must be replaced every 35^{th} year following installation. In a hypothetical financial decision, if we desire to return the cost of our investment in 40 years, as modules are replaced once every 35^{th} year. The output values for each of the three economic scenarios are as follows as shown in table 4.5. 1^{st} scenario using the same module until the expected system life, 2^{nd} scenario replacing the modules for same price used for installation, and 3^{rd} scenario replacing the system modules for lower costs in future market.
The table 4.6 summarizes the comparison of economic scenarios and their impact on energy yield and LCOE. According to the report [91] the average home power price in Spain (without taxes and levies) is 0.14 € per kWh. Grid parity and total investment recovery is easily achievable in specific locations like as Almeria, Spain, with a residential plant operating for a minimum of five years (because the levelized cost of energy is 0.10 € per kWh) under any of the patterns of behavior.

Table 4.5: LCOE value and Energy produced in 40 years at Steppe climate - Almeria.

Economic scenario	LCOE [€ per kWh]	Energy Produced [MWh]
Scenario 1	0.039	416
Scenario 2	0.044	428.3
Scenario 3	0.041	428.3

Table 4.6: Comparison between economic scenarios and their impacts at steppe climate - Almeria.

Comparison	Additional energy yield [%]	Change in LCOE [%]
Scenario 1 and 2	3%	12.8%
Scenario 1 and 3	3%	5%

Sensitivity analysis is conducted by adjusting the discount rate variable by 3%, 5%, 7%, and 10% for the third economic scenario. Increases in the discount rate result in an increase in the LCOE value over the entire range as seen in figure 4.4c. The LCOE at a 3%, 5%, 7%, and 10% discount rate for a 40-year investment recovery is listed in table 4.7, respectively. Comparing a default discount rate of 5% to a default discount rate of 10%, we see that a 5% increase in the discount rate results in a 43% rise in the LCOE. By comparing the default discount rate of 5% to the default discount rate of 3%, we see that a 2% reduction in the discount rate results in a 14% reduction in the LCOE.

Table 4.7: Sensitivity analysis using discount rate at Steppe climate - Almeria.

Discount rates[%]	LCOE [€ per kWh]
3	0.035
5(default)	0.041
7	0.048
10	0.059

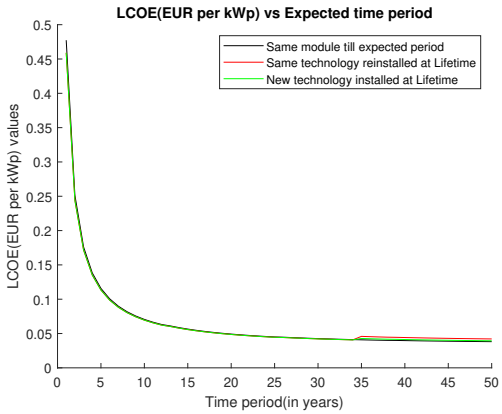

(a) LCOE results for 3 scenarios at Almeria.

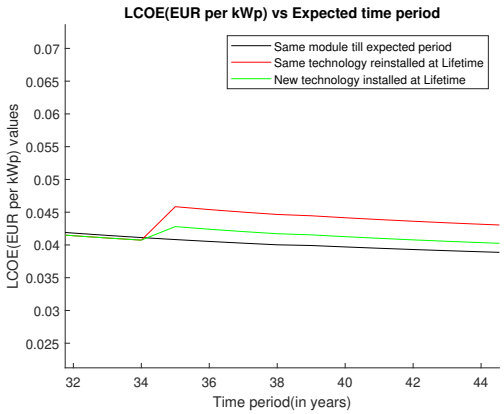

(b) LCOE result with 34 years replacement cycle at Almeria.

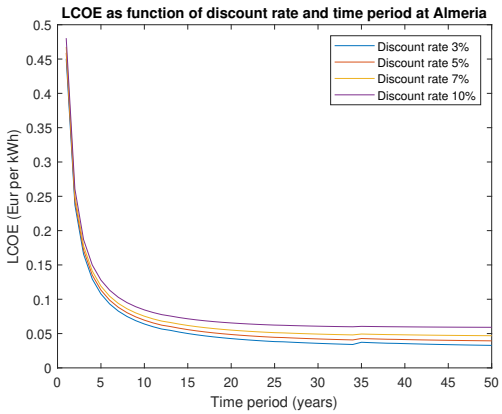

(c) Sensitivity analysis with Discount rate for 3rd scenario at Almeria.

Figure 4.4: Financial assessment of Steppe climatic zone.

4.4.2. FINANCIAL ANALYSIS AT TROPICAL CLIMATE - BANGKOK

The LCOE values for Bangkok, Thailand are shown in the figure 4.5a for the three scenarios mentioned previously, as well as a sensitivity analysis at the site shown in the figure 4.5c.

Bangkok's tropical environment is expected to have a 13-year life expectancy with extremely high degradation values as reviewed in section 3.6.1. As a result, to maintain the system's functionality for 50 years, the photovoltaic module must be replaced three times after installation. The same hypothetical financial decision is made to recover the entire investment cost over a 40-year period. The LCOE values and energy produced in each scenario are listed in table 4.8.

Table 4.8: LCOE value and Energy produced in 40 years at Tropical climate-Bangkok.

Economic scenario	LCOE [€ per kWh]	Energy Produced [MWh]
Scenario 1	0.051	316.1
Scenario 2	0.075	346.9
Scenario 3	0.065	346.9

Different economic scenarios are compared and their impacts are as presented in table 4.9. Due to the module being replaced every 13 years, increases in LCOE values can be noted in the figure 4.5b. According to the report's [92], the average residential electricity price in Thailand is 0.06 € per kWh (excluding taxes and levies). In scenario 1, a residential photovoltaic system in Thailand can attain grid parity after a minimum of 33 years of operation (When the levelized cost of electricity is 0.054 € per kWh). Grid parity and total recovery is only possible in scenarios 2 and 3 if the working duration exceeds 50 years.

Table 4.9: Comparison between economic scenarios and their impacts at Tropical-Bangkok.

Comparison	Additional energy yield [%]	Change in LCOE [%]
Scenario 1 and 2	9.7%	47%
Scenario 1 and 3	9.7%	27.4%

As in the previous instance, a sensitivity analysis is conducted on the discount rate variable. In scenario 3, the LCOE values for discount rates of 3%, 5%, 7%, and 10% at 40^{th} year are presented in table 4.10, respectively. Comparing the default 5% instance to the 10% scenario demonstrates that a 5% increase in discount rate results in a 35.3% rise in LCOE. By contrast, comparing the default scenario to the 3% discount rate case demonstrates that a 2% reduction in the discount rate results in a 10% reduction in the LCOE value.

Table 4.10: Sensitivity analysis using discount rate at Tropical climate - Bangkok.

Discount rates[%]	LCOE [€ per kWh]
3	0.058
5(default)	0.065
7	0.074
10	0.088

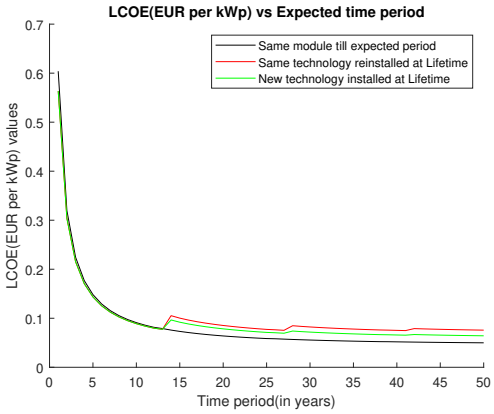

(a) LCOE results for 3 scenarios at Bangkok

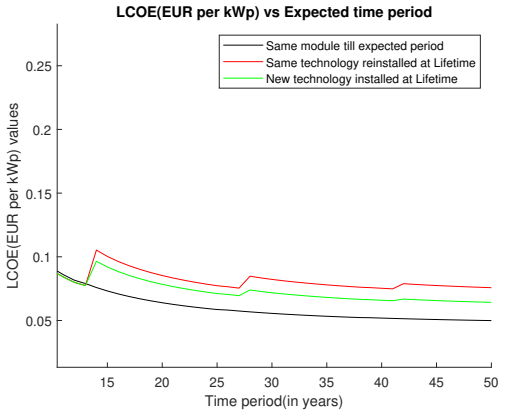

(b) LCOE result with 13 year replacement cycle at Bangkok.

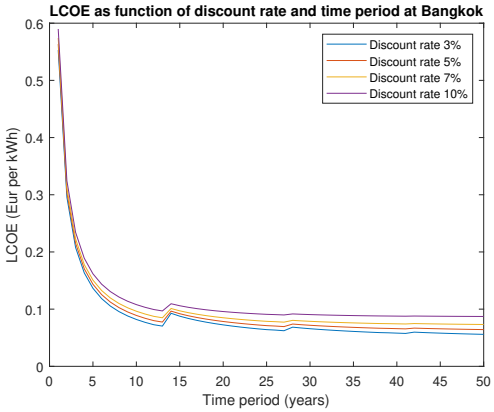

(c) Sensitivity analysis with Discount rate for 3rd scenario at Bangkok.

Figure 4.5: Financial assessment of Tropical climatic zone.

4.4.3. FINANCIAL ANALYSIS AT COLD CLIMATE - MINNEAPOLIS

The LCOE values for Minneapolis, located in USA, are provided in the figure 4.6a for the three scenarios discussed previously, as well as a sensitivity analysis at the site, as shown in the figure 4.6b.

Minneapolis's lifespan in a cold climate is projected to be 56 years with extremely low degradation values, as examined in section 3.6.1. As a result, they do not need to be replaced for the duration of our case study, which is 50 years. The same hypothetical financial decision is maintained for investment recovery over a 40-year period. The LCOE value for the 40^{th} year recovery period is identical in all cases because the PV modules are not changed until the 56^{th} year, at which point the LCOE value is 0.047 € per kWh. According to the report's [93], the average residential electricity price in Minnesota state is 0.11 € per kWh (excluding taxes and levies). A household photovoltaic (PV) system in Minneapolis can achieve grid parity and investment recovery in all scenarios with a minimum of seven years of operation (When the levelized cost of electricity is 0.10 € per kWh).

Sensitivity analysis is performed on the Minneapolis case with various discount rates. The LCOE values for discount rates of 3%, 5%, 7%, and 10% at 40^{th} year are liste in table 4.11, respectively. Analyzing the default 5% example with a 10% discount rate demonstrates that a 5% increase in discount rate results in a 50% spike in LCOE. In comparison, analysis of the 3% and default discount rate cases demonstrates that a 2% reduction in the discount rate results in a 17% reduction in the LCOE value.

Table 4.11: Sensitivity analysis using discount rate at Cold climate - Minneapolis.

Discount rates[%]	LCOE [€ per kWh]
3	0.040
5(default)	0.047
7	0.056
10	0.071

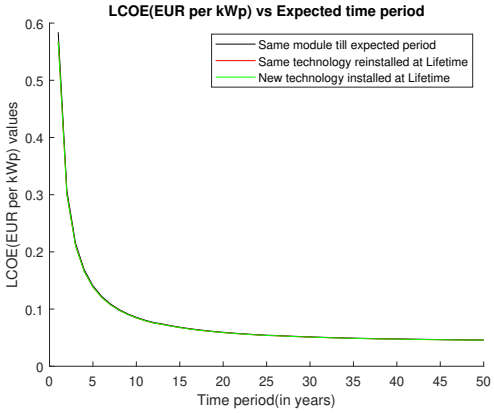

(a) LCOE results for 3 scenarios at Minneapolis.

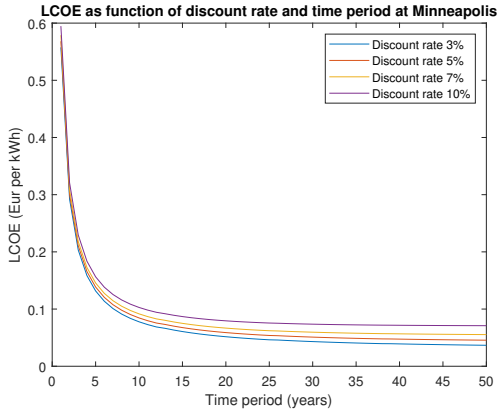

(b) Sensitivity analysis with Discount rate for 3rd scenario at Minneapolis.

Figure 4.6: Financial assessment of cold climatic zone.

4.5. CONCLUSION:

We present a study on significance of LCOE and implementation in PVMD toolbox. Additionally, we demonstrate how the LCOE is impacted by tropical climates with severe degradation, steppe climates with moderate degradation, and cold climates with low degradation available in Bangkok, Almeria, and Minneapolis respectively, as well as a sensitivity analysis of the discount rate in each site. To investigate the effect on LCOE, a hypothetical system was created with the following parameters: system cost, module count, and temporal variables, as shown in table 4.4.

We find that in locations such as Almeria, Spain, where the degradation is moderate their life expectancy is estimated to be 34 years, as discussed in the section 3.6.1. Comparing the LCOE for a 40-year recovery in 2^{nd} and 3^{rd} scenarios to the 1^{st} scenario reveals that for a 3% increase in energy, the LCOE should be increased by 12.8% and 5%, respectively. In order to achieve grid parity and investment costs in Spain, a residential system such as ours must operate for at least five years, resulting in an LCOE of 0.10 € per kWh. Sensitivity study of the discount rate revealed that increasing DR to 10% from the default 5% would result in a 43 percent increase in LCOE, while dropping it to 3% would result in a 14 percent decrease in LCOE. The same example is recreated for Bangkok, Thailand, with a high degradation rate and a lifetime of 13 years. Comparing the LCOE for a 40-year recovery in 2^{nd} and 3^{rd} scenarios to the 1^{st} scenario reveals that to achieve 9.7 percent energy savings, the LCOE needs be increased by 47% and 27.4%, respectively. To reach grid parity and investment costs in Thailand, the system must operate for at least 33 years with a levelized cost of energy (LCOE) of 0.054 € per kWh in scenario 1 and for more than 50 years in other scenarios. Sensitivity analysis indicates that increasing the discount rate from 5% to 10% results in a 35.3% increase in LCOE while dropping the discount rate to 3% results in a 10% decrease in LCOE. Finally, in locations such as Minneapolis, Minnesota, USA, with the lowest degradation rate and a 55-year life expectancy. In all cases, the LCOE required to recover the investment cost over a 40-year period is 0.047 € per kWh, as modules are not changed over the estimated plant operational period. Grid parity and return on investment are achieved after at least seven years of operation at an LCOE of 0.10 € per kWh. Sensitivity study revealed that a discount rate of 10% results in a 50% increase in LCOE when compared to default, while a discount rate of 3% results in a 17% decrease in LCOE.

In conclusion, we observe that tropical climates have the highest LCOE compared to other location and the greatest fluctuation in LCOEs when compared to other scenarios. We discover that when discount rates are varied from their default value, cold climates have the most variance, indicating a strong sensitivity to parameters, followed by tropical climates and steppe climates.

5

TANDEM MODULES

At the moment, crystalline silicon modules account for a significant portion of the PV industry. Despite their commercial dominance, crystalline silicon modules are reaching their theoretical efficiency limit of 29% [94]. As a result, new novel technologies are required to improve the performance of photovoltaic modules. Tandem modules are one such technologies that enables higher performance photovoltaic modules to be built on the same compact package as crystalline silicon modules. They work by stacking various cells with varied bandgaps on top of one another. Solar cells with a large band gap are positioned on top to absorb the sun's high energy spectrum, while solar cells with a small band gap are placed on the bottom to absorb the sun's low energy spectrum. One such combination is perovskite and silicon, which has earned considerable attention due to the intriguing properties of perovskite cells, which include a tunable band gap, high external photoluminescent quantum yield, and low-cost fabrication processes capable of achieving a high efficiency with theoretical limit of 45% [95] [96].

In perovskite(pvk)/silicon(si) tandem cells, among multiple structures the most prominent are: 2 terminal tandem cells (2T cells) and 4 terminal tandem cells (4T cells). 2 terminal tandem cells are constructed by monolithic connection of top perovskite cell with bottom silicon cell in series and 4 terminal tandem cell is constructed by mechanically placing perovskite top cell on silicon bottom cell. There are a few issues with perovskite/silicon tandem cells. The first is determining the optimal combination of perovskite cell composition for a two-terminal monolithic tandem cell in order to maximize efficiency. It was discovered that the perovskite/silicon tandem module is most efficient when the perovskite cell has a bandgap of 1.71 eV [97]. This restriction is necessary because current mismatch is a significant issue in 2T cells, where the top and bottom cells are connected in series. As a result, the top cell must be tuned to create the same amount of current as the bottom cell, so restricting the efficiency [97]. The second difficulty is the stability of perovskite cells, which has significantly improved in recent years [98]. Solving both of these issues would result in increased power and stability, which are essential for perovskite silicon tandem cells to be commercialized in the photovoltaic industry. High-quality perovskite silicon tandem cells may be created utilizing the widely available and cost-effective silicon wafer cell manufacturing sector, providing a significant advantage for commercializing perovskite silicon tandem cells. Thus, while making perovskite silicon cells costs more than silicon wafers, the additional cost is offset by the increased energy production and efficiency of perovskite/silicon tandem cells.

Recent research demonstrates that perovskite exhibits both reversible and irreversible degradation. The irreversible degradation occurred as a result of moisture and oxygen infiltrating the perovskite film and forming non-functional chemicals [99]. Asserting that real-world operating conditions have an effect on the performance, energy generation, lifetime, and financial viability of perovskite silicon tandem cells. To accurately assess the performance and economic viability of tandem modules, the individual degradation of the perovskite and silicon cells, as well as the device design that affects the module's overall degradation, must be assessed.

The purpose of this study is to determine the annual degradation rate allowed in perovskite top layer with a 2T or 4T configuration in order to maintain a 20% power loss during the lifetime of independent crystalline silicon module at the same location. The overall degradation rate determined throughout the analysis is utilized to compute the energy produced by the 2T and 4T modules. Finally, economic evaluations of 2T and 4T modules are conducted in comparison to silicon modules at the location in terms of perovskite degradation rate and manufacturing costs.

5.1. SPECIFICATIONS AND PVMD TOOLBOX IMPLEMENTATION

This section discusses tandem structure used in evaluation and implementation of tandem degradation model in PVMD toolbox.

5.1.1. TANDEM CELL SPECIFICATION

The efficiency of perovskite/silicon tandem cells, which is now well known, has been published as 26.2%. This can be improved further by utilizing a wide bandgap perovskite layer, although broader bandgap perovskite cells suffer from significant V_{oc} losses [100]. Losses in V_{oc} are caused by factor such as low photoluminescence quantum yields, phase instabilities, and an ineffective selective layer. Perovskite cells with a bandgap of 1.7eV exhibit low Fill Factor (FF) qualities (about 77%) in perovskite/silicon tandem cells. The primary reason for low FFs is a high ideality factor (n) of roughly 1.4 to 1.8; thus, decreasing the ideality factor results in increased FFs. The revolutionary structure provided in the report cite solved both V_{oc} losses and high ideality factor [101].

To address the issues raised above, a hole selective layer composed of the methyl group substitution Me-4PACS ([4-(3,6- dimethyl-9H-carbazol-9-yl)butyl]phosphonic acid) was developed. This combination reduced light-induced halide segregation while simultaneously improving photoluminescence quantum yield, resulting in high V_{oc}, high FF, and stability at high temperatures. The structure that has been proposed is depicted in the figure 5.1. The bottom cell is a hetero-junction silicon cell with a thickness of 250μm, and the top cell is a perovskite cell with a 1.68eV and a perovskite(PVK) layer composition of $Cs_{0.05}(FA_{0.77}MA_{0.23})_{0.95}Pb(I_{0.77}Br_{0.23})_3$. It has been proposed that the perovskite cell structure is composed of the following elements: $LiF/Ag/IZO/\ SnO2/C_{60}/LiF/PVK/HTL/ITO$. Monolithic tandem cells with the above combination and structure had an open circuit voltage (Voc) of 1.9 eV, a Fill factor of 79.4 - 85 %, an short circuit current density of 19.24 mA/cm^2 and a power conversion efficiency of 29.15 %. Using the PVMD toolbox, tandem module consisting of 72 cells is constructed for 2T and 4T configurations, yielding P_{stc} values of 556.08 W and 556.31 W with a 29.15 % under STC conditions, respectively.

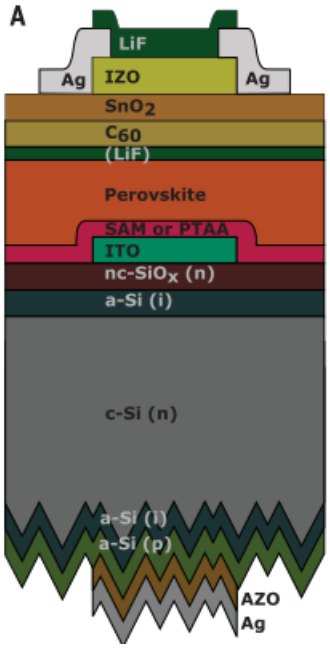

Figure 5.1: monolithic tandem cell structure.

5.1.2. PVMD TOOLBOX IMPLEMENTATION

The nonlinear power loss due to degradation by climatic stress factors in crystalline silicon bottom layer is

computed using the Kaaya model, as explained in chapter 3. Regarding the degradation in perovskite layer, a new GUI is designed that allows the user to specify a linear degradation (in percentage) value for the top layer as an input variable, as shown in figure 5.2. Thus, the overall power loss of the tandem module is estimated using the linear degradation value provided by the user for top perovskite layer and the non-linear power loss value calculated using the Kaaya model for the bottom silicon layer.

The new GUI for top pvk layer degradation has been integrated into the "ELECTRICAL" section of the PVMD toolbox, where the electrical system is built by configuring the structure, electrical losses, bypass diode, cell configuration, and top layer degradation value. After the entire system is configured, the individual currents for the top (I_1) and bottom (I_2) layer are computed, as well as the individual voltages for each layer, denoted by V_1 and V_2. Later, utilizing weighted percentages derived from simulating various degradation rate scenarios described in the report [102] for a 25-year guaranteed silicon module using a Negev site with a 24-year life expectancy.

The total linear degradation value of the top layer is applied to I_1 and V_1. I_1 receives 70% percent of the total linear degradation, whereas V_1 receives the remaining 30%. The bottom silicon layer proceeds in the same manner, now by utilizing nonlinear power loss values obtained from the Kaaya model and weighted percentages. 70% of the total nonlinear power loss is applied to I_2, while 30% is applied to V_2. The degraded IV parameters of each layer(I_1,V_1,I_2 and V_2) are used to calculate the tandem module overall output power. The computed output power with degradation along with output power without degradation (ideal case) of the tandem module is utilized to determine the overall power loss in tandem devices as a function of the specified top layer degradation's.

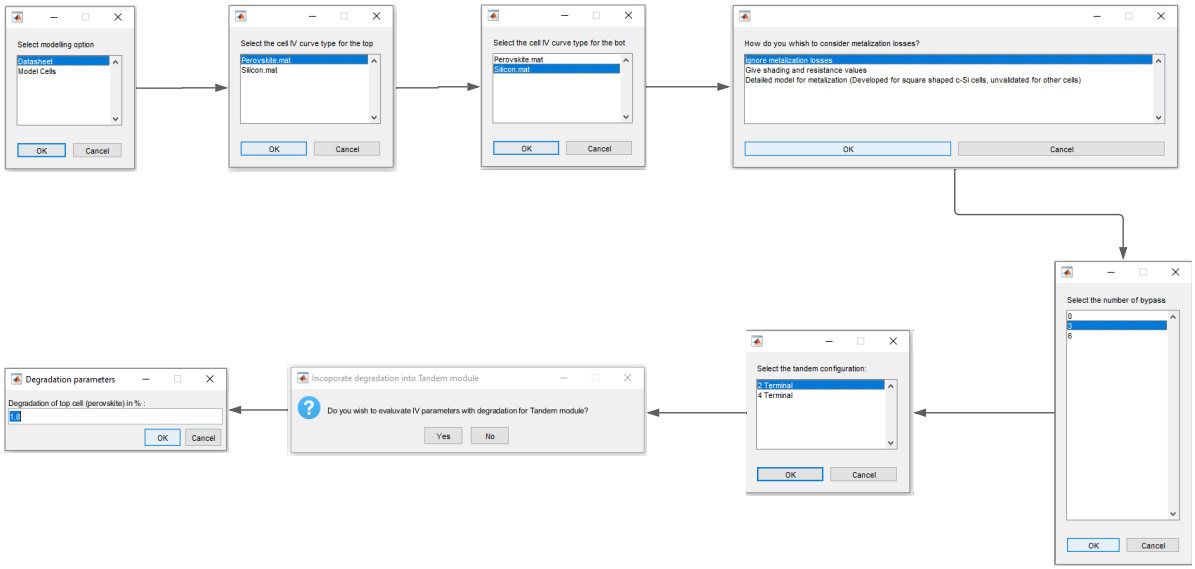

Figure 5.2: GUI flowchart for implementing degradation in Tandem modules.

5.2. VALIDATION OF TANDEM DEGRADATION:

The degradation section is validated using data from the report [102] for perovskite/silicon tandem devices. The modelled perovskite/silicon tandem module in PVMD toolbox has a 29.15% efficiency and a P_{STC} value of 556 W. According to Jiadong Qian, a 2T and 4T perovskite/silicon tandem module should have a perovskite top layer degradation rate of 0.9% and 1.3% per year to retain its 80 percent performance in 25 years, while a silicon bottom layer with a degrades at rate of 0.8% per year.
Similar scenario is replicated in PVMD toolbox using Negev meteorological data to simulate the degradation model for silicon bottom layer. At Negev, it is seen that the performance of independent crystalline silicon module decreases by 20% after operating for 24 years with degradation of 0.75% as seen in section 3.4. This location has similar lifetime of crystalline silicon module as the reference case. Therefore, it is used for vali-

dation of the model in PVMD toolbox. As shown in the table 5.1, the modelled performance of a 2 terminal perovskite/silicon tandem module decreases by 20% after 24 years if the perovskite layer degrades at a rate of 0.9% per year, and 4 terminal perovskite/silicon tandem module if the perovskite layer degrades at a rate of 1.4% per year. The computed parameters are same as reference perovskite layer degradation values in the reference report [102]. Thus validating our model in PVMD toolbox.

Table 5.1: Tandem module degradation with respect to configuration.

Configuration	Reference degradation rate [%]	Modelled degradation rate [%]
2 Terminal	0.9%	0.9%
4 Terminal	1.3%	1.4%

5.3. RESULTS AND DISCUSSION

To investigate various output parameters for 2T and 4T tandem module. We designed a case study with a $Cs_{0.05}(FA_{0.77}MA_{0.23})_{0.95}Pb(I_{0.77}Br_{0.23})_3$ perovskite layer on top and a crystalline silicon layer on the bottom, both with the cell structure shown in figure 5.1. The PVMD toolbox uses GenPro4 software to create the cell structure. Irradiation is computed using sky maps and sensitivity maps. The module's temperature is calculated using a fluid dynamic model. For the case study, the electrical system is configured in the "ELECTRICAL" section, and the process is as illustrated in the figure 5.2, *"Model cells" − > Perovskite top layer − > silicon bottom layer − > ignore metalization losses − > 3 bypass diodes − > 2T or 4T − > evaluate IV parameters with degradation − > Top pvk layer degradation rate "*. This results in the development of a 2T tandem module having 72 cells with a 29.15% efficiency, a short circuit current Isc_{STC} of 4.89A, an open circuit voltage Voc_{STC} of 133.31V, and a power output P_{STC} of 556.08 W under STC conditions. The same design resulted in a 4T tandem module with a 29.15% efficiency, a short circuit current of 4.84A and 4.92A in the top and bottom layer, an open circuit voltage of 81.79V and 51.52V in the top and bottom layer, and a power output of 556.30 Watts. Both configurations exhibited a fill factor of about 85.2%.

5.3.1. NORMALIZED POWER RESULTS FOR 2T AND 4T TANDEM MODULE

Silicon is used as the bottom layer in both tandem module designs. The Kaaya degradation model mentioned in section 3.2.3 is used to calculate the normalized power(NP) output of a silicon bottom layer with tandem structure (as the structure affects the bottom layer temperature, an important parameter for evaluating silicon degradation). We acquired power loss (calculated as $= 1 - NP$) and the lifespan of the bottom silicon layer after computing the degradation model for silicon in order to achieve a 20% performance decline. Two constraints/assumptions are used to compute the degradation of the total tandem module. To begin, the tandem module's temporal computation is restricted by the lifetime of an independent crystalline silicon module at the site for correlation purpose. Second, due to a lack of data on the performance of perovskites, it is anticipated to decrease linearly each year. Using the constraints/assumptions we initiated a tandem module with a defined lifetime, assessed power loss in the bottom layer, and specified linear degradation in the top layer.

The subsequent linear degradation rate of the top layer is varied between 0.2 and 3% per year and the normalized power of the tandem module is determined for each degradation rate at Almeria (with independent crystalline silicon module lifetime of 35 years and avg 0.51% DR). As illustrated in 5.3, a contour map is used to depict the normalized power of tandem module with varying top layer degradation rates (0.2 to 3% per year) and a non-linear simulated bottom layer power loss. The X-Axis indicates the number of years till the tandem module reaches its temporal limit (i.e., the lifetime of the independent crystalline silicon module), the Y-Axis the various degradation rates of the top layer, and the Z-Axis the tandem module's normalized power.

In figure 5.3a and 5.3b, the maximum observed normalized power (z value) is indicated by a light contour code (96%) whilst the lowest observed normalized power (<65%) is indicated by a dark contour code and the area enclosed by blue bounds represents the 80% performance area. Over a 35-year period, we see a 20% reduction in performance for 2T tandem module, while perovskite module degrades at a linear rate of 0.5% per year and 4T tandem module at a linear rate of 0.8% per year. At 0.3% greater DR than the degradation rate of 2T pvk layer, the 4T tandem module achieves its 20% performance loss in 35 years. This is because the top

and bottom layers in the 4T configuration are not coupled, eliminating losses caused by current mismatch and thereby enhancing module performance. When the maximal degradation rate of perovskite is assumed (3% per year), the initial normalized power is around 96% but rapidly declines to 66% near the end (i.e 35 years). While the lowest degradation rate of perovskite (0.2% per year) shows that the initial normalized power was around 96% but it gradually degrades to 85% in both configurations.

Table 5.2: Optimal tandem degradation rate for 35 years lifetime.

Tandem configuration	Optimal degradation rate[% per year]	Lifetime
2 Terminal	0.5	35
4 Terminal	0.8	35

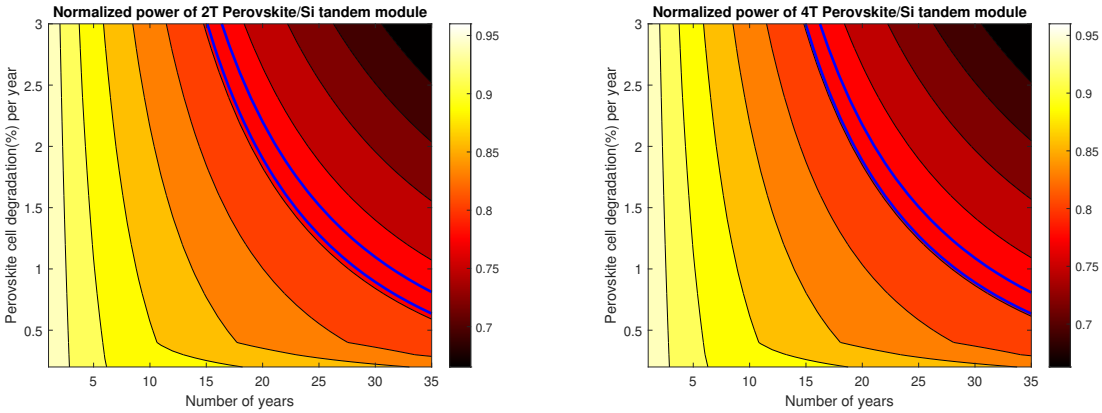

(a) Normalized power for 2T tandem.

(b) Normalized power for 4T tandem.

Figure 5.3: Normalized power as function of top perovskite layer degradation and time at Almeria, Spain.

5.3.2. ENERGY PRODUCTION RESULTS FOR 2T AND 4T TANDEM MODULE

The energy generated by the tandem module is simulated as the sum of the module's power output for each hour in a year with degradation. As with the preceding section, the energy generated is displayed as a function of the degradation rate and time of the perovskite layer. The contour plot in figure 5.4a and 5.4b illustrates the total energy generated by tandem module during that particular year. The X-axis indicates the number of years, the Y-axis indicates the degradation rate of perovskite, which ranges from 0.2 to 3% per year, and the Z-axis indicates the amount of energy produced in kWh per year at Almeria. The yellow contour shows the most amount of energy generated, while the blue contour indicates the least amount of energy generated.

According to the previous section 5.3.1, a recommended perovskite degradation rate of 0.5% in a 2T tandem module results in a 20% reduction in performance upon 35 years (the same lifespan as a independent crystalline silicon module); under these conditions, the 2T tandem module generates 32.3 MWh over 35 years. As illustrated in figure 5.4c, the perovskite layer with the lowest degradation rate (0.2% per year) produces the most energy (33.3 MWh) over a 35-year period, while the layer with the highest degradation rate (3% per year) produces the least energy (29.5 MWh) over the same period as seen in table 2.3b. Thus, for a place such as Almeria with degradation rate of 0.51% for silicon module, constructing a tandem module with the lowest degradation rate for top pvk layer, which requires more resources, produces 13% more energy than designing a perovskite layer with a high degradation rate.

As demonstrated in figure 5.4c, it is recommended that the perovskite layer in a 4T tandem module degrades at a rate of 0.8% per year, resulting in a 20% degradation in performance after 35 years; under these conditions, the 4T tandem would generate 32.4 MWh of energy over its lifetime. When a degradation rate of 0.2% per year is considered, 33.8 MWh of energy is generated over a 35-year period, while a degradation rate of

3% per year generates 29.9 MWh of energy over the same period. Thus, if we create a tandem module with low pvk degradation, we can generate 13% more energy than if we construct a module with high pvk degradation.

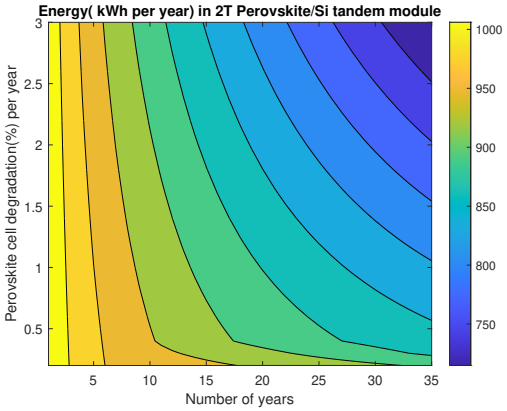

(a) Energy produced by 2T tandem.

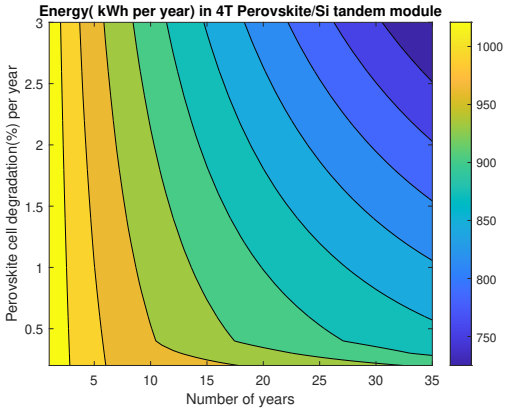

(b) Energy produced by 4T tandem.

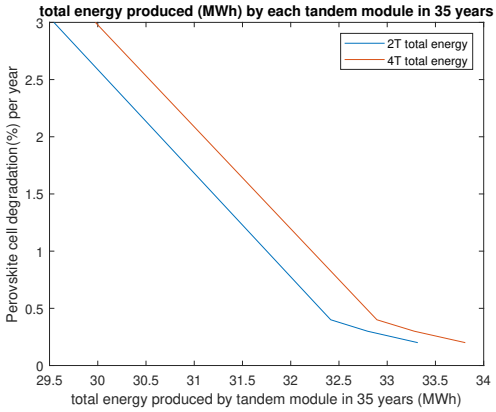

(c) Total energy produced by 4T and 2T in 35 years.

Figure 5.4: Energy produced as function of top perovskite layer degradation at Almeria, Spain.

5.3.3. ENERGY COMPARISON OF 2T AND 4T TANDEM MODULE WITH CRYSTALLINE SILICON MODULE

Moreover, we compare the energy generated by tandem modules to that produced by independent crystalline silicon modules at the location-Almeria. We examine the ratio of energy produced each year by tandem module to energy produced by crystalline silicon module in each year as a function of the degradation rate of the perovskite top layer. A contour plot is used for this purpose, as illustrated in figures figure 5.5a and 5.5b, where the X-axis represents the number of years, the Y-axis represents the degradation rate of the perovskite top layer, and the Z-axis represents the ratio of energy produced by tandem module and independent crystalline silicon module at the location for each year. The violent code represents the highest energy ratio (1.24), while the blue code represents the lowest energy ratio (1). For example, a 2T tandem module with a perovskite degradation rate of 1% per year on 10^{th} year would generate 22% more energy than a typical crystalline silicon module at the site, while a 4T tandem module would generate 23% more energy on 10^{th} year. In other example, a 2T tandem module with a DR of 2% each year would produce 13% more energy than crystalline silicon, whereas a 4T tandem module would produce 15% more energy than a conventional silicon module in that year.

When a 2T tandem module is configured, it is compared to a crystalline silicon module with a degradation rate of 0.51%, a module efficiency of 24.39% and P_{STC} of 458.54 W. The highest conceivable yearly energy

ratio is 1.22 for 0.2% perovskite degradation in first year, while the lowest possible annual energy ratio is 1 for a 3% degradation rate in the 35^{th} year. In a 4T tandem module, we observe a maximum annual energy ratio of 1.24 in the first year for a 0.2% degradation rate of perovskite and a minimum of 1 for a 3% degradation rate in the 35^{th}year.

The figures 5.5c show the ratio of total energy generated by tandem module and crystalline silicon module over a 35-year period. We observe that a perovskite layer with a DR of 0.2%, 0.5%, or 3% per year in a 2T tandem module would generate 26%, 22%, or 11% more energy than a crystalline silicon module. At 0.2%, 0.8%, and 3% DR each year, a 4T tandem module would produce 28%, 23%, and 13% more total energy than crystalline silicon module. It is interesting to note that 4T module generates more energy than 2T when compared with crystalline silicon modules in all cases of top layer degradation.

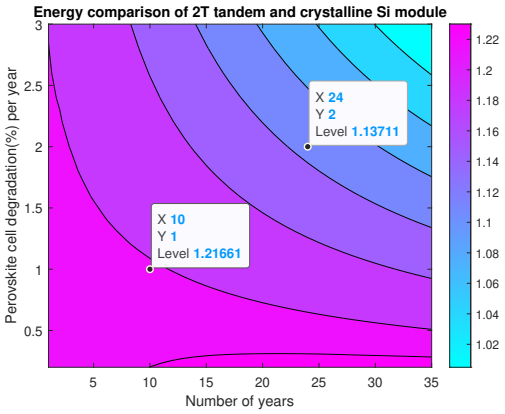

(a) Ratio of energy produced each year by 2T and crystalline silicon module.

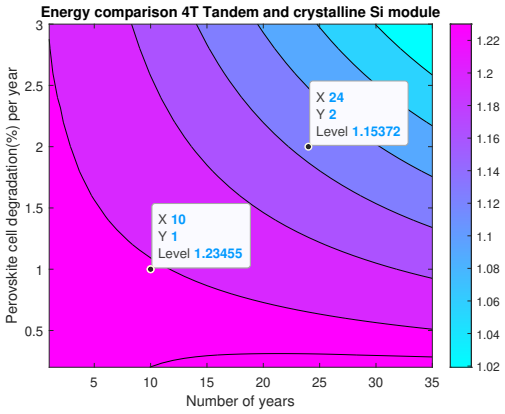

(b) Ratio of energy produced each year by 4T and crystalline silicon module.

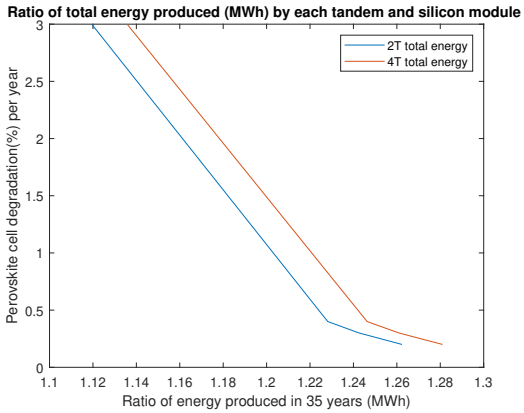

(c) Ratio of total energy produced from 4T and 2T by crystalline silicon in 35 years.

Figure 5.5: Energy comparison as function of top layer degradation and configuration at Almeria, Spain.

5.3.4. FINANCIAL ANALYSIS OF TANDEM MODULE

Economic feasibility is critical when it comes to commercializing any technology or project. As a result, we conducted a study comparing the LCOE of 2T or 4T tandem modules to that of crystalline silicon modules. We give the ratio of the LCOE of a tandem module with a 2T or 4T configuration to that of an independent crystalline silicon module as a function of the degradation rate of the perovskite top layer. This variable can be used to assess the economic benefit of using a tandem module rather than a standard crystalline silicon module at a particular location. We use the same location as in prior experiments - Almeria, Spain - for this study. The figures 5.6a and 5.6b denote the ratio of the LCOE of a 2T and an independent crystalline silicon module, and of a 4T and a crystalline silicon module, respectively, as a function of perovskite degradation. Due to the fact that perovskite modules are not yet commercially viable, there is a lack of financial data re-

garding perovskite modules. As a solution, we made a few assumptions, one of which is that the cost of manufacturing tandem modules is a certain percentage higher than the cost of manufacturing crystalline silicon modules. The percentages used to calculate the cost of tandem module manufactured are 5,10,20,40,60, and 80%, meaning cost of tandem module [€ per kW] =*crystalline silicon module cost per kW+crystalline silicon cost per kW∗x%* (where x is the specified percentage). This modelled module cost of tandem is used to calculate the module costs inputs for the table 4.1 built in the PVMD toolbox's LCOE section 4.2.1. A comparable setup to that utilized in section 4.4 is replicated for tandem module, but with a fixed and grid-connected residential system rated at 7.2 kW. As mentioned in section 4.2.1, the cost of crystalline silicon modules was 395.5 € per kW. Applying a cost percentage of 5, 10, 20, 40, 60, and 80% to determine tandem module costs results in 415.2, 435, 474.5, 553.6, 632.8, and 771.85 € per kW. Electrical, inverter, structural, and operation and maintenance costs are assumed to be identical, i.e. 193.53, 151.45, 84.14, and 16.8 € per kW, respectively. In each case of tandem module costing, the LCOE for total investment recovery for 35 year is determined.

The ratio of LCOEs is defined as function degradation rate of perovskite layer and additional manufacturing cost. The additional cost of manufacturing tandem module is depicted in figure 5.6 as a blue cross, red circles, yellow plus, purple asterisk, green square, and blue diamonds for percentages of 5, 10, 20, 40, 60, and 80%. The X-axis indicates the ratios of LCOEs, the Y-axis reflects the degradation rate of perovskites, and the curves represent production costs.For instance, suppose a 2T tandem module costs 40% more than crystalline silicon modules and the perovskite layer in this tandem module declines at an optimal rate of 0.5% each year. The LCOE required to repay the investment cost of a tandem module is 13% greater than the LCOE of a crystalline silicon module after 35 years. In worst possible combination if tandem modules are made at a cost of 80% more than silicon modules and perovskite degrades at a rate of 3% per year, the LCOE of tandem modules should be 40% higher than silicon modules. The LCOE of a 4T tandem module at 40% higher cost and 0.8% optimal degradation is 12% more than that of a crystalline silicon module. In 4T, the worst combination requires a 38% increase in LCOE. In other case If tandem modules are operated at a 10% higher cost and the perovskite layer degrades at a 0.2% annual rate, the LCOE of the 2T and 4T tandem module is 2% and 4% lower than that of the silicon module. Indicating that employing tandem modules is more cost effective than using crystalline silicon modules in this combination.

As mentioned previously in section 5.3.1, we are interested in the degradation rate of perovskite at 0.5 and 0.8% for 2T and 4T, respectively, in Almeria. For a 2T tandem module with a degradation rate of 0.5 percent and manufacturing costs increasing by 5,10,20,40,60, and 80 percent, the LCOE value increases by 0.3, 2, 6, 13, 19.5, and 32%, respectively. With 0.8 percent perovskite degradation and manufacturing costs increasing by the above percentages, the LCOE values of the 4T tandem module increase by -1,1,5,12,19, and 30%, respectively. It is interesting to observe that at 5% additional cost and optimal degradation rates 2T reaches equilibrium with silicon module but 4T LCOE is in forward equilibrium indicating tandem module have lower LCOE than crystalline silicon module.

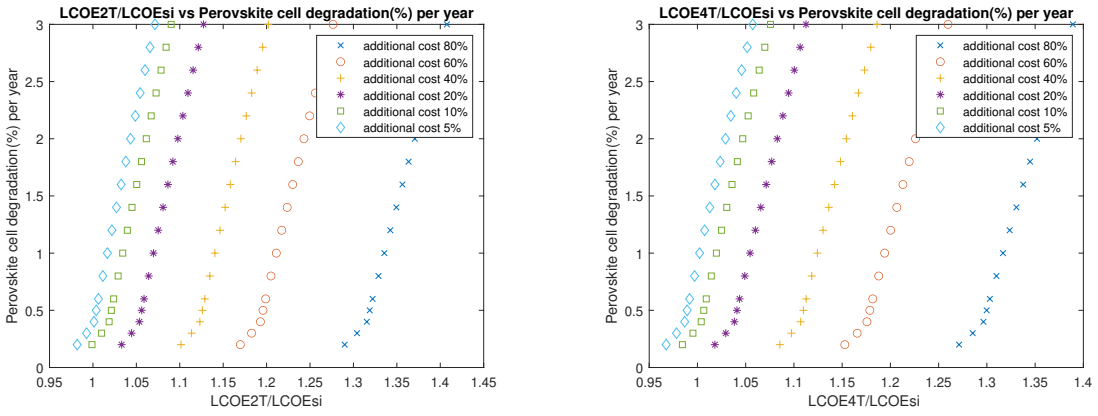

(a) LCOE ratios of 2T and crystalline silicon module.

(b) LCOE ratios of 4T and crystalline silicon module.

Figure 5.6: LCOE comparison of tandem module and silicon module as function of perovskite degradation and manufacturing cost.

5.4. CONCLUSION

We built a degradation model for perovskite silicon tandem module in this study and combined it with the module's IV parameters, as well as implemented it in the PVMD toolbox. A tandem structure as mentioned in figure 5.1 is used to design a module in PVMD toolbox with 72 cells resulted in 556.08W for 2T and 556.31W for 4T tandem under STC conditions. The current electrical model in the PVMD toolbox has been updated to account for tandem module degradation effects using weighted averages. To conduct the study on tandem modules, a few constraints were imposed: (1) the computation period for degradation in tandem modules is limited to the lifetime of an independent crystalline silicon module at the location (calculated using the Kaaya model from section 3.2.3) to be able to correlate them; and (2) the perovskite top layer is assumed to degrade linearly with time due to a dearth of data on perovskite performance. This model was validated using data from the report [102], which indicates that 2T and 4T perovskite silicon tandem modules with degradation rates of 0.9% and 1.3% respectively, meet the manufacturers' 25-year warranty. Negev with lifetime of 24 years and 0.74% DR is utilized to simulate the scenario described in the paper. It demonstrated that when 2T and 4T perovskite layer degradation rate is 0.9% or 1.4% per year, respectively, the anticipated performance of 2T and 4T tandem module decreases by 20%. Thus, the model's validation is completed.

Further studies are performed for Almeria, Spain where Kaaya model predicts a 35-year lifetime for the crystalline silicon tandem module. Tandem module performance ratios was investigated here. Degradation rates of 0.2 to 3% per year for perovskite top layer generate performance ratios of 96 to 66%. Tandem modules at Almeria are expected to last for 35 years (lifetime silicon modules), with a maximum degradation rate of 0.5% and 0.8% per year for 2T and 4T top perovskite layer, respectively. The total energy generated by 2T and 4T tandem modules is also investigated.
To add intrigue to the result, we investigate the total energy generated by 2T and 4T tandem modules over a 35-year period using independent crystalline silicon modules. It is shown that 0.5% degradation (optimal) in a 2T tandem module result in 22% greater total energy than crystalline silicon module at the location. At the site, a 4T tandem module with a degradation rate of 0.8% (optimal) generates 23% more total energy than the market-dominant crystalline silicon modules. When extreme degradation rates of 0.2% and 3% are investigated, we see both 2T and 4T produce 13% more energy in 0.2% DR.

Financial analysis is crucial in determining the feasibility of a project. Thus, the LCOE of 2T and 4T tandem modules is compared to the LCOE of an independent crystalline silicon module for Almeria as a function of the degradation rate of the perovskite layer over a 35-year recovery period. To compare the LCOEs of tandem and crystalline silicon modules, a ratio of their LCOEs is utilized. Due to a shortage of data on tandem module costs, they are assumend to have produced at additional cost of 5,10,20,40,60, and 80% than silicon modules. For a 35-year lifetime, a 2T tandem with an ideal perovskite degradation rate of 0.5% and 40% greater production costs requires a 13% higher LCOE than crystalline silicon. Similarly, 4T requires 12% higher LCOE than crystalline silicon for the perovskite's with ideal degradation rate of 0.8% and 40% additional cost. Economic equilibrium is obtained when a 2T tandem module operates at a DR of 0.5% and a manufacturing cost of 5%, with the LCOE of tandem being roughly identical to that of crystalline silicon. At 0.8% DR and 10% higher manufacturing cost, the 4T tandem achieves economic equilibrium. It's worth noting that 4T tandem at 0.8% DR and 5% additional manufacturing cost require cheaper LCOE than crystalline silicon.

6

CONCLUSION

This chapter presents a summary of findings and work done for the objectives provided in the chapter 1.1 in this MSc thesis project along with recommendations for future development that can be carried out.

The main goal for the project to is

Evaluate lifetime yield of crystalline silicon and perovskite/silicon tandem module along with financial analysis and implementation in PVMD Toolbox.

Section 6.1 discusses how the main goal was achieved through three objectives. Improvements made in PVMD toolbox are presented in section 6.2 and finally, the recommendation for future work are presented in section 6.3.

6.1. FINAL CONCLUSION

The section 3.2 described the construction of a hybrid model that incorporates both statistics and physics-based models. We selected to address the gaps in knowledge found in the literature study by implementing Ismail Kaaya's hybrid model (referred to as the Kaaya model). We use the mathematical models described to calculate the degradation rates associated with the major mechanisms of degradation, namely hydrolysis, photo, and thermo-mechanical degradation, and then integrate them into a single total degradation rate variable. The computed degradation rate, in conjunction with the model parameters , initiate the non-linear power loss model, which is described in detail in section 3.2.3, along with a flowchart illustrating the methods used. To assess crystalline silicon module degradation under various climatic circumstances, five Koppen-Geiger photovoltaic (KGPV) classed climatic zones are used. The characteristics of these climate zones are as follows. The tropical zone with high irradiation (AH) in Bangkok, Thailand, has a degradation rate of 1.31% and a lifetime of 13.4 years, the desert with extremely high high irradiation (BK) in Atacama, Chile, has a degradation rate of 0.53% and a lifetime of 33.4 years, the steppe with high irradiation (CH) in Almeria, Spain, has a degradation rate of 0.52% and a lifetime of 24 years, temperate with high irradiation (DH) in Atlanta, USA has 0.67% degradation rate and 26.2 years lifetime ,and cold with medium irradiation in Minneapolis, USA has 0.33% degradation rate with 55.9 years. Tropical climates degrade the most in in all mechanisms, while cold climates degrade the least in all mechanisms except thermo-mechanical degradation caused by large temperature changes. Contrary to popular belief, tropical climes outperformed desert regions in terms of photo-degradation due to the presence of higher relative humidity. The overall degradation data indicated that tropical has the greatest loss of power, followed by temperate, steppe, and desert, and finally cold. The final power loss in the desert and steppe zones seems to be equal because the average stress in the desert is offset by a single high stressor(i.e, temperature) in the steppe. It is critical to highlight that the Atacama location chosen for the desert zone is close to the ocean, resulting in a greater relative humidity than average.

The financial analysis is conducted using the LCOE measure. Tropical, steppe, and cold climates are chosen as extreme, intermediate, and least degraded areas, respectively. For the case study, a hypothetical residential fixed and grid-connected system with a rated power of 6.5kW is constructed. The results indicate that for a 40-year investment recovery period in Almeria (steppe climate), replacing degraded modules with new modules at the same price will result in a 12.8% increase in LCOE, while replacing with new modules at a lower price of that time will result in a 5% increase in LCOE. Sensitivity analysis utilizing the discount rate revealed that increasing the discount rate from 5% to 10% results in a 43% increase in LCOE, while decreasing it to 3% results in a 2% drop in LCOE. At the moment, grid parity and investment recovery can be achieved

with a minimum of five years of operation of a photovoltaic project in Almeria. Similar research conducted in Bangkok (tropical environment) revealed LCOE increase of 47.4% and 27.4% for scenarios 2 and 3 that is using the same price module and lower priced modules, respectively. Sensitivity analysis revealed a 35.3% and 10% rise in LCOE, respectively, when the discount rate was increased from 5% to 10% and 3%. Grid parity and investment recovery are possible in Bangkok for residential systems after 33 years of operation; scenarios 2 and 3 take more than 50 years. Because Minneapolis (cold climate) has a 56-year life expectancy, the module does not need to be updated over the 40-year investment recovery period, leading in no change in the LCOE for any scenario. Perhaps sensitivity study revealed that a 5% to 10% change in discount rate results in a 50% reduction in LCOE and a 2% reduction for a 5% to 3% change. These findings indicate that switching to new, less expensive modules in Tropical (high degradation) climates has a great influence on LCOE than in steppe climates (moderate degradation). Discount rate variation has the greatest impact on LCOE in cold climates (lowest DR), followed by tropical and steppe regions.

The method and results of tandem module degradation are presented in section 5.1. In PVMD toolbox, a 72-cell tandem module utilizing perovskite and silicon cells is produced with a 29.15% efficiency and an output power of 556W and 556.30W for 2T and 4T, respectively. To achieve a 35-year lifetime for a tandem module, i.e., the lifetime of a crystalline silicon module at the location calculated using the Kaaya degradation model in a steppe climate such as Almeria, perovskite cells must degrade at a degradation of 0.5% and 0.8% per year for 2T and 4T configurations, respectively, and as a result, they yield 22% and 23% more energy than crystalline silicon modules, respectively. It is critical to note that the 0.3% leverage observed in the 4T module is due to the absence of a current mismatch resulting in a performance loss. The 2T and 4T modules are compared to the market-leading crystalline silicon modules, which have a power output of 458.54W and an efficiency of 24.4% and are likely to be commercialized in the next decade. At a least degradation rate of 0.2%, 2T and 4T generate 26% and 28% more energy than crystalline silicon, respectively; at a high degradation rate of 3%, we see 11% and 13% more energy than silicon modules. The financial analysis compares the LCOE of tandem modules with crystalline silicon. The cost of tandem modules is specified as being 5, 10, 20, 40, 60, and 80% higher than the cost of contemporary silicon modules. 2T modules with a 0.5% degradation and a 40% increase in manufacturing cost resulted in a 13% higher LCOE than silicon modules, whereas 4T modules with a 0.8% degradation and a 40% increase in manufacturing cost resulted in the same 13 percent higher LCOE as silicon modules. Indicating that both the 2T and 4T modules function identically at optimal degradation and added cost. Economic equilibrium is established in 2T at a degradation rate of 0.5% for the pvk layer and 5% additional cost for the tandem, and in 4T at a degradation rate of 0.8% and 10% additional cost. It is intriguing that 4T at 0.8% DR and 5% additional cost results in forward equilibrium with tandem, demonstrating that tandem modules are a preferable investment than silicon in Almeria's steppe climate.

6.2. IMPLEMENTATION IN PVMD TOOLBOX:

The developed model are integrated into the toolbox and validated for performance. They are provide with user interactive GUI for better experience. Implementations include:

1. Degradation Model: A new degradation section has been added to the toolbox, complete with a graphical user interface for specifying the location's name and operation period till which normalized power are calculated irrelevant to lifetime. The weather section is updated in accordance with the input required to create the degradation model. The degradation section generates two graphical and MATLAB variables. The graphical result includes a representation of the normalized power due to each degradation mechanism as well as the total degradation during the lifetime of the module. Variable output include degradation rates and normalized power values as a result of the degradation.

2. Financial section: A new financial section has been included to compute the LCOE. The interactive graphical user interface (GUI) displays the number of modules, system costs (segregated), discount rate, and other economic scenarios, as well as the annual growth rate. The output includes a visual representation of the annual LCOE necessary to recover the investment in that year as a function of economic scenarios and MATLAB variable. The MATLAB variable contains the LCOE and discounted energy values, as well as the total amount of actual energy produced and the overall system cost for the selected operational time.

3. Tandem section: The electrical section has been modified to account for degradation in the IV char-

acteristics of silicon and pvk/si tandem modules. The updated graphical user interface now offers the ability to specify the rate of perovskite degradation. The final output is a MATLAB variable including degraded parameters for each year, such as DC power and average normalized power.

6.3. RECOMMENDATIONS

Some improvement that are possible for future studies are as following:

1. A weather research and forecast model can be used to increase the accuracy of the degradation model by predicting environmental stress values such as relative humidity, ambient temperature's and UV radiations in future.
2. Conducting research on PV module recycling solutions can be employed in the financial area, as recycling generates revenue for degraded modules that must be replaced.
3. Financial assessment can be further improved by incorporating variable to account new efficient power generating module for energy calculation in future.

BIBLIOGRAPHY

[1] A. J. Curran, C. Birk Jones, S. Lindig, J. Stein, D. Moser, and R. H. French, *Performance loss rate consistency and uncertainty across multiple methods and filtering criteria,* in 2019 IEEE 46th Photovoltaic Specialists Conference (PVSC) (2019) pp. 1328–1334.

[2] S. Lindig, I. Kaaya, K. Weiss, D. Moser, and M. Topic, *Review of statistical and analytical degradation models for photovoltaic modules and systems as well as related improvements,* IEEE Journal of Photovoltaics **8**, 1773 (2018).

[3] D. C. Jordan, C. Deline, M. G. Deceglie, A. Nag, G. M. Kimball, A. B. Shinn, J. J. John, A. A. Alnuaimi, A. B. A. Elnosh, W. Luo, A. Jain, M. U. Saleh, H. von Korff, Y. Hu, J. Jaubert, and F. Mavromatakis, *Reducing interanalyst variability in photovoltaic degradation rate assessments,* IEEE Journal of Photovoltaics **10**, 206 (2020).

[4] K. Ismail, M. Koehl, A. P. Mehilli, M. Sidrach-de Cardona, and K. Weiss, *Photovoltaic lifetime forecast: Models for long-term photovoltaic degradation prediction and forecast,* UMA Editorial **PP**, 22 (2020).

[5] I. Kaaya et al., *Photovoltaic lifetime forecast: Models for long-term photovoltaic degradation prediction and forecast,* (2020).

[6] J. Ascencio-Vasquez, K. Brecl, and M. Topic, *Methodology of köppen-geiger-photovoltaic climate classification and implications to worldwide mapping of pv system performance,* Solar Energy **191**, 672 (2019).

[7] A. Jasevics, L. Zemite, and L. Petrichenko, *A comparative assessment of the deployment of pv technologies in the baltics and in the european union,* 2018 IEEE 6th Workshop on Advances in Information, Electronic and Electrical Engineering (AIEEE), , 1 (2018).

[8] L. Oberbeck, K. Alvino, B. Goraya, and M. Jubault, *Ipvf's pv technology vision for 2030,* Progress in Photovoltaics: Research and Applications **28**, 1207 (2020).

[9] A. Ndiaye, A. Charki, A. Kobi, C. M. Kébé, P. A. Ndiaye, and V. Sambou, *Degradations of silicon photovoltaic modules: A literature review,* Solar Energy **96**, 140 (2013).

[10] G. Belluardo, P. Ingenhoven, W. Sparber, J. Wagner, P. Weihs, and D. Moser, *Novel method for the improvement in the evaluation of outdoor performance loss rate in different pv technologies and comparison with two other methods,* Solar Energy **117**, 139 (2015).

[11] S. Lindig, I. Kaaya, K.-A. Weiß, D. Moser, and M. Topic, *Review of statistical and analytical degradation models for photovoltaic modules and systems as well as related improvements,* IEEE Journal of Photovoltaics **8**, 1773 (2018).

[12] A. B. Subramaniyan, R. Pan, J. Kuitche, and G. TamizhMani, *Quantification of environmental effects on pv module degradation: A physics-based data-driven modeling method,* IEEE Journal of Photovoltaics **8**, 1289 (2018).

[13] A. Limmanee, S. Songtrai, N. Udomdachanut, S. Kaewniyompanit, Y. Sato, M. Nakaishi, S. Kittisontirak, K. Sriprapha, and Y. Sakamoto, *Degradation analysis of photovoltaic modules under tropical climatic conditions and its impacts on lcoe,* Renewable Energy **102**, 199 (2017).

[14] I. de France (IPVF), *30 cube goal for modules,* (2014).

[15] A. Abate, *Perovskite solar cells go lead free,* Joule **1**, 659 (2017).

[16] K. Jansen and A. Delahoy, *A laboratory technique for the evaluation of electrochemical transparent conductive oxide delamination from glass substrates,* Thin Solid Films **423**, 153 (2003).

[17] M. Köntges, S. Kurtz, C. Packard, U. Jahn, K. Berger, K. Kato, T. Friesen, H. Liu, M. Van Iseghem, j. Wohlgemuth, D. Miller, M. Kempe, P. Hacke, F. Reil, N. Bogdanski, W. Herrmann, C. Buerhop, G. Razongles, and G. Friesen, *Review of failures of photovoltaic modules,* (2014).

[18] F. Pern, *Ethylene-vinyl acetate (eva) encapsulants for photovoltaic modules: Degradation and discoloration mechanisms and formulation modifications for improved piiotostability,* Die Angewandte Makromolekulare Chemie **252**, 195 (2003).

[19] M. Köntges, I. Kunze, S. Kajari-Schröder, X. Breitenmoser, and B. Bjørneklett, *The risk of power loss in crystalline silicon based photovoltaic modules due to micro-cracks,* Solar Energy Materials and Solar Cells **95**, 1131 (2011).

[20] S. Richter, M. Werner, S. Swatek, and C. Hagendorf, *Understanding the snail trail effect in silicon solar modules on microstructural scale,* (2012).

[21] D. Lausch, V. Naumann, A. Graff, A. Hähnel, O. Breitenstein, C. Hagendorf, and J. Bagdahn, *Sodium outdiffusion from stacking faults as root cause for the recovery process of potential-induced degradation (pid),* Energy Procedia **55**, 486 (2014).

[22] K. Kato, *PVRessQ!: a research activity on reliability of PV systems from an user's viewpoint in Japan,* in Reliability of Photovoltaic Cells, Modules, Components, and Systems IV, Vol. 8112, edited by N. G. Dhere, J. H. Wohlgemuth, and K. W. Lynn, International Society for Optics and Photonics (SPIE, 2011) pp. 159 – 167.

[23] V. Sharma and S. S. Chandel, *Performance and degradation analysis for long term reliability of solar photovoltaic systems: A review,* Renewable and Sustainable Energy Reviews **27**, 753 (2013).

[24] D. Jordan, T. Silverman, J. Wohlgemuth, S. Kurtz, and K. VanSant, *Photovoltaic failure and degradation modes: Pv failure and degradation modes,* Progress in Photovoltaics: Research and Applications **25** (2017), 10.1002/pip.2866.

[25] R. L. D. DeGraaff and Z. Campeau, *Degradation mechanisms in si module technologies observed in the field; their analysis and statistics,* Presentation at PV Module Reliability Workshop, NREL (2011).

[26] A. Skoczek, T. Sample, and E. Dunlop, *The results of performance measurements of field-aged crystalline silicon photovoltaic modules,* Progress in Photovoltaics: Research and Applications **17**, 227 (2009).

[27] S. Sakamoto and T. Oshiro, *Field test results on the stability of crystalline silicon photovoltaic modules manufactured in the 1990s,* (2003) pp. 1888 – 1891 Vol.2.

[28] D. Jordan and S. Kurtz, *Photovoltaic degradation rates—an analytical review,* Progress in Photovoltaics: Research and Applications **21** (2013), 10.1002/pip.1182.

[29] A. M. Reis, N. T. Coleman, M. W. Marshall, P. A. Lehman, and C. E. Chamberlin, *Comparison of pv module performance before and after 11-years of field exposure,* in Conference Record of the Twenty-Ninth IEEE Photovoltaic Specialists Conference, 2002. (2002) pp. 1432–1435.

[30] S. Sakamoto and T. Oshiro, *Field test results on the stability of crystalline silicon photovoltaic modules manufactured in the 1990s,* (2003) pp. 1888 – 1891 Vol.2.

[31] D. King, M. Quintana, J. Kratochvil, D. Ellibee, and B. Hansen, *Photovoltaic module performance and durability following long-term field exposure,* Progress in Photovoltaics: Research and Applications **8**, 241 (2000).

[32] A. Realini, N. Cereghetti, D. Chianese, and S. Rezzonico, *Performance of old pv modules: measurement of 25 years old crystalline silicon module,* (2006).

[33] G. Saleh IM, Abouhdima I, *Performance of thirty years stand alone photovoltaic system,* (2009).

[34] N. G. Dhere, S. A. Pethe, and A. Kaul, *Photovoltaic module reliability studies at the florida solar energy center,* in 2010 IEEE International Reliability Physics Symposium (2010) pp. 306–311.

[35] J. Adelstein and B. Sekulic, *Performance and reliability of a 1-kw amorphous silicon photovoltaic roofing system,* in Conference Record of the Thirty-first IEEE Photovoltaic Specialists Conference, 2005. (2005) pp. 1627–1630.

[36] J. . S. W. McNutt, P.; Adelstein, *Performance evaluation of a 1.5-kwdc a-si pv array using the pvusa power rating method at nrel's outdoor test facility,* (2005).

[37] M. P. S. F. F. T. Y. O. F. Apicella, V. Giglio, *Thin film modules: Long term operational experience in mediterranean climate,* (2008) pp. 3422 – 3425.

[38] Z. S. H.-D. Musikowski, *Analysis of the operational behavior and long-term performance of a cis pv system,* (2010) pp. 3942 – 3946.

[39] D. C. Jordan and S. R. Kurtz, *Thin-film reliability trends toward improved stability,* in 2011 37th IEEE Photovoltaic Specialists Conference (2011) pp. 000827–000832.

[40] B. Meyers, M. Tabone, and E. Kara, *Statistical clear sky fitting algorithm,* (2018).

[41] M. J. Reno and C. W. Hansen, *Identification of periods of clear sky irradiance in time series of GHI measurements,* Renewable Energy **90**, 520 (2016).

[42] T. Huld, G. Friesen, A. Skoczek, R. Kenny, T. Sample, M. Field, and E. Dunlop, *A power-rating model for crystalline silicon pv modules,* Solar Energy Materials and Solar Cells - SOLAR ENERG MATER SOLAR CELLS **95**, 3359 (2011).

[43] C. Jennings, *Pv module performance at pg e,* in Conference Record of the Twentieth IEEE Photovoltaic Specialists Conferen (1988) pp. 1225–1229 vol.2.

[44] C. M. Whitaker, T. U. Townsend, H. J. Wenger, A. Iliceto, G. Chimento, and F. Paletta, *Effects of irradiance and other factors on pv temperature coefficients,* in The Conference Record of the Twenty-Second IEEE Photovoltaic Specialists Conference - 1991 (1991) pp. 608–613 vol.1.

[45] G. Belluardo, P. Ingenhoven, W. Sparber, J. Wagner, P. Weihs, and D. Moser, *Novel method for the improvement in the evaluation of outdoor performance loss rate in different pv technologies and comparison with two other methods,* Solar Energy **117** (2015), 10.1016/j.solener.2015.04.030.

[46] M. Malvoni, N. Manoj Kumar, S. Chopra, and N. Hatziargyriou, *Performance and degradation assessment of large scale grid-connected solar photovoltaic power plant in tropical semi-arid environment of india,* Solar Energy **203**, 101 (2020).

[47] A. Phinikarides, G. Makrides, B. Zinsser, M. Schubert, and G. Georghiou, *Analysis of photovoltaic system performance time series: Seasonality and performance loss,* Renewable Energy **77**, 51 (2015).

[48] C. C. Holt, *Forecasting seasonals and trends by exponentially weighted moving averages,* International Journal of Forecasting **20**, 5 (2004).

[49] A. Phinikarides, G. Makrides, and G. Georghiou, *Comparison of analysis methods for the calculation of degradation rates of different photovoltaic systems,* (2013).

[50] A. Phinikarides, N. Kindyni, G. Makrides, and G. Georghiou, *Review of photovoltaic degradation rate methodologies,* Renewable and Sustainable Energy Reviews **40**, 143–152 (2014).

[51] K. Ismail, S. Lindig, K. Weiss, A. Virtuani, M. Sidrach-de Cardona, and D. Moser, *Photovoltaic lifetime forecast model based on degradation patterns,* Progress in Photovoltaics: Research and Applications **28** (2020), 10.1002/pip.3280.

[52] M. Kempe, G. Jorgensen, K. Terwilliger, T. McMahon, C. Kennedy, and T. Borek, *Acetic acid production and glass transition concerns with ethylene-vinyl acetate used in photovoltaic devices,* Solar Energy Materials and Solar Cells **91**, 315 (2007).

[53] A. Masuda, N. Uchiyama, and Y. Hara, *Degradation by acetic acid for crystalline si photovoltaic modules,* Japanese Journal of Applied Physics **54**, 04DR04 (2015).

[54] R. Pan, J. Kuitche, and G. Tamizhmani, *Degradation analysis of solar photovoltaic modules: Influence of environmental factor,* (2011) pp. 1 – 5.

[55] B. Braisaz, C. Duchayne, M. Van Iseghem, and K. Radouane, *Pv aging model applied to several meteorological conditions,* (2014).

[56] L. Escobar and W. Meeker, *A review of accelerated test models,* Statistical Science **21** (2007), 10.1214/088342306000000321.

[57] D. Jordan and S. Kurtz, *Analytical improvements in pv degradation rate determination,* (2010) pp. 002688 – 002693.

[58] A. Halm, A. Schneider, V. Mihailetchi, L. Koduvelikulathu, L. Popescu, G. Galbiati, H. Chu, and R. Kopecek, *Potential-induced degradation for encapsulated n-type ibc solar cells with front floating emitter,* (2015).

[59] U. J. M. H. P. H. Marc Köntges, Gernot Oreski and K.-A. Weiss, *Assessment of photovoltaic module failures in the field : International energy agency photovoltaic power systems programme,* IEA PVPS Task 13, Subtask 3 : report IEA-PVPS (2017).

[60] P. Hacke, S. Spataru, K. Terwilliger, G. Perrin, S. Glick, S. Kurtz, and J. Wohlgemuth, *Accelerated testing and modeling of potential-induced degradation as a function of temperature and relative humidity,* IEEE Journal of Photovoltaics **5**, 1 (2015).

[61] E. Annigoni, M. Jankovec, F. Galliano, H.-Y. Li, L.-E. Perret-Aebi, M. Topic, F. Sculati-Meillaud, A. Virtuani, and C. Ballif, *Modeling potential-induced degradation (pid) in crystalline silicon solar cells: From accelerated-aging laboratory testing to outdoor prediction,* (2016).

[62] J. Hattendorf, R. Löw, W.-M. Gnehr, L. Wulff, M. Koekten, D. Koshnicharov, A. Blauaermel, and J. Esquivel, *Potential induced degradation in mono-crystalline silicon based modules: An acceleration model,* (2012), 10.4229/27thEUPVSEC2012-4BV.2.51.

[63] M. Koentopp, M. Kroeber, M. Schütze, and C. Taubitz, *Potential induced degradation: Model calculations and correlation between laboratory tests and outdoor occurrence,* (2014).

[64] L. Dunn, M. Gostein, and B. Stueve, *Literature review of the effects of uv exposure on pv modules.* (2013).

[65] M. Muñoz-García, N. Vela, F. Chenlo, and M. Alonso-Garcia, *Early degradation of silicon pv modules and guaranty conditions,* Solar Energy **85** (2011).

[66] M. Köhl, D. Philipp, N. Lenck, and M. Zundel, *Development and application of a uv light source for pv-module testing,* Proc. SPIE **7412** (2009), 10.1117/12.825939.

[67] N. Bosco, T. Silverman, and S. Kurtz, *Climate specific thermomechanical fatigue of flat plate photovoltaic module solder joints,* Microelectronics Reliability **62** (2016), 10.1016/j.microrel.2016.03.024.

[68] M. Kempe, *Evaluation of the uncertainty in accelerated stress testing,* 2014 IEEE 40th Photovoltaic Specialist Conference, PVSC 2014 , 2170 (2014).

[69] G. Gaines, R. E. Thomas, G. Noel, T. S. Shilliday, V. Wood, and D. Carmichael, *Development of an accelerated test design for predicting the service life of the solar array at mead, nebraska. quarterly report,* (1979).

[70] A. Bala Subramaniyan, R. Pan, J. Kuitche, and G. Tamizhmani, *Quantification of environmental effects on pv module degradation: A physics-based data-driven modeling method,* IEEE Journal of Photovoltaics **8**, 1 (2018).

[71] E. G. Goma, *Development of cell to system annual energy yield toolbox for bifacial modules,* (2019).

[72] J. G. Etxebarria, *Toolbox for the design and simulation of a floating bifacial pv plant with reflectors,* (2018).

[73] L. Wald, *A simple algorithm for the computation of the spectral distribution of the solar irradiance at surface,* (2018), 10.13140/RG.2.2.17025.76648.

[74] A. L. Buck, *New equations for computing vapor pressure and enhancement factor,* Journal of Applied Meteorology **20**, 1527 (1981-12-01).

[75] I. Kaaya, J. Ascencio-Vásquez, K.-A. Weiss, and M. Topič, *Assessment of uncertainties and variations in pv modules degradation rates and lifetime predictions using physical models,* Solar Energy **218**, 354 (2021).

[76] K. Ismail, M. Koehl, A. P. Mehilli, M. Sidrach-de Cardona, and K. Weiss, *Modeling outdoor service lifetime prediction of pv modules: Effects of combined climatic stressors on pv module power degradation,* IEEE Journal of Photovoltaics **PP**, 1 (2019).

[77] A. Bouaichi, C. Hajjaj, A. Merrouni, A. El Amrani, C. Messaoudi, H. Zitouni, and A. Ghennioui, *In-situ inspection and measurement of degradation mechanisms for crystalline and thin film pv systems under harsh climatic conditions,* Energy Procedia **157**, 1210 (2019).

[78] M. EL-Shimy, *Viability analysis of pv power plants in egypt,* Renewable Energy **34**, 2187 (2009).

[79] Wiki-solar, *"utility-scale solar in 2018 still growing thanks to australia and other later entrants",* .

[80] D. Yue, F. You, and S. Darling, *Domestic and overseas manufacturing scenarios of silicon-based photovoltaics: Life cycle energy and environmental comparative analysis,* Solar Energy **105**, 669 (2014).

[81] R. Burrett, C. Clini, R. Dixon, M. Eckhart, M. El-Ashry, D. Gupta, A. Haddouche, D. Hales, K. Hamilton, C. House, et al., *Renewable energy policy network for the 21st century,* (2009).

[82] E.-S. Mohamed, *Analysis of levelized cost of energy (lcoe) and grid parity for utility-scale photovoltaic generation systems,* in Conference: 15th International Middle East Power Systems Conference (MEPCON '12).

[83] M. Campbell, P. Aschenbrenner, J. Blunden, E. Smeloff, and S. Wright, *The drivers of the levelized cost of electricity for utility-scale photovoltaics,* White paper: SunPower corporation (2008).

[84] K. Branker, M. Pathak, and J. M. Pearce, *A review of solar photovoltaic levelized cost of electricity,* Renewable and sustainable energy reviews **15**, 4470 (2011).

[85] M. El-Shimy, *Viability analysis of pv power plants in egypt,* Renewable Energy **34**, 2187 (2009).

[86] K. Branker, M. Pathak, and J. M. Pearce, *A review of solar photovoltaic levelized cost of electricity,* Renewable and sustainable energy reviews **15**, 4470 (2011).

[87] F. ISE, *Current and future cost of photovoltaics. long-term scenarios for market development, system prices and lcoe of utility-scale pv systems,* Study on behalf of Agora Energiewende. (2015).

[88] Olindo, *Lcoe calculations,* .

[89] R. Fu, D. J. Feldman, and R. M. Margolis, US solar photovoltaic system cost benchmark: Q1 2018, Tech. Rep. (National Renewable Energy Lab.(NREL), Golden, CO (United States), 2018).

[90] OECD, *Projected Costs of Generating Electricity: 2015 Edition,* International Energy Agency , 215 (2015).

[91] Eurostat, *Household energy prices in the EU increased compared compared with 2017,* , 1.

[92] metropolitan electricity authority, *Residential service,* (2015).

[93] EIA, *Average Price of Electricity to Ultimate Customers by End-Use Sector,* U.S. Energy Information Administration **2020**, 2020 (2021).

[94] A. Richter, M. Hermle, and S. W. Glunz, *Reassessment of the limiting efficiency for crystalline silicon solar cells,* IEEE journal of photovoltaics **3**, 1184 (2013).

[95] J. Werner, B. Niesen, and C. Ballif, *Perovskite/silicon tandem solar cells: Marriage of convenience or true love story?–an overview,* Advanced Materials Interfaces **5**, 1700731 (2018).

[96] B. Chen, S.-W. Baek, Y. Hou, E. Aydin, M. De Bastiani, B. Scheffel, A. Proppe, Z. Huang, M. Wei, Y.-K. Wang, et al., *Enhanced optical path and electron diffusion length enable high-efficiency perovskite tandems,* Nature communications **11**, 1 (2020).

[97] E. Unger, L. Kegelmann, K. Suchan, D. Sörell, L. Korte, and S. Albrecht, *Roadmap and roadblocks for the band gap tunability of metal halide perovskites,* Journal of Materials Chemistry A **5**, 11401 (2017).

[98] W. Tress, K. Domanski, B. Carlsen, A. Agarwalla, E. A. Alharbi, M. Graetzel, and A. Hagfeldt, *Performance of perovskite solar cells under simulated temperature-illumination real-world operating conditions,* Nature energy **4**, 568 (2019).

[99] S. Gomez, Sanchez, M. Campoy-Quiles, and Abate, *Topological distribution of reversible and non-reversible degradation in perovskite solar cells,* Nano Energy **45**, 94 (2018).

[100] M. Jost, L. Kegelmann, L. Korte, and S. Albrecht, *Monolithic perovskite tandem solar cells: A review of the present status and advanced characterization methods toward 30% efficiency,* Advanced Energy Materials **10**, 1904102 (2020).

[101] A. Al-Ashouri, E. Köhnen, B. Li, A. Magomedov, H. Hempel, P. Caprioglio, J. A. Márquez, A. B. M. Vilches, E. Kasparavicius, J. A. Smith, et al., *Monolithic perovskite/silicon tandem solar cell with> 29% efficiency by enhanced hole extraction,* Science **370**, 1300 (2020).

[102] J. Qian, M. Ernst, N. Wu, and A. Blakers, *Impact of perovskite solar cell degradation on the lifetime energy yield and economic viability of perovskite/silicon tandem modules,* Sustainable Energy & Fuels **3**, 1439 (2019).

7
APPENDIX